D.C. Water Resources Research Institute
Annual Technical Report
FY 2015

Introduction

District of Columbia is totally urban and its waterways are impacted due to urban runoff and combined sewer outfalls. Consequently, the designated uses that directly relate to human use of the District's waters are generally not supported, such as swimming and fishing. Moreover, the uses related to the quality of habitat for aquatic life is not supported. It is also noted that the water quality of the District's waterbodies continues to be impaired. The mission of the DC Water Resources Research Institute (WRRI), here on called the Institute is to identify the problems and contribute to their solution through applied research and training funded through the seed grants.

This report is a summary of the research activities of the Intitute for the period of March 1, 2015 through February 28, 2016. Hosted under the College of Agriculture, Urban Sustainability and Environmental Sciences (CAUSES) of the University of the District of Columbia, the DC WRRI continued to coordinate water related research, training and outreach activities in the District of Columbia in order to enhance the quality and quantity of DC waterways.

Since 2005, the Institute has provided seed grants for 89 research projects and trained hundreds of graduate and undergraduate students. The seed grants created opportunities for students and new faculty in creating innovative researches and getting trained in water technologies. The seed grant also helped new faculty leverage extramural funding. Through the Institute, the University of the District of Columbia has received about $2 million in financial support to build state-of-the-art research and training laboratories for environmental and water quality testing, as well as modeling and simulation.

In 2015, the Institute funded and implemented eight research projects that address key water issues in the District. The overarching goal of this project includes identifying city water resources and environmental problems, and contributing to their solutions. About 20 graduate and undergraduate students were directly involved in the research projects, but more than 100 students were trained in the water quality testing technologies through lab and field experiences.

Partially funded through the administrative project, the Institute also manages two state-of-the-art laboratories: water and environmental quality testing laboratory, and water and environmental quality modeling and simulation laboratory. The water and environmental quality testing laboratory became accredited by the National Environmental Laboratory Accreditation Program (NELAP) with NELAC standard in October, 2015 though the State of New Hampshire Environmental Laboratory Accreditation Program. The lab is now nationally accredited for trace metals, minerals and water hardness potable and non-potable waters. The lab is now in the process of expanding its NELAP accreditation for pesticides analysis in water, and trace metal analysis in soil and biosolids. This NELAP accreditation is the 1st of its kind in DC and the metropolitan area, has a significant impact, in enhancing the research and training capacity of UDC in preparing future water scientists.

Even if there was no funded information transfer project during the reporting time, the Instute continued conducting successful information transfer projects through training workshops and the regional annual water symposium. The Institute continued building collaboration with other centers within the hosting institution and beyond for conducting information transfer activities. In collaboration with the American Water Resources Association in the National Capitol Region (AWRA-NCR), the Institute organized the 4th Annual Water Symposium on April 8, 2016, at the University of DC. This one-day symposium sought to bring together experts from governmental agencies, academia, the private sector, and non-profits to present and discuss rethinking the value of water: innovations in research, technology, policy, and management. In close collaboration with other land-grant centers in CAUSES, such as the Center for Sustainable Development, the Institute continued in conducting outreach activities by organizing training workshop, distributing newsletters,

media releases and fact sheets. The Institute will work closely with both internal and external colaborators to build on its current success of information transfer activities.

Research Program Introduction

In FY 2015, the Institute funded eight research projects that address three areas: hydrology and flooding, water quality, policy and green infrastructure. The progress report of Dr. MacAvo's project introduces the effectiveness of green roofs for limiting nittrogen, phosphorous, dissolved organic carbon (DOC) and suspended solids. Based on the traditional green roofs (soil-based) and Aqualok roofs (foam-based) installed at the American University several years ago, green roofs of any type show higher Total Suspended Solids (TSS) and phosphorus than rainwater. The planted and unplanted roofs are all better options than asphalt roofs with respect to phosphorous, though neither are better than the asphalt roof with respect to TSS.

The progress report of Drs. Nian Zhang and Pradeep Behera investigates the application of a least-squares support vector machine (LS-SVM) model to improve the accuracy of stream flow forecasting. Cross-validation and grid-search methods are used to automatically determine the LS-SVM parameters in the forecasting process. Based on streamflow records from the U.S. Geological Survey (USGS) gaging station 1652500 on Four Mile Run of the Potomac River, the performance of the LS-SVM model is compared with the recurrent neural network model trained by Levenberg-Marquardt backpropagation algorithm. The results of the comparison indicate that the LS-SVM model is a useful tool and a promising new method for streamflow forecasting.

The progress report of Dr. Massoudieh's demonstrates the application flexible framework for modeling the multi-dimensional processes of hydrological and water quality in urban environments that wish to incorporate stormwater green infrastructure (GI) and explore its potential performance and effectiveness. The framework models a GI system using a set of blocks and connectors representing different functional components of the GI. The computational engine of this flexible model solves equations describing critical mechanisms related to GI model performance that can be grouped into three categories: 1) hydraulics, 2) particle fate and transport, and 3) coupled dissolved and particle-associated reactive transport of water quality constituents. The proposed method can be applied to evaluate the hydraulic performance of a bioretention system.

The progress report of Dr. Phelps introduces the importance of biomonitoring in identify persistent bioaccumulated and toxic pesticides in the Anacostia watershed. This project looked for the path transferring chlordane from Maryland tributary sources and the tidal Anacostia to DC food fish of three trophic levels. This study identified that chlordane-contaminated surface sediment from Maryland is the likely source of chlordane contamination in DC part of Anacostia watershed.

The progress report of Dr. Knee assesses how hydraulic fracturing ("fracking") could affect dissolved metal concentrations and other water quality parameters in Washington, DC's water source, the Potomac River. Based on 73 samples collected from stream sites in parts of the Potomac watershed that overlie the Marcellus shale in the states of Virginia, West Virginia and Maryland, fracking sites had significantly higher concentrations of strontium, a metal that has been associated with fracking in previous studies, as well as one isotope of radium, 224Ra.

The progress report of Drs. Xu and Song work introduces the application of a nanotechnology or "smart" switchable surfactant responsive to UV light that serves as a template system for water pollutant removal. The proposed research is very much useful for the District of Columbia because it can help improve the efficiency and capacity of wastewater treatment to meet the increasing volume of wastewater, especially in metropolitan area.

The progress report of Dr. Song introduces an analytical method able to provide rapid, sensitive, easy and reliable detection of water soluble organic and inorganic phosphorus (P) in water samples using 31P Nuclear Magnetic Resonance spectroscopy. The research finding showed that the high sensitivity of 31P NMR makes

the technique a reliable analytical tool in phosphorus analysis.

The progress report of Dr. Behera introduces the impact of extreme wet-weather events on DC waterways and transportation infrastructure. The study considers the extreme events include 100 year storm and a 10 feet river surge during hurricanes or extreme events. During the extreme events, what percentage of roads are affected is assessed through digital maps which provides the vulnerability assessment of the transportation network during the extreme events.

Listed below are the eight grants awarded to researchers for FY 2016 104B grants and associated Principal Investigator:

Title: Performance evaluation of urban stream restoration using process-based modeling, Dr. Arash Massoudieh, Assistant Professor, Catholic University of America.

Title: Analysis of perchlorate in drinking water, surface water by AxION Direct sample analysis (DSA) /Time of flight (TOF) Mass Spectrometer, Sebhat Tefera and Yacov Assa, College of Agriculture, Urban Sustainability and Environmental Sciences, University of the District of Columbia.

Title: 31P NMR Studies on the oxidative degradation of Glyphosate and its primary metabolite aminomethylphosphonic acid (AMPA) by transition metal oxide nanomaterilas in soil, water and sediment samples, Xueqing Song, School of Arts and Sciences, University of the District of Columbia.

Title: Analysis of External and Internal Storm Event Characteristics for Washington DC based on different IETDs, Pradeep Behera, professor, School of Engineering and Applied Sciences, University of the District of Columbia.

Title: A Comparative Study of Nearest-Neighbor Method (NNM) and Extended Nearest-Neighbor (ENN) Method for Annual Streamflow Prediction, Nian Zhang and Pradeep Behera, School of Engineering and Applied Sciences, University of the District of Columbia

Title: Development of A Novel Stormwater Runoff Collection and Treatment System for Urban Agriculture and Food Security, Jiajun Xu, School of Engineering and Applied Sciences, University of the District of Columbia

Title: Assessing the effectiveness of interactive signage at advancing communicating, promoting, and educating the public on green infrastructure projects in public spaces, Kamran Zendehdel, Harris Trobman and Xiaochu Hu, College of Agriculture, Urban Sustainability and Environmental Sciences, University of the District of Columbia

Title: Influence of consistently high levels of ammonium on food web dynamics in the Anacostia River. Dr. Caroline Solomon, Department of Sciences, Technology and Mathematics, Gallaudet University.

Evaluating Long-term water quantity and quality performance of Bioretention systems in Washington, DC using monitoring and modeling

Basic Information

Title:	Evaluating Long-term water quantity and quality performance of Bioretention systems in Washington, DC using monitoring and modeling
Project Number:	2015DC168B
Start Date:	3/1/2015
End Date:	2/28/2016
Funding Source:	104B
Congressional District:	District of Columbia
Research Category:	Engineering
Focus Category:	Water Quality, Water Quantity, Models
Descriptors:	None
Principal Investigators:	Arash Massoudieh

Publication

1. Massoudieh,Arash, Haydee De Clippeleir, Ahmed Al-Omar, Heather Stewart and Jamal Alikhani, 2016. Optimization of Mainstream Deammonification Operation. In: "Rethinking the Value of Water: Innovations in Research, Technology, Policy, and Management", the 2016 NCR-AWRA 4th Annual Water Symposium,Friday, April 8, 2016.

Progress Report: Development of a flexible model for performance evaluation of green infrastructure

Author: Arash Massoudieh

Abstract:

A flexible framework is introduced for modeling the multi-dimensional processes of hydrological and water quality in urban environments that wish to incorporate stormwater green infrastructure (GI) and explore its potential performance and effectiveness. The framework models a GI system using a set of blocks and connectors representing different functional components of GI. The blocks are used to represent any spatial feature with the ability to store water (e.g. pond, soil, benthic sediments, manhole, a storage zone, etc.) and water quality constituents and the connectors represent the flow and mass transfer between each pair of blocks. Each block and connector can be assigned different constitutive relationships controlling the head-storage (H-S) and head-flow (H-Q) relationship depending on their identity. The computational engine of this flexible model solves equations describing critical mechanisms related to GI model performance that can be grouped into three categories:1) hydraulics, 2) particle fate and transport, and 3) coupled dissolved and particle-associated reactive transport of water quality constituents (e.g., pollutants). Regarding the hydraulics, the model can solve a combination of Richard's equation, kinematic/diffusive wave, Darcy, and other user-provided flow models simultaneously. The particle transport model is based on performing mass-balance

on particles in different phases including for example mobile and deposited in soil and constitutive theories controlling their transport, settling, deposition and release. The reactive transport modules allows constituents to be in dissolved, sorbed, or bound to particles and also to undergo user-defined transformations. The numerical solution is based on an adaptive time-step implicit Newton-Raphson method. A graphical user interface has been added that allows users to visualize the conceptual layout of the GI system being modeled as well as define and parameterize the transport and fate mechanisms. An applications of the modeling framework consisting of the hydraulic performance of a bioretention system is demonstrated.

Keywords: Low Impact Developments, Rain Garden, Bioretention, modeling fate and transport

1. Introduction

Urban stormwater GI are practices also referred to as low impact developments (LIDs) that are designed to reduce the volume and peak flow as well as the contaminant loading associated with stormwater runoff. GI design relies on processes such as infiltration, evapotranspiration, sedimentation, filtration, deposition, and plant uptake for mitigating stormwater impacts. A wide range of GI types are used for stormwater management. To name a few there are dry and wet ponds, infiltration basins, constructed wetlands, bioretention systems, rain gardens, rain barrels, green roofs, infiltration trenches, bio-swales, and porous pavements, see the review by Ahiablame, et al. (2013). Innovative or non-conventional approaches including combining multiple types of GIs or using non-standard GI designs have also been proposed and proven to be effective in some cases (Dickson, et al., 2011, Liu, et al., 2015, Page, et al., 2012).

To be able to evaluate the long-term performance of GI design and explore potential improvements it is important to be able to consider the relative importance of processes affecting GI hydraulics and the fate and transport of contaminants fluxing through these facilities. Field studies have shown that the performance of stormwater GIs can be highly dependent on their design configuration and the properties of the medium within the structure that interacts with the stormwater that they are designed to treat (Liu, et al., 2014). It has also been shown that GI performance is dependent on the intensity and duration of rain events (Berndtsson, 2010, Qin, et al., 2013). Recommended design standards for GIs are often different among jurisdictions in the United States and around the world (He and Davis, 2010).

Process-based mathematical modeling provides a cost-effective way to examine the effects of various design guidelines on the performance of GIs tailored to specific sites and geographies to optimize their performance while meeting hydraulic and water quality goals and also to test different hypotheses about the relative importance of the various treatment processes within GIs. Most available models for GI performance analysis are either developed for catchment scale, see summaries by Elliott and Trowsdale (2007); and Li and Babcock Jr (2014) and hence lack the details needed to consider site-specific design aspects. For those that are process-based they have been developed for a specific type of GI with predefined structures (e.g. for bioretention systems see (Dussaillant, et al., 2005, Dussaillant, et al., 2004, He and Davis, 2010, Palhegyi, 2009) and for Permeable Pavements see Lee, et al. (2014)). Therefore, their application is restricted to configuration consistent with the one they are intended for. General purpose models such as those designed for modeling flow and transport in unsaturated soil or surface water hydraulics and water quality have also been used to study certain aspects of GI performance (e.g. (Brown, et al., 2013, Hilten, et al., 2008, Massoudieh and Ginn, 2008, Meng, et al., 2014).

General purpose models such as models designed for flow in unsaturated media (e.g. Hydrus, (Šimůnek, et al., 2008) has also been used to evaluate the performance of GIs (Hilten, et al., 2008, Meng, et al., 2014, Šimůnek, et al., 2008) however, the performance of GIs are often controlled by the combination of various processes in multiple media types such as flow and transport in variably saturated soil, aggregate or underdrain layers, overland flow, and pipes that cannot be easily modeled using the general purpose models typically developed based on a single medium.

A flexible process-based modeling framework is described here with the ability to evaluate the hydrological and water quality performance of a wide range of GIs with user-defined structure and levels of complexity. The modeling framework was developed to account for three critical aspects of GI performance including the modeling of 1) hydraulics, 2) particle/colloid transport and 3) dissolved and particle-bound reactive transport of contaminants. The flexibility of the hydraulic component allows for flow considerations in different media often seen in stormwater GIs including ponds, overland flow, saturated and unsaturated porous media, storage layers or structures, pressurized or free-surface flow in pipes as well as evaporation and transpiration. The tool also allows users to introduce new media with user-defined H-S and H-Q relationships. The particle/colloid transport module allows introduction of multiple particle types, each with different transport properties. Particles are considered to be present in different phases including mobile, reversibly deposited, irreversibly deposited or bound to the air-water interface while undergoing exchange between these phases. The number and nature of the phases each particle class can be present in as well as the exchange between the phases can be specified by the user. Particle transport is especially important in predicting the water quality effects of GIs because particle retention is one of the most important mechanisms for removal of

contaminants with high affinity to solid materials. The contaminant reactive transport module allows consideration of multiple reactive components based on user-provided networks and stoichiometric coefficients. Contaminants can undergo sorption-desorption with the soil matrix as well as mobile and immobile particles. Build-up, wash-off and atmospheric exchange of contaminants can also be considered. The main goal of this research was to demonstrate the basics of the modeling framework, the governing equations that can be attributed to different compartments and the numerical approach to solve the hydraulic, particle transport and the transport and transformation of water quality constituents. Three demonstration applications of the modeling framework on a bio-retention system, a porous pavement system, and a wet pond are also briefly presented.

2. Model Framework and Components

2.1 Hydraulics:

A GI system is modeled with GIFMod using a number of "blocks" that are connected using "interfaces". Each block represents one spatial feature such as an unsaturated/saturated soil element, pond, manhole, stream segment, among many other. The expressions determining how the flow is computed between the blocks are specified for each interface. This expression could be in any equation form specified by the user or come from pre-defined relationships including Richard's equation for unsaturated medium, Darcy's law for saturated medium, Hazen-Williams for pipes, or Manning equation for ponds, streams and overland flow. Generally, the existing software tools used for GI modeling tools provide a pre-defined set of equations to choose from. For example, SWMM offers three categorical methods (Horton's Equation, Green-Ampt Method

and Curve Number Method) to model infiltration, but not the Richard's equation. While the other options may be adequate for many modeling scenarios, this flexible framework provides the user an option to choose hydraulic processes and equations that best represent the modeled scenario.

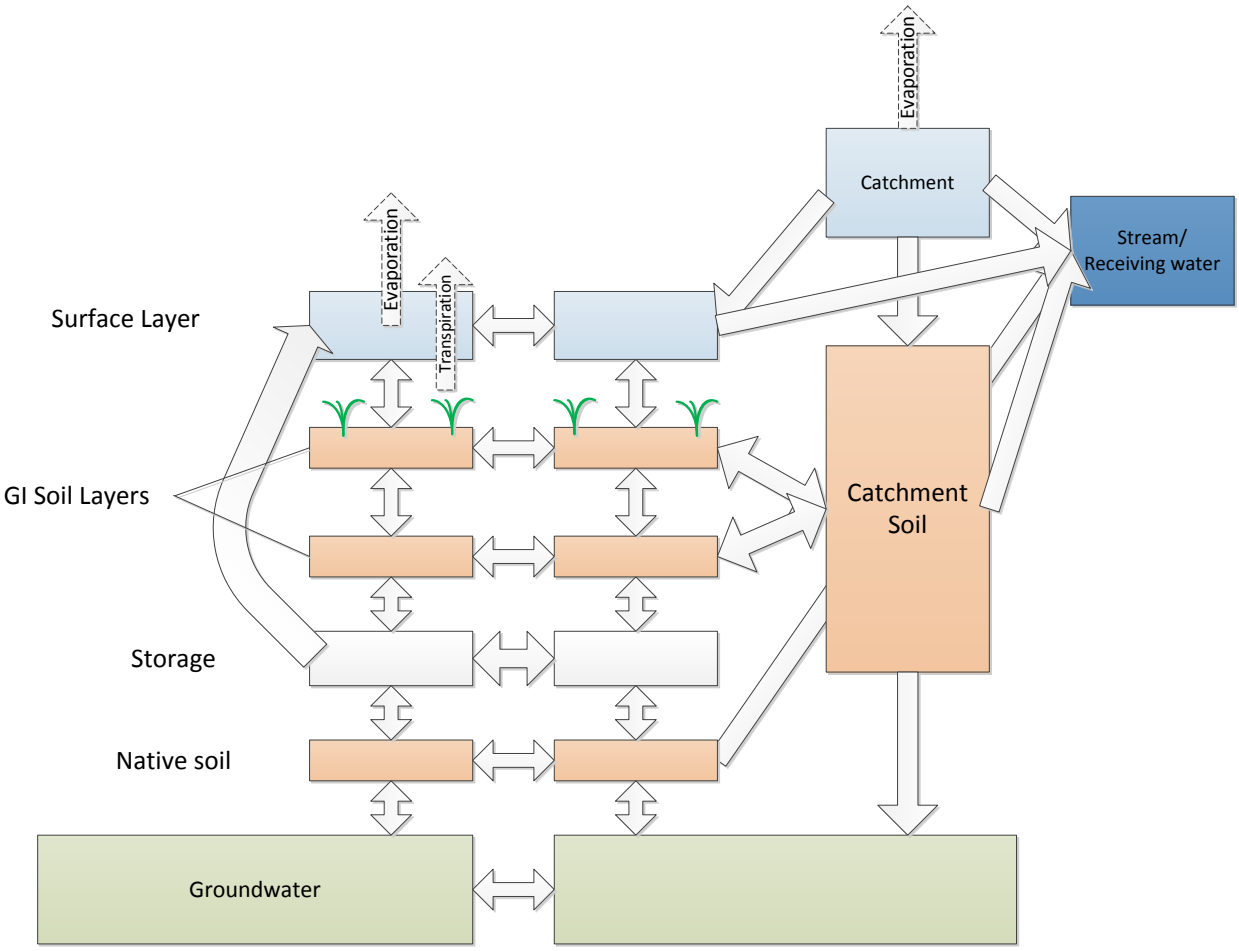

Figure 1: An example depiction of how blocks and connectors can be used to represent a GI system consisting of different components. The boxes represent block and arrows represent connectors. Each block and connector can be assigned governing equations controlling their hydraulic and transport properties.

The water balance equation for each block can be written as:

$$\frac{dS_i}{dt} = -\sum_{j=1}^{nj} Q_{w,ij} - \sum_{j=1}^{nj} Q_{ev,ij} + \sum_{j}^{ns} Q_{Si,j} \qquad (1)$$

where S_i [L^3] is the water storage (volume) in block *i*, $Q_{w,ij}$ [L^3/T] is the liquid water flow from block *i* to block *j* ($Q_{w,ij} = -Q_{w,ij}$), *nj* is the number of neighboring blocks exchanging water with block *i*, $Q_{ev,ij}$ [L^3/T] is the water vapor flow from block *i* to block *j,* which simplistically is determined using a diffusive term proportional to the void area occupied by the air phase and other factors such as temperature. $Q_{Si,j}$ is source or sink of water flow within the block *i* due to direct precipitation, external inflow or evapotranspiration [L^3/T], and *ns* is the number of sources/sinks within block *i*. In order to solve the system of ordinary differential equations consisting of the Eq. (1) applied to all of the blocks a relationship between Q and S is needed. This is typically done by linking both Q and S to the hydraulic head in the block.

$$h_i = f\left(S_i, \boldsymbol{\Theta}\right) \tag{2a}$$

$$Q_{w,ij} = -Q_{w,ji} = g\left(h_i, h_j, \boldsymbol{\Theta}\right) \tag{2b}$$

$$Q_{ev,ij} = -Q_{ev,ji} = g_{ev}\left(S_i, S_j, \boldsymbol{\Theta}\right) \tag{2b}$$

Where $\boldsymbol{\Theta}$ represent all other physical parameters controlling the H-S and Q-H relationships. Six generic GI media types including unsaturated and saturated soil, pond, stream, overland flow, storage are provided with the framework. Other media types can be customized by the user by providing the H-S relationship for the blocks and Q-H relationships for the interfaces. It should be noted that the unsaturated soil media type can perform under a saturated condition, but when a block is known to be saturated throughout the modeling time series, choosing a saturated block typereduces the computational burden. The H-S and Q-H relationships for the aforementioned six block types are listed in Tables 1 and 2 respectively. In addition to the default (Q-H) relationships shown in Table 2, the user can select from three other default interface types

including rating curve, free surface and pressurized flow in pipe (via Hazen-Williams equation) and normal flow. Similar to other models, the storage variation in pipes or other such interfaces are not accounted for in the calculations assuming the flow in and out of such interfaces is always equal. This simplification is justified since the storage variation in pipes in GI systems is typically insignificant.

Evapotranspiration can be modeled using generic evaporation and transpiration models provided in the framework for example the aerodynamic model for evaporation (Chow, et al., 2013) or several commonly used root water uptake models (RWU) either by expressing the functional dependence of the vegetation water stress factor based on soil moisture or soil matric potential by providing the field capacity and wilting point moisture and matric suction by the user. Alternative expressions for calculation of evaporation and transpiration rates can also be introduced by the user.

2.2 Particle Transport

A particle transport module allows simulation of multiple types (classes) of particles with different transport behavior including settling, resuspension, reversible and irreversible attachment to the solid matrix, entrapment into air-water interface (AWI) and other user-defined processes. Each particle type/class can be present in different phases as specified by the user. For example, a particle class can be specified in mobile aqueous phase, in reversibly or irreversibly attached phase or trapped in AWI. The general form of the transport equation for particles can be written as the following single equation:

$$\frac{d\Gamma_{i,l}G_{p,l,i}}{dt} = \underbrace{\alpha_l \left| \sum_{\cdot,\cdot}^{nj} pos\left(Q_{w,ij} + v_{s,p,ij}A_{ij}\right)G_{p,l,j} - \sum_{\cdot,\cdot}^{nj} pos\left(-Q_{w,ij} - v_{s,l,ij}A_{ij}\right)G_{p,l,i} \right|}_{Advection}$$
$$\underbrace{-S_i\left(\sum_{\cdot,\cdot}^{nl_p}\mathbf{K}_{l,l'}G_{p,l,i} - \sum_{\cdot,\cdot}^{nl_p}\mathbf{K}_{l',l}G_{p,l',i}\right)}_{mass\ exchange\ between\ phases\ (e.g.\ mobile\ phase\ and\ attached\ phase)} \quad \underbrace{+\alpha_l \sum_{\cdot,\cdot}^{nj} A_{ij}\frac{D_{p,ij}}{d}\left(G_{p,l,j} - G_{p,l,i}\right)}_{dispersion/diffusion} \tag{3}$$

Equation (3) is a general equation that describes the mass balance of colloid class p in phase l in block i which lumps together the sets of equations representing the mass balance of mobile and immobile colloids (Massoudieh and Ginn, 2008, Massoudieh and Ginn, 2010). In Eq. (3) $\Gamma_{i,l}$ is referred to as the capacity of phase l in block i. For example, in the case of a two-phase colloid transport model with an aqueous phase and a reversibly or irreversibly captured colloidal phase soil, $\Gamma_{i,0} = S_i$ or $\Gamma_{i,0} = S_i + K_{aw}S_{aw}$ when equilibrium entrainment of particles into AWI with an interface area of S_{aw} and equilibrium air-water partition coefficient of K_{aw} or $\Gamma_{i,1} = \rho_b V$ when the captured colloidal phase is expressed as colloid mass per mass of soil matrix or $\Gamma_{i,1} = f_i V$ when the attached particles are expressed as mass of particles per surface area of soil matrix. ρ_b [M/L^3] is the bulk density and f_i [L^2/L^3] is the specific surface area. Also α_l is an indicator representing the mobility of particle phase l (0 when phase l is immobile and 1 when it is mobile), $G_{p,l,i}$ is the concentration of particles of class p in phase l and block i, nj represent the number of connectors attached to block i, $pos(x) = xH(x)$, H is the Heaviside function, $v_{s,p,ij}$ is the settling velocity of particle class p projected on the direction of interface ij, A_{ij} is the area of the interface ij, nl_p is the number of phases particles of class p can be in, $\mathbf{K}_{l,l'}$ is particle mass transfer rate from phase l to l' which can be a function of concentration in the destination

phase (due to blocking), flow velocity, or other factors and $D_{p,ij}$ is the dispersion coefficient or particles in class p in interface ij which can be a function of flow velocity and other factors. It should be noted that the user interface allows $v_{s,p,ij}$, $\mathbf{K}_{l,l'}$, $D_{p,ij}$ to be expressed as expressions.

2.3 Coupled particle-bound and/or dissolved reactive transport

A coupled particle-bound and dissolved reactive transport module can solve the transport phenomena as of multiple reactive species both in the aqueous phase or as sorbed to mobile particles. The adsorption and desorption both to the immobile soil matrix and immobile particles can be accounted for. Most models used for GI modeling in the past ignore the fact that some contaminants can move not only in dissolved phase but as bound to mobile particles. Colloid-facilitated transport can play an important particularly in transport of consituents with high affinity to solid material. In modeling GIs this can be particularly important when sedimentation result in removal of contaminants due to the settling of particle-bound contaminants. Processes such as atmospheric exchange and pollutant build-up on soil or other surfaces can also be considered via user-defined expressions indicating their flux. The mass balance equation for a compound in any of these phases can be represented by the following equation:

$$\begin{aligned}\frac{d\Gamma_{i,p,l}C_{p,l,i,k}}{dt} = {} & \underbrace{\alpha_{p,l}\left|\sum^{nj} pos\left(Q_{w,ij}+v_{s,p,ij}A_{ij}\right)G_{p,l,j}C_{p,l,j,k}-\sum^{nj} pos\left(-Q_{w,ij}-v_{s,p,ij}A_{ij}\right)G_{p,l,i}C_{p,l,i,k}\right|}_{advection} \\ & \underbrace{-S_i\left(\sum^{nl_p}\mathbf{K}_{l,l'}G_{p,l,i}C_{p,l,i,k}-\sum^{nl_p}\mathbf{K}_{l',l}G_{p,l',i}C_{p,l',i,k}\right)}_{mass\ exchange\ due\ to\ colloid\ exchange}+\underbrace{\alpha_{p,l}\sum^{nj}A_{ij}\frac{D_{s,i,j,k}}{d}\left(G'_{p,l,i}C_{p,l,j,k}-G'_{p,l,i}C_{p,l,i,k}\right)}_{Dispersion/Diffusion} \\ & \underbrace{+S_i\sum^{np}\sum^{nl_p}\boldsymbol{\kappa}_{p,p'}\left(\frac{C_{p',l',i,k}}{\phi_{\cdot,\cdot}}-\frac{C_{p,l,i,k}}{\phi_{\cdot,\cdot}}\right)}_{adsorption-desorption}+\underbrace{S_i\sum^{nr}\psi_{r,k}R_r}_{transformation/reaction}+\underbrace{S\,\xi}_{mospheric\ Exchange} \\ & \underbrace{+\sum^{ns} pos\left(Q_{Si,j}G_{p,l,in}C_{p,l,in,k}\right)-\sum^{ns} pos\left(-\beta_{p,l,j}Q_{Si,j}G_{p,l,in}C_{p,l,in,k}\right)}_{Sink/sources}\end{aligned} \quad (4)$$

where $\Gamma_{i,p,l}$ [dimension depends on the phase] is the capacity of particle class p in phase l in block i ($p=0$ is reserved for the aqueous phase and $p=-1$ indicates the constituent fraction sorbed to the solid matrix), $C_{p,l,i,k}$ is the concentration of chemical constituent k adsorbed to phase l of particle class p in block i, $\alpha_{p,l}$ is the mobility indicator for phase l of particle type p (i.e. $\alpha_{p,l}=1$ for mobile phases and $\alpha_{p,l}=0$ for immobile phases), $D_{s,i,j,k}$ is the dispersion/diffusion coefficient of chemical constituent k, $G'_{p,l,i}$ is the concentration of particulate class p in phase l for $p\neq 0$ and equal to 1 for $p=0$ (aqueous phase), $\boldsymbol{\kappa}_{p,p'}$ is the direct mass exchange rate between particle type p and p', $\phi_{k,p}$ is partition coefficient of constituent k with respect to particle size class p which is equal to 1 for aqueous phase ($p=0$), R_r is the rate of reaction/process number r and $\psi_{r,k}$ is the stoichiometric constant of constituent k in process number r which is negative when the constituent k is used as a result of the process, $\xi_{p,l,i,k}$ is the source of constituent k as bound to particle class p or in aqueous phase of adsorbed to soil matrix ($p=0$) which is determined using a user defined expression. It should be noted that typically the elements of matrix $\boldsymbol{\kappa}_{p,p'}$ are zero except for the case when either p or p' is zero or one of the phases is the aqueous phase as the constituent mass transfer typically occurs through the aqueous phase. $\beta_{p,l,j}$ is a switch that determines whether a water sink (such as evaporation or transpiration) also result in uptake of a particular constituents. The code allows expressing both R_r and $\psi_{r,k}$ as a function of other constituent concentrations and some given process parameters through external input files. The reaction rate expressions and stoichiometric constants can be entered as a Petersen matrix (Russell, 2006) into the program.

2.4 Numerical solution

By moving all the terms to the right hand side in Eqs. (1), (3) and (4) they all can be written in the general form:

$$\frac{dg(X)}{dt} - f(X) = 0 \qquad (5)$$

Applying Euler's approximation and Crank-Nicholson time weighting with non-equal weighting, the descretized form of Eq. (5) can be written as:

$$\mathbf{F}\left(\mathbf{X}^{t+\Delta t}; \mathbf{X}^{t}, \Delta t\right) = \frac{g\left(\mathbf{X}^{t+\Delta t}\right) - g\left(\mathbf{X}^{t}\right)}{\Delta t} - \omega f\left(\mathbf{X}^{t}\right) - (1-\omega) f\left(\mathbf{X}^{t+\Delta t}\right) = 0 \qquad (6)$$

where $\mathbf{X}$ is the vector of all state variables, the super-script indicates the time at which $\mathbf{X}$ will be evaluated and ω is the time weighting factor. $\mathbf{F}$ is the residual vector and the goal at each time-step is to find the $\mathbf{X}^{t+\Delta t}$ that results in $\mathbf{F} = 0$. Solving Eq. (6) using Newton-Raphson (NR) method requires evaluating the Jacobian matrix $J = \partial \mathbf{F}(\mathbf{X}^{t+\Delta t}) / \partial \mathbf{X}^{t}$ numerically which is a computationally intensive task. So here an approach was adopted to reuse the Jacobian matrix as long as it is possible. For this purpose the NR equation is modified as:

$$\mathbf{X}_{i+1}^{t+\Delta t} = \mathbf{X}_{i}^{t+\Delta t} - \frac{\Delta t_t}{\Delta t_J} \left(\mathbf{J}_J\right)^{-1} \mathbf{F}(\mathbf{X}_{i}^{t+\Delta t}) \qquad (7)$$

where $\mathbf{J}_J$ is the Jacobian matrix calculated at a previous time-step that is being reused and Δt_J is the time-step size at the time the Jacobian matrix has been calculated and Δt_t is the current time step size. Subscripts i and $i+1$ indicate the NR iteration counter. The iterations continue until the norm of residual is below a given threshold ($\left|\mathbf{F}(\mathbf{X}_{i}^{t+\Delta t})\right|_2 < \varepsilon$. To save computational time the inverse of the Jacobian matrix, $\left(\mathbf{J}_J\right)^{-1}$ is stored in the memory. The adaptive time step algorithm works based on limiting the number of NR iterations to achieve convergence. At each time step,

the time step size is either increase or decrease or remain unchanged based on the number of iterations required in the previous time step:

$$\Delta t^{t+\Delta t} = \begin{cases} \Delta t^t \left(1+\gamma\right) & NI < NI_{\min} \\ \Delta t^t \left(1+\gamma\right)^{-1} & NI > NI_{\max} \\ \Delta t^t & otherwise \end{cases} \qquad (8)$$

where NI is the number of iterations to reach convergence at the previous time step, $NI_{\min}$ and $NI_{\max}$ are some thresholds and γ is the time-step expansion factor.

Checking for dry blocks

When modeling GI systems, it often occurs that some of the blocks become completely dry or stay dry for a long duration for example in pond, stream, storage or catchment components. This results in a stiff system of equations and requires very small time-step sizes. In order to avoid this problem a new method is implemented that is based on changing the state variables to the outflow from a block when it is known that the block is entering a zero storage condition. When the calculated storage in a block is calculated as a negative number, the calculation is redone by setting $S_i^{t+\Delta t} = 0$ and modifying the descretized form of Eq. (1) as:

$$\frac{0 - S_i^t}{\Delta t} = \sum_{j=1}^{nj} pos\left(Q_{ij}\right) + \sum_{j=1}^{ns} pos\left(Q_{Sij}\right) - \upsilon_i \left[\sum_{j=1}^{nj} pos\left(-Q_{ij}\right) + \sum_{j=1}^{ns} pos\left(-Q_{Sij}\right) \right] \qquad (9)$$

where υ_i is called flow correction factor which reduces the outflows in order to satisfy the dryness condition at time $t + \Delta t$. For a dry block υ_i is treated as a state variable to be solved using the NR approach. The dryness condition will be maintained until the υ_i is calculated to be larger than 1 which indicates starting of a wet stage for the block at this time the mass balance equation for the block is switched to the normal (wet) form.

3. Demonstration Application: A dual-cell bioretention system

Site Description

First we demonstrate how GIFMod can be used to model a GI system in Cincinnati, OH consisting of two rain gardens built as bioretention facilities and placed in series to mitigate stormwater volume and pollutant loading to a combined sewer. The two rain gardens are connected by an underdrain pipe which carries runoff from the aggregate storage zone of the upper cell to the surface of the lower cell. The system is designed to control stormwater flow and pollution from a catchment of 94,500 ft^2 (Dumouchelle and Darner, 2014) (Figure 1). The runoff produced over the wooded area and the parking lot is collected by at a catch basin within the parking lot and is diverted to the upper rain garden through an underground 12" PVC pipe (solid arrow in Figure 2). This pipe carries the main inflow to the upper rain garden. In our model conceptualization the contribution of direct runoff from the sloped grassed area to the upper rain garden is considered minor and, therefore, ignored for storms with average intensity, which was confirmed by field observations.

Figure 2. Aerial image of St. Francis Apartment rain gardens.

The inflow to the upper rain garden infiltrates through at least 24 inches (0.61m) of engineered soil (a mixture of sand, soil, and compost) laying above 15 inches (0.38m) of gravel aggregate , where it gradually percolates to the underneath native soil. The excess water at the aggregate layer is collected by a porous 6" PVC pipe situated at the top of this layer (dashed-line arrows in Figure 2) and is diverted to a manhole. The excess water from the ponding at the rain garden surface is also collected by the same manhole. The manhole diverts excess water to the lower rain garden using a 12" PVC pipe (solid arrow in Figure 1). The contribution of the direct runoff to the lower rain garden from the sloped grassed area and the sidewalk between upper and lower rain garden (total area of 15,300 ft^2) is considered negligible. The lower rain garden has been designed with similar specifications to the upper rain garden as shown in Table 3. The excess water from the lower rain garden is discharged to the city's combined sewer system (CSO?).

Table 3. Design specifications of St. Francis rain gardens. Source: (Dumouchelle and Darner, 2014) and design maps.

Media	Parameter	Value
Pond	Area	Upper: 3,816 ft^2 (354.52 m^2) + Lower: 3,241 ft^2 (301.10 m^2)
Input PVC Culvert	Diameter	12 inches (0.30 m)
Soil Layer	Texture	Engineered Soil
	Minimum Depth	24 inches (0.61 m)
Underdrain Aggregate Layer	Depth	15 inches (0.38 m)
Underdrain PVC Pipe	Diameter	6 inches (0.15 m)
	Slope	0.50%

The flow in and out of each of the bioretention cells have been monitored over a period of three years (2012-2014). The inflow to the upper and lower rain gardens was continuously measured using a pressure transducer -V-Notch weir system. The evapotranspiration was estimated at the site based on ASCE standardized reference evapotranspiration equation (Walter et al., 2005). The required climatic data for this evapotranspiration equation are air temperature, humidity, solar radiation, and wind speed. These data were continuously collected using a Campbell Scientific ET107 station (ET 107 Instruction Manual) located at the upper rain garden. The precipitation at the site was also measured using a tipping bucket rain gage.

St. Francis GI Model Setup

Each rain garden was divided into three vertical compartments each containing a surface water component a soil column representing multiple layers, a storage layer and a single soil layer at the bottom representing the native soil. The horizontal segmentation was performed to take into account the irregular surface topography of the rain gardens and the possibility of short-circuiting. That is, the middle section of each rain garden receives the inflow, and has the lowest surface elevation. Hence more ponding of water and infiltration is expected to occur here. Unless there is a high volume of storm runoff the two adjacent segments (??) usually remain unsaturated.

Figure 2 shows the cross sectional topography of the rain gardens as obtained through surveying during March 2015. The cross sectional profile of the lower rain garden represents the width-averaged surface elevation..

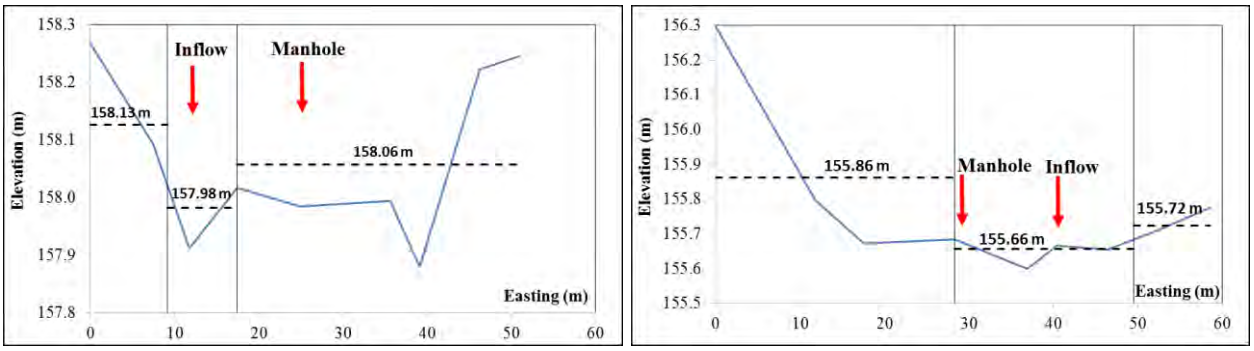

Figure 3. Profiles of the upper (left) and the lower (right) rain gardens. The dash lines represent the average surface elevation of the segments, ref figure 3..

Based on the surface topography (Figure 2), the surface elevations and areas of the three compartments were determined as presented in Table 4. Based on this simplified surface topography, the inflow initially enters the middle column of the upper rain garden. However, if excess ponding forms and the water elevation exceeds the surface elevation of other columns, the

the ponded water flows into adjacent surface water components accordingly based on the flow value determined using Manning equation. The water flow in the lower cell is similar to the upper one with the exception that the effluent from the upper cell is the main inflow into the lower cell.

Table 4. Description of the soil columns of the rain gardens.

Parameter	Upper Rain Garden			Lower Rain Garden		
	Western	Middle	Eastern	Western	Middle	Eastern
Surface Elevation (m)	158.13	157.98	158.06	155.86	155.66	155.72
Soil Depth (m)	0.76	0.61	0.69	0.81	0.61	0.67
Surface Area (m^2)	61.67	85.71	207.14	182.14	98.00	20.97
Easting Length (m)	9.17	8.24	33.57	28.29	21.18	9.06

Figure 3 shows the model representation of the system. To better represent the moisture distribution in the upper unsaturated soil layer, each soil column was discretized into 5 horizontal layers.

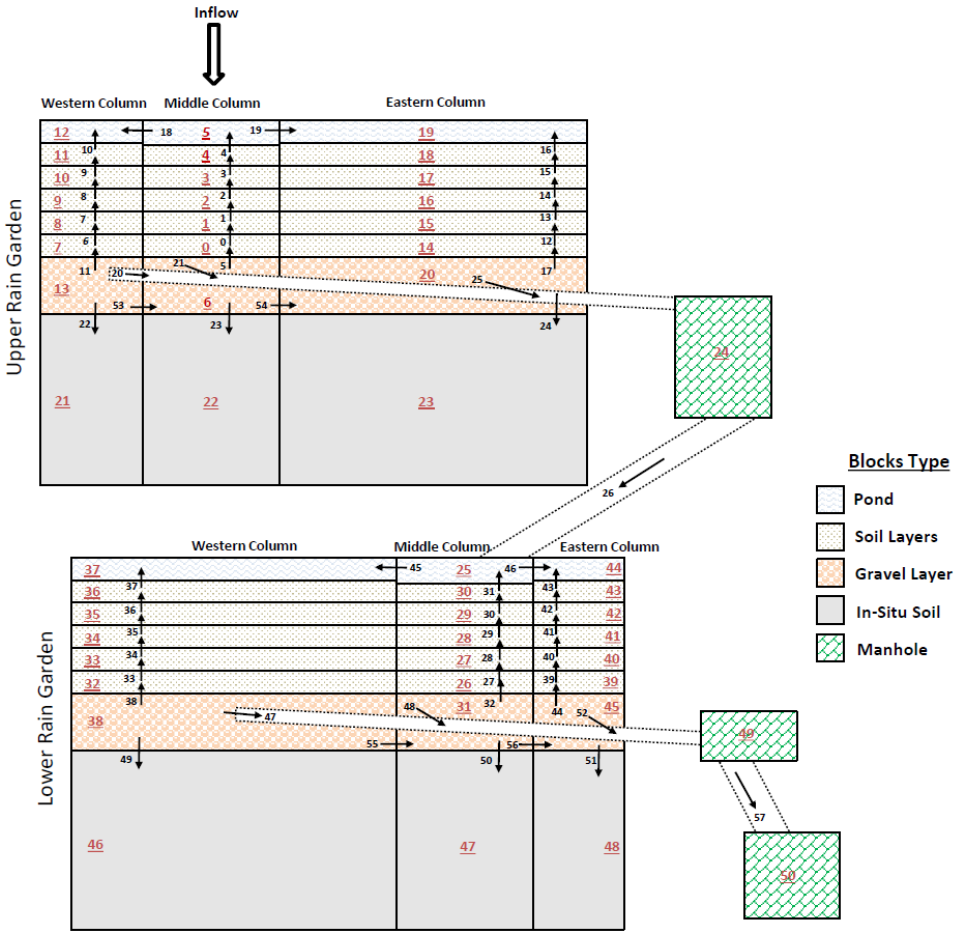

Figure 3. Block-Connector Model for the St. Francis Apartment Rain Gardens.

Based on this simplified surface topography, the inflow enters to the middle column of the upper rain garden while precipitation and evapotranspiration are assumed at the surface for all the pond blocks (blocks 5, 12, 19, 25, 37, 44). The drainage pipe at the gravel layer collects the excess water from all three aggregate layers and discharges it to the manhole block (block 24). The manhole discharges excess water to the pond block of the middle column (block 25) in the lower rain garden.

The proper definition of the connectors and their governing equations are critical since they control the water transport in the system. In the set-up chosen here, the pond to pond connectors

(connectors 18, 19, 45, 46) were based on diffusive wave equation with a Manning coefficient of 0.035. This value is consistent with calibrated values for a vegetated surface according to Krebs et al. (2014). However, it should be pointed out that due to the fact that the travel time from surface pond to surface pond is substantially smaller than the time-scale of simulation, this value has little effect on the final outcome. The connectors between soil layer blocks were based on the van-Genuchten relationship (van-Genuchten 1980) for the soil-water characteristics with the typical parameters of K=3m/d, θ_r=0.10, θ_s=0.35, α=3.0m^{-1}, n=2.94, and λ=0.5. The flow between the gravel layer blocks (connectors 53, 54, 55, 56) were based on Darcy equation with K=50 m/d which results in quick horizontal equilibrium between the three aggregate blocks. The hydraulic conductivity of the native soil was obtained as K=0.0045 m/d by calibration. The flow rate in pipe connectors (20, 21, 25, 26 47, 48, 52, 57) were based on Hazen-Williams equation (ref??) with PVC roughness coefficient of 150.

Model Results

The modeling was conducted over the period of March 27 to June 30, 2014. The comparison of the outflows from the upper (i.e. connector 26) and lower (i.e. connector 57) rain gardens with the observations are displayed in Figure 4. The model response to the stormwater outflows follows the observed trend. However, the model underestimates the highest outflow peak of 4/3/14 which is attributed to the contribution of runoff from the grassed slopes during that long and intense storm which was represented in the model.

The model predictions are better for the upper rain garden with a coefficient of determination R^2=0.86 and Nash- Sutcliffe efficiency coefficient NSE=0.83 than the lower rain garden with R^2=0.51 and NSE=0.49. This is attributed to the fact that the uncertainty in the model predictions for the lower rain garden is influenced by the model uncertainty from the upper rain garden in

addition to the modeling uncertainty for the lower rain garden system. A rigorous calibration and validation using another portion of the dataset is needed to obtain more reliable calibrated parameters; however, this is beyond the scope of this model application demonstration.

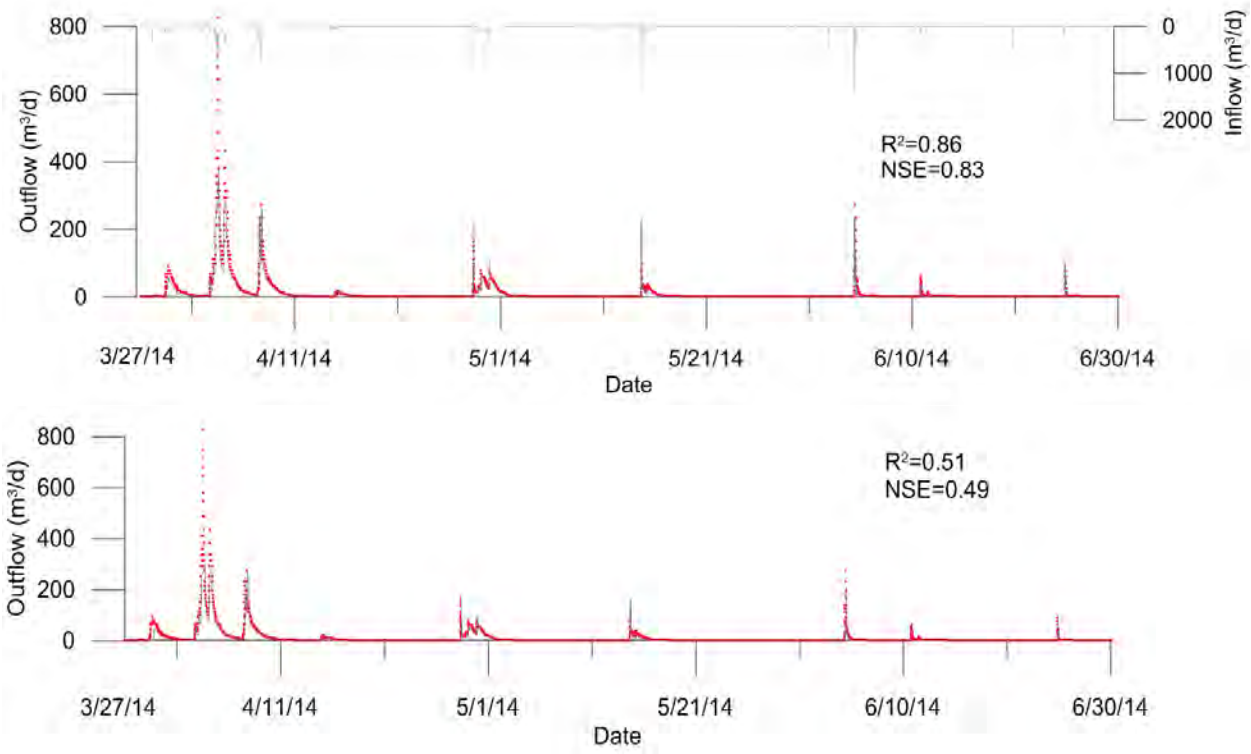

Figure 4. Comparison of the predicted outflow from the upper rain garden (top) and from the lower rain garden (bottom) with the observations.

Tables:

Table 1: Six default media types implemented in the model and the H-S equations. In the equations h [L] is the hydraulic head, S [L^3] is the storage, A_s [L^2] is the surface/bottom area, ε and n_s are matric suction parameters for storage blocks under near dry condition (Brooks and Corey, 1964), $s_e = (\theta - \theta_r)/(\theta_s - \theta_r)$ is the effective saturation , n is the Van Genuchten soil retention parameter, S_s [1/L] is specific storage, z_0 is the bottom elevation, h_0 is the top elevation of the block, $H()$ is the Heaviside function and $pos(x) = H(x)x$.

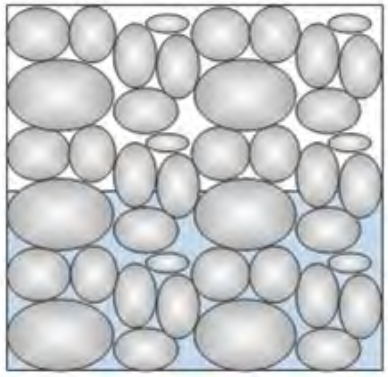 Storage $h = \frac{S}{A_s \theta_s} - \frac{\varepsilon}{s_e^{n_s}}$	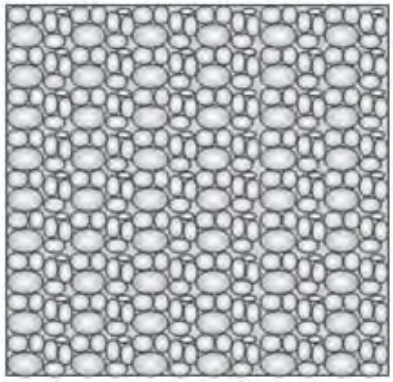 Saturated soil/Darcy $h = h_0 + \frac{\theta - \theta_s}{S_s}$	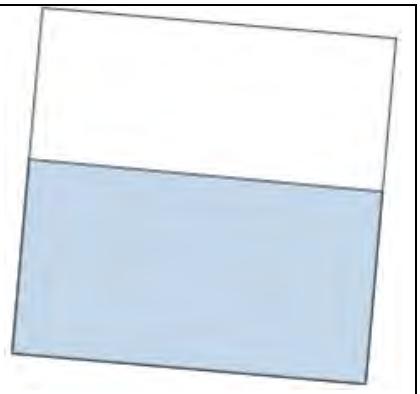 Pond $h = z_0 + \frac{S}{A_s}$
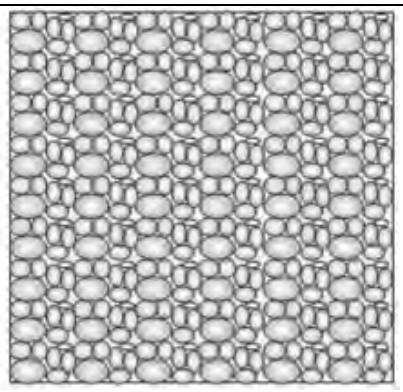 Unsaturated Soil $h = z_0 - \frac{H(\theta_s - \theta)}{\alpha}\left(s_e^{n/(1-n)} - 1\right)^{1/n} + \frac{pos(\theta - \theta_s)}{S_s}$	 Stream segment $h = z_0 + \frac{S}{A_s}$	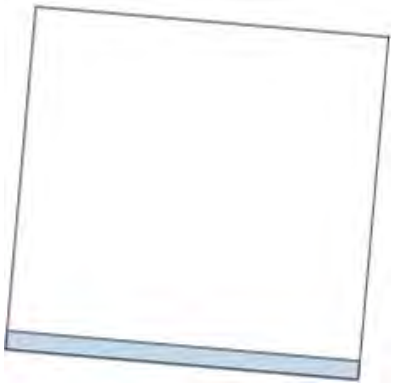 Overland flow $h = z_0 + \frac{S}{A_s}$

Table 2: Default Q-H equations for interfaces between different or similar media. i **and** j **are indicators for the blocks being connected,** A **[L²] is the cross-sectional area of the interface,** K_s **[L/T] is the saturated hydraulic conductivity** m **and** λ **are Van Genuchten soil retention parameters,** d **is the presumed length of the interface or the distance between the centerfolds of the blocks being connected,** $y = h - z_0$ **[L] is the water depth,** W **[L] is the width of the interface,** n_m **is Manning's roughness coefficient .**

j\i	Soil	Pond	Storage	Catchment	Darcy	Stream
Soil	$AK_s s_e^{\lambda}\left[1-\left(1-s_e^{1/m}\right)^m\right]^2$	$\frac{2AK_s s_e^{\lambda}\left[1-\left(1-s_e^{1/m}\right)^m\right]^2}{d}\frac{h_i-h_j}{d}$	$\frac{2AK_s s_e^{\lambda}\left[1-\left(1-s_e^{1/m}\right)^m\right]^2}{d}$ $\times\frac{pos\left[h_i-h_j\right]}{d}$ $z_{0,i} > z_{0,j}$	User-defined	$2AK_s s_e^{\lambda}\left[1-\left(1-s_e^{1/m}\right)^m\right]^2\frac{h_i-h_j}{d}$	User-defined
Pond	$2AK_s s_e^{\lambda}\left[1-\left(1-s_e^{1/m}\right)^m\right]^2$	$\frac{W}{n_m}\sqrt{\frac{h_i-h_j}{d}}\left(\frac{y_i+y_j}{2}\right)^{5/3}$	$K_s\frac{h_i-h_j}{d}$	$\frac{W}{n_m}\left[\sqrt{\frac{pos(h_i-h_j)}{d}}(y_i)^{5/3}\right.$ $\left.-\sqrt{\frac{pos(h_j-h_i)}{d}}(y_j)^{5/3}\right]$	$2AK_s\frac{h_i-h_j}{d}$	$\frac{W}{n_m}\left[\sqrt{\frac{pos(h_i-h_j)}{d}}\left(\frac{y_i+y_j}{2}\right)^{5/3}\right.$ $\left.-\sqrt{\frac{pos(h_j-h_i)}{d}}\left(\frac{y_i+y_j}{2}\right)^{5/3}\right]$
Storage	$2AK_s s_e^{\lambda}\left[1-\left(1-s_e^{1/m}\right)^m\right]^2$ $\times\frac{pos\left[h_i-\max\left(z_i,h_j\right)\right]}{d}$ $z_{0,i} > z_{0,j}$	$K_s\frac{h_i-h_j}{d}$	$\begin{cases}K_s\frac{h_i-h_j}{d} & horizontal\\ K_s\frac{h_i-z_i}{d} & vertical\end{cases}$	$-\frac{W}{n_m}\sqrt{\frac{pos(h_j-z_j)}{d}}(y_j)^{5/3}$	$\begin{cases}K_s W\frac{h_i+h_j}{2}\frac{h_j-h_i}{d} & horizontal\\ K_s A\frac{h_i-h_j}{d} & vertical\end{cases}$	User-defined
Catchment	User-defined	$\frac{W}{n_m}\left[\sqrt{\frac{pos(h_i-h_j)}{d}}(y_i)^{5/3}\right.$ $\left.-\sqrt{\frac{pos(h_j-h_i)}{d}}(y_j)^{5/3}\right]$	$\frac{W}{n_m}\sqrt{\frac{pos(h_j-z_j)}{d}}(y_j)^{5/3}$	$\frac{W}{n_m}\left[\sqrt{\frac{pos(h_i-h_j)}{d}}(y_i)^{5/3}\right.$ $\left.-\sqrt{\frac{pos(h_j-h_i)}{d}}(y_j)^{5/3}\right]$	User-defined	$\frac{W}{n_m}\left[\sqrt{\frac{pos(h_i-h_j)}{d}}(y_i)^{5/3}\right.$ $\left.-\sqrt{\frac{pos(h_j-h_i)}{d}}(y_j)^{5/3}\right]$
Darcy	$2AK_s s_e^{\lambda}\left[1-\left(1-s_e^{1/m}\right)^m\right]^2$	$\frac{2AK_s}{d}\frac{h_i-h_j}{d}$	$\begin{cases}K_s A\frac{pos(h_i-h_j)}{d} & horizontal\\ K_s A\frac{h_i-h_j}{d} & vertical\end{cases}$	User-defined	$AK_s\frac{h_i-h_j}{d}$	$AK_s\frac{h_i-h_j}{d}$
Stream	User-defined	$\frac{W}{n_m}\left[\sqrt{\frac{pos(h_i-h_j)}{d}}\left(\frac{y_i+y_j}{2}\right)^{5/3}\right.$ $\left.-\sqrt{\frac{pos(h_j-h_i)}{d}}\left(\frac{y_i+y_j}{2}\right)^{5/3}\right]$	User-defined	$\frac{W}{n_m}\left[\sqrt{\frac{pos(h_i-h_j)}{d}}(y_i)^{5/3}\right.$ $\left.-\sqrt{\frac{pos(h_j-h_i)}{d}}(y_j)^{5/3}\right]$	User-defined	$\frac{W}{n_m}\left[\sqrt{\frac{pos(h_i-h_j)}{d}}-\sqrt{\frac{pos(h_j-h_i)}{d}}\right]$ $\times\left(\frac{y_i+y_j}{2}\right)^{5/3}$

References

Ahiablame, L. M., Engel, B. A., and Chaubey, I. (2013). "Effectiveness of low impact development practices in two urbanized watersheds: Retrofitting with rain barrel/cistern and porous pavement." *Journal of environmental management*, 119, 151-161.

Berndtsson, J. C. (2010). "Green roof performance towards management of runoff water quantity and quality: A review." *Ecological Engineering*, 36(4), 351-360.

Brown, R., Skaggs, R. W., and Hunt, W. (2013). "Calibration and validation of DRAINMOD to model bioretention hydrology." *Journal of Hydrology*, 486, 430-442.

Chow, V., Maidment, D., and Mays, L. (2013). *Applied Hydrology, 2nd Edition*, McGraw-Hill Companies,Incorporated.

Dickson, D. W., Chadwick, C. B., and Arnold, C. L. (2011). "National LID Atlas: A collaborative online database of innovative stormwater management practices." *Marine Technology Society Journal*, 45(2), 59-64.

Dussaillant, A., Cuevas, A., and Potter, K. (2005). "Raingardens for stormwater infiltration and focused groundwater recharge: Simulations for different world climates." *Water Science and Technology: Water Supply*, 5(3-4), 173-179.

Dussaillant, A. R., Wu, C. H., and Potter, K. W. (2004). "Richards equation model of a rain garden." *Journal of Hydrologic Engineering*, 9(3), 219-225.

Elliott, A., and Trowsdale, S. (2007). "A review of models for low impact urban stormwater drainage." *Environmental modelling & software*, 22(3), 394-405.

He, Z., and Davis, A. P. (2010). "Process modeling of storm-water flow in a bioretention cell." *Journal of Irrigation and Drainage Engineering*, 137(3), 121-131.

Hilten, R. N., Lawrence, T. M., and Tollner, E. W. (2008). "Modeling stormwater runoff from green roofs with HYDRUS-1D." *Journal of Hydrology*, 358(3), 288-293.

Lee, J. G., Borst, M., Brown, R. A., Rossman, L., and Simon, M. A. (2014). "Modeling the hydrologic processes of a permeable pavement system." *Journal of Hydrologic Engineering*, 20(5), 04014070.

Li, Y., and Babcock Jr, R. W. (2014). "Green roof hydrologic performance and modeling: a review." *Water Science & Technology*, 69(4).

Liu, J., Lucas, W., Chan, I., She, N., and Wu, L. "Innovative Design of the LID Facilities of Congdu Ecological Grange." *Proc., International Low Impact Development Conference 2015@ sLID: It Works in All Climates and Soils*, ASCE, 331-341.

Liu, J., Sample, D. J., Bell, C., and Guan, Y. (2014). "Review and research needs of bioretention used for the treatment of urban stormwater." *Water*, 6(4), 1069-1099.

Massoudieh, A., and Ginn, T. R. (2008). "Modeling colloid-enhanced contaminant transport in stormwater infiltration basin best management practices." *Vadose Zone Journal*, 7(4), 1261-1268.

Massoudieh, A., and Ginn, T. R. (2010). "Colloid-facilitated contaminant transport in unsaturated porous media." *Modelling of pollutants in complex environmental systems*, 2, 263-292.

Meng, Y., Wang, H., Chen, J., and Zhang, S. (2014). "Modelling Hydrology of a Single Bioretention System with HYDRUS-1D." *The Scientific World Journal*, 2014.

Page, J., Winston, R., and Hunt III, W. F. "Stormwater monitoring of innovative street retrofits in urban Wilmington, NC." *Proc., World Environmental and Water Resources Congress 2012: Crossing Boundaries*.

Palhegyi, G. E. (2009). "Modeling and sizing bioretention using flow duration control." *Journal of Hydrologic Engineering*, 15(6), 417-425.

Qin, H.-p., Li, Z.-x., and Fu, G. (2013). "The effects of low impact development on urban flooding under different rainfall characteristics." *Journal of environmental management*, 129, 577-585.

Russell, D. L. (2006). *Practical Wastewater Treatment*, Wiley.

Šimůnek, J., van Genuchten, M. T., and Šejna, M. (2008). "Development and applications of the HYDRUS and STANMOD software packages and related codes." *Vadose Zone Journal*, 7(2), 587-600.

Does hydraulic fracturing pose a threat to DC™s water supply? A field and modeling study.

Basic Information

Title:	Does hydraulic fracturing pose a threat to DC™s water supply? A field and modeling study.
Project Number:	2015DC169B
Start Date:	3/1/2015
End Date:	2/28/2016
Funding Source:	104B
Congressional District:	District of Columbia
Research Category:	Water Quality
Focus Category:	Hydrogeochemistry, Water Quality, Water Supply
Descriptors:	None
Principal Investigators:	Karen Knee

Publications

1. This work has been presented at the NCR Water Resources Symposium at UDC on April 8, 2016. The graduate student in charge of the project, Colin Casey, has also had abstracts accepted at the Association for Environmental Studies and Sciences meeting (Washington, DC, June 8-11, 2016) and the 6th International Radium-Radon Workshop (Girona, Spain, July 17-21, 2016).
2. This work has been presented at the NCR Water Resources Symposium at UDC on April 8, 2016. The graduate student in charge of the project, Colin Casey, has also had abstracts accepted at the Association for Environmental Studies and Sciences meeting (Washington, DC, June 8-11, 2016) and the 6th International Radium-Radon Workshop (Girona, Spain, July 17-21, 2016).

Cover Page

Does hydraulic fracturing pose a threat to DC's water supply?

Progress Report

Dr. Karen L. Knee, Principal Investigator

Department of Environmental Science, American University

April 22, 2016

1. Executive Summary

The goal of this project was to assess how hydraulic fracturing ("fracking") could affect dissolved metal concentrations and other water quality parameters in Washington, DC's water source, the Potomac River. The fracking process involves injecting fluids into shale plays in order to fracture them and release the oil and gas trapped within. Shale plays may contain higher levels of heavy metals and naturally occurring radioactive elements than rocks at the surface that are normally in contact with surface and groundwater. Additionally, fracking fluids may be re-used many times and become very saline, increasing the solubility and mobility of some elements. A significant fraction of the fluid used in fracking returns to the surface to be recycled, stored, or disposed of. This is known as flowback water or produced water. If it comes in contact with aquifers, streams or rivers, it could contaminate these water bodies. Although anecdotal evidence of surface and groundwater pollution exists and a few studies have documented specific impacts on surface or groundwater, the potential threat that fracking may pose to the water sources of major metropolitan areas – including DC – had not been investigated scientifically.

The present study addressed this important data gap through a combined field and modeling approach. Field work was conducted in summer 2015. We sampled 73 stream sites in parts of the Potomac watershed that overlie the Marcellus shale in the states of Virginia, West Virginia and Maryland. Maryland currently has a moratorium on fracking, and although the state of Virginia permits fracking, it has not been initiated in that part of the state. Thus, Maryland and Virginia served as "controls" while West Virginia was the "fracking" group. We measured concentrations of dissolved metals, the naturally occurring radioactive elements radium and radon, and ancillary water quality parameters (dissolved oxygen, turbidity, pH, specific conductance, temperature). We also measured the stream discharge at every sampling site.

Fracking sites had significantly higher concentrations of strontium, a metal that has been associated with fracking in previous studies, as well as one isotope of radium, ^{224}Ra. No other significant differences between the fracking and control groups were observed. We are currently working on investigating whether the vulnerability of small watershed units to fracking (as quantified by Entrekin et al., 2015) is related to any of the measured water quality parameters. The Entrekin et al. paper provides a much more sophisticated way of quantifying fracking impact than simply looking at the density of well permits upstream of each site, as we had initially planned to do. Additionally, using internal funding, we are planning one follow-up sampling trip to West Virginia this summer to sample about 20 additional sites with high levels of vulnerability to fracking.

The final component of the project, which is still ongoing, will be to use the results of field and lab analysis, combined Entrekin et al. (2015)'s modeling framework and freely available hydrologic data, to construct a simple model of how fracking in the Potomac's watershed may influence pollutant concentrations and loadings at Great Falls, where the District of Columbia obtains its drinking water. Once this step is completed, I will provide a follow-up report to DCWRRI and relevant DC authorities.

2. Introduction

The District of Columbia's water source is the Potomac River. Much of the Potomac's watershed overlies the Marcellus Shale, an unconventional natural gas play that can be exploited by hydraulic fracturing ("fracking"). Little conclusive evidence about the impact of fracking on surface water quality exists. However, a few studies (Entrekin et al. 2011, Vidic et al. 2013, Warner et al. 2013) and a small pilot project that I conducted during summer 2013 suggested that fracking activity within a watershed may be associated with elevated conductivity and dissolved metal concentrations in stream water. The goal of this study was to assess whether fracking activity upstream in the Potomac watershed could affect the quality of DC's water source in terms of conductivity, dissolved metals and dissolved radium. This is a critical problem because high levels of these pollutants could be associated with increased water treatment costs and/or health impacts for DC residents, as well as impacts on aquatic life in the Potomac and in Chesapeake Bay.

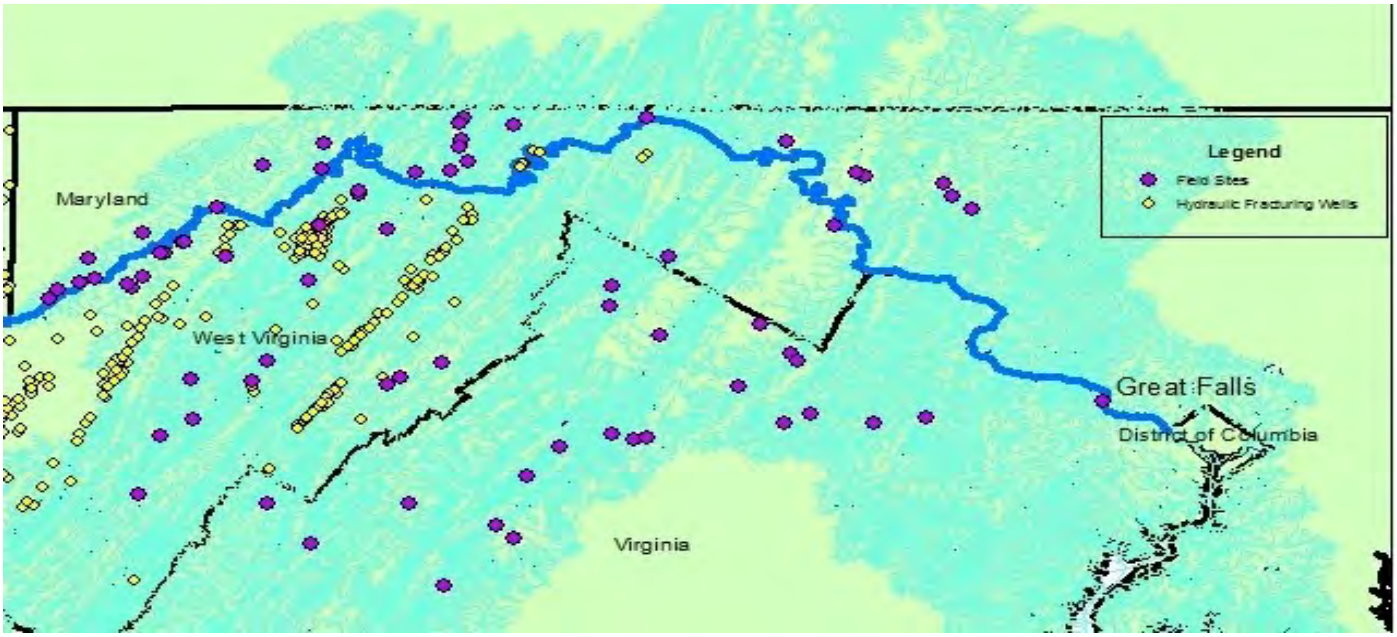

Figure 1: Potomac River watershed (cyan) with the locations of unconventional natural gas permits shown with yellow dots and the locations of stream sites sampled in this study shown with purple dots. State/district boundaries are indicated with black lines and the main stem of the Potomac River is indicated with a bold blue line.

The specific objectives of this research were: (1) to measure selected aspects of water quality, including conductivity, dissolved metal and radium concentrations, in tributaries of the Potomac River overlying the Marcellus Shale, (2) to determine whether water quality in Potomac tributaries ***with*** fracking activity occurring in the watershed differs significantly from that in comparable tributaries ***without*** fracking activity, (3) to assess whether there is a relationship between watershed exposure or vulnerability to fracking and stream water quality, (4) to model the fate and transport of pollutants related to

fracking as they travel downstream in the Potomac River system, and (5) to provide data and recommendations to DC Water regarding the potential threat of fracking to the quality of DC's water supply.

3. Methodologies

Field Work: This component of the project took place during three 5-day sampling trips during summer 2015. A total of 73 stream sites on tributaries of the Potomac River that overlie the Marcellus Shale in Virginia, West Virginia, and Maryland were sampled. At each site, a YSI Professional Plus multiparameter instrument was used to measure temperature, dissolved oxygen, total dissolved solids, and pH and a Hanna portable turbidimeter to measure turbidity. The location of each stream sampling site was determined using a hand-held Garmin GPS. Stream discharge was measured using the standard velocity-area method, with a USGS Pygmy Meter used to measure the water velocity. It was important to measure the stream discharge because it can be used to convert pollutant concentrations to loadings, which are more relevant to the impact on DC's water supply. Samples for radon, radium, nutrient, and dissolved metal analysis were collected in the field for later analysis. Radon samples were collected in 2-L bottles and analyzed within one week on a RAD-7 radon detector with the Big Bottle grab sample accessory (Durridge Co., Billerica, MA, USA). Large-volume (100-L) water samples for radium analysis were collected with a submersible pump and 20-L collapsible water carriers and filtered through a plastic column containing manganese-coated acrylic fiber following the procedure described by Knee et al. (2010) to quantitatively extract the radium. Samples for nutrient (nitrate, nitrite, phosphate, silicate and ammonium) analysis were syringe-filtered in the field with a 0.2 μm filter and frozen until analysis. Filtering and freezing the samples ensures that any particles that could leach nutrients into the water are removed and prevents biological activity from altering nutrient concentrations. Samples for dissolved metal analysis were filtered in the field with a 0.2 μm filter and acidified to pH 2 with trace metal clean nitric acid. Additionally, a sample of sediment from the stream bottom was collected in a Ziploc bag at each site because previous work (Warner et al. 2013) had suggested that Ra from fracking pollution might be more likely to be present in sediments rather than in the water.

Laboratory methods: Activities of ^{223}Ra and ^{224}Ra were measured using a Radium Delayed Coincidence Counter (RaDeCC system). ^{226}Ra activities are currently being measured using a RAD7 radon detector and the procedure described by Dimova et al (2007). Nitrate and phosphate concentrations have been measured using standard colorimetric methods on an EasyChem discrete analyzer (Systea Scientific, Oak Brook, IL, USA), and ammonium analysis is ongoing. Dissolved metal concentrations have been measured on an inductively coupled plasma – optical emission spectrometer (ICP-OES) at American University. Sediment samples were transported to Dr. Natasha Dimova's lab at the University of Alabama, Tuscaloosa, for ^{226}Ra analysis on a gamma counter. This analysis is ongoing.

Geographic and statistical analysis: I had intended to perform geographic analysis roughly assessing the fracking impact in all West Virginia watersheds for this project, but

recently a paper (Entrekin et al. 2015) was published, detailing a more sophisticated modeling framework for quantifying watershed vulnerability to fracking at the hydrologic unit code 12 (HUC-12) level. A HUC-12 is a subwatershed unit, with an average area of about 100 km^2. The vulnerability index developed by Entrekin et al. (2015) was based on exposure (how much fracking was occurring in the subwatershed) and sensitivity (how different subwatershed characteristics, such as slope, stream density, and land use, would modulate the impact of fracking on water quality). I am currently in the process of overlaying the water quality data we collected with the HUC-12 vulnerability data provided by Sally Entrekin and Kelly Maloney. HUC-12 charcteristics will be matched up with the sampling sites they contain using ArcGIS, and potential correlations will be investigated.

We assessed whether there were significant differences between samples from fracking (West Virginia) and control (Virginia and Maryland) streams using the Kruskal-Wallis non-parametric test with a significance criterion of $p<0.05$. We are currently working on assessing whether a significant positive correlation exists between the vulnerability score of the HUC-12 and any of the water quality parameters measured. Microsoft Excel and/or R are being used for statistical analysis.

4. Results and Discussion

Seventy-three stream sites (23 in Virginia, 25 in West Virginia, and 25 in Maryland) were sampled in summer 2015 (Fig. 2). In terms of radium and radon, ^{224}Ra activities were significantly higher in West Virginia (fracking) streams compared to Maryland and Virginia (control) streams, but no significant difference was observed for ^{223}Ra, ^{228}Th (the parent isotope of ^{224}Ra) or Rn. Measurements of long-lived Ra isotopes (^{226}Ra and ^{228}Ra) in stream water and ^{226}Ra in sediment samples collected from the stream bottom are ongoing.

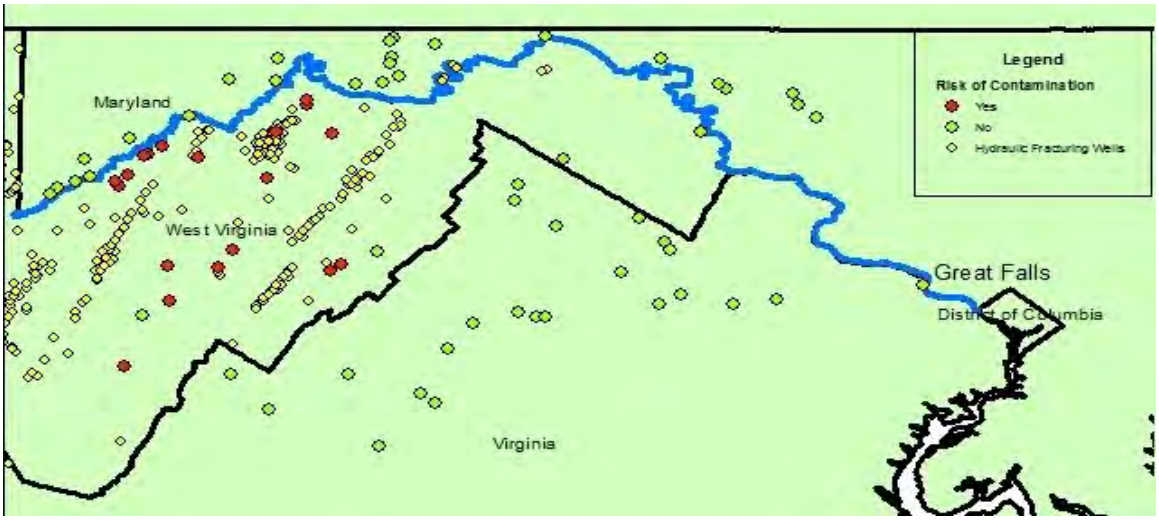

Fig. 2. Map indicating the location of permitted hydraulic fracturing wells, sampling sites downstream of hydraulic fracturing wells (red) and sampling sites with no current risk of hydraulic fracturing contamination (green) in Maryland, Virginia and West Virginia.

Parameter	No Hydraulic Fracturing (± standard error)	Hydraulic Fracturing (± standard error)
^{223}Radium (dpm/100L)	**0.23** (± 0.04)	**0.17** (± 0.06)
^{224}Radium (dpm/100L)	**8.6** (± 1.3)	**14** (± 3)
^{228}Thorium (dpm/100L)	**1.4** (± 0.2)	**1.6** (± 0.4)
Radon (Bq/m^3)	**900** (± 300)	**700** (± 200)

Table 1: Mean and standard error of radioisotope activities measured in streams in Maryland and Virginia (no hydraulic fracturing) and West Virginia (hydraulic fracturing).

Based on pilot data comparing dissolved metal data from streams in southwestern Pennsylvania (where a high degree of fracking activity exists) and western Maryland (where no fracking is occurring) I hypothesized that dissolved metal concentrations would be significantly higher in West Virginia than in Maryland and Virginia. However, this was generally not the case. Aluminum, arsenic, barium, calcium, chromium, iron, potassium, magnesium, manganese, sodium and strontium were measured on the ICP-OES. Of these, six metals (barium, iron, potassium, manganese, sodium and strontium) had field blank concentrations similar to the analytical blank, good calibration curves, and concentrations well above the method detection limit for at least some samples. The data for these metals is summarized in Table 2.

	Concentration (mg/L)	
Metal	**No Hydraulic Fracturing**	**Hydraulic Fracturing Present**
	(± standard error)	**(± standard error)**
Barium	**0.06** (±0.02)	**0.05** (± 0.00)
Iron	**0.02** (± 0.01)	**0.01** (± 0.01)
Potassium	**2.1** (± 0.2)	**2.7** (± 0.3)
Manganese	**0.10** (± 0.06)	**0.9** (± 0.9)
Sodium	**7.7** (± 1.0)	**5.5** (± 0.9)
Strontium	**0.21** (± 0.02)	**0.31** (± 0.07)

Table 2: Mean and standard error of dissolved metal concentrations measured in streams in Maryland and Virginia (no hydraulic fracturing) and West Virginia (hydraulic fracturing).

In general, dissolved metal concentrations in streams were similar between fracking and non-fracking sites. The only metal that was significantly higher in fracking compared to non-fracking streams was strontium, and even then the difference was not that large. No metals were significantly higher in non-fracking streams. The only one of these metals for which the EPA sets an aquatic life criterion is iron. The criterion is 1000 μg/L (1 mg/L), which is 50-100 times higher than the concentrations we measured in these streams. Thus, it appears that the streams we measured are healthy in terms of dissolved metal concentrations, and we did not find any evidence that hydraulic fracturing is leading to unhealthy conditions in terms of dissolved metals in this area.

Other water quality parameters measured were also similar among the three states and did not appear to be affected by fracking. We had hypothesized that specific conductance and

turbidity, which are measures of dissolved and suspended solids, respectively, would be higher in West Virginia (fracking) compared to Maryland and Virginia (control); however, this was not the case. With the exception of dissolved oxygen, which was signigicantly lower in West Virginia than in the two other states (Table 3), there were no significant differences observed in any of the water quality paramters. We are not sure why dissolved oxygen was so much lower in West Virginia than in the other two states, but we do not feel that it is necessarily due to fracking.

Parameter	Virginia	Maryland	West Virginia
Dissolved Oxygen (%)	81	87	45
Dissolved Oxygen (mg/L)	7.0	7.8	3.8
Specific Conductance (µS/cm)	281.6	482.8	396.4
Conductivity (µS/cm)	266.6	423.6	374.5
pH	7.95	7.90	7.76
Turbidity (NTU)	7.63	10.56	6.47
Nitrate (ppm)	0.69	0.58	0.65

Table 3: Summary of means for other water quality parameters in Virginia, Maryland and West Virginia streams.

The field work described in the initial proposal has been completed. However, we were able to obtain internal funding to conduct one additional field sampling trip, focusing on the sites with the highest level of vulnerability to fracking within the Potomac watershed. These sites are located near the towns of Romney and Keyser, WV. Having more sites at the highest end of the impact spectrum will provide greater statistical power for the study. We are also continuing to work on the geographic analysis, using the vulnerability indices developed by Entrekin et al. (2015).

5. Project outcomes, presentations, publications (book chapter journals or conference proceedings)

This work has been presented at the NCR Water Resources Symposium at UDC on April 8, 2016. The graduate student in charge of the project, Colin Casey, has also had abstracts accepted at the Association for Environmental Studies and Sciences meeting (Washington, DC, June 8-11, 2016) and the 6th International Radium-Radon Workshop (Girona, Spain, July 17-21, 2016).

The research supported by this grant will form the main component of Colin Casey's masters thesis, which will be completed in spring semester, 2017. Additionally, I plan to write one or more manuscripts for submission to scientific journals based on the results. I anticipate submitting the first of these articles by May 2017.

6. Student supports

Colin Casey, a master's student in Environmental Science, has been supported by this grant, and the research described in this report comprises the bulk of his thesis research (although the analysis and writing are ongoing). In addition to Colin, the following students participated in field and lab work for this project and benefited by the training

opportunities provided: Jessica Balerna (undergraduate environmental science major at AU), Gabriel Santos (undergraduate exchange student from Brazil), John Doherty (masters student in environmental science at AU), Charlotte Hovland (undergraduate student at University of Chicago), and Preston Pisano (undergraduate student in environmental science at AU).

7. Extramural funding

I have not received any extramural funding for this project, but I am currently in the process of preparing an NSF CAREER proposal focused on the topic of fracking and water quality, using the research described here as preliminary results.

8. Conclusion

This project investigated differences in stream water quality between areas with and without fracking in parts of the Potomac watershed overlying the Marcellus shale. In general, few significant differences were observed, although concentrations of ^{224}Ra and Sr were higher in fracking areas compared to non-fracking areas. No evidence of serious contamination that would impact the health of humans or aquatic life was observed. Geographic analysis linking water quality parameters to the vulnerability index of each subwatershed is ongoing.

9. Acknowledgements

I thank the DC Water Resources Research Institute and American University (through matching funds and a competitive Faculty Research Support Grant) for funding this project. Sally Entrekin and Kelly Maloney generously shared the source data from their 2015 manuscript, allowing us to use it for our geographic analysis. Thank you also to Jessica Balerna, Gabriel Santos, John Doherty, Charlotte Hovland and Preston Pisano for their invaluable assistance in the field and lab.

10. References

Dimova, N., W.C. Burnett, E.P. Horwitz and D. Lane-Smith. 2007. Automated measurement of ^{224}Ra and ^{226}Ra in water. Applied Radiation and Isotopes 65: 428-434.

Entrekin, S.A. , M.A. Evans-White, B. Johnson, and E. Hagenbuch. 2011. Rapid expansion of natural gas development poses a threat to surface waters. Frontiers in Ecology and the Environment 9: 503-511.

Entrekin, S.A., K.O. Maloney, K.E. Kapo, A.W. Walters, M.A. Evans-White, and K.M. Klemow. 2015. Stream vulnerability to widespread and emergent stressors: A focus on unconventional oil and gas. PLoS ONE 10(9): e0137416

Knee, K.L., J.H. Street, E.E. Grossman, A.B. Boehm, and A. Paytan. 2010. Nutrient inputs to the coastal ocean from submarine groundwater discharge in a groundwater-dominated system: Relation to land use (Kona Coast, Hawai`i, USA). Limnology and Oceanography 55: 1105-1122.

Vidic, R.D., S.L. Brantley, J.M. Vandenbossche, D. Yoxtheimer, and J.D. Abad. 2013. Impact of shale gas development on regional water quality. Science 340: 1235009

Warner, N.R., C.A. Christie, R.B. Jackson, and A. Vengosh. 2013. Impacts of shale gas wastewater disposal on water quality in Western Pennsylvania. Environmental Science and Technology 47: 11849-11857.

Evaluation of figreen rooffl effectiveness for nitrogen, phosphorus and suspended solid reduction in runoff from precipitation events

Basic Information

Title:	Evaluation of figreen rooffl effectiveness for nitrogen, phosphorus and suspended solid reduction in runoff from precipitation events
Project Number:	2015DC170B
Start Date:	3/1/2015
End Date:	2/28/2016
Funding Source:	104B
Congressional District:	District of Columbia
Research Category:	Water Quality
Focus Category:	Sediments, Non Point Pollution, Nutrients
Descriptors:	None
Principal Investigators:	Stephen E. MacAvoy

Publications

1. MacAvoy SE, Ewers E, Bushaw-Newton K. (2009). Nutrients, oxygen dynamics, stable isotopes and fatty acid concentrations of a freshwater tidal system, Washington, D.C. Journal of Environmental Monitoring 11:1622-1629
2. Connor NC, Sarraino S, Frantz D, Bushaw-Newton K, MacAvoy SE. (2014). Geochemical characteristics of an urban river: influences of an anthropogenic landscape. Applied Geochemistry 47:209-216.
3. MacAvoy, SE and E Petersen. 2015. American Geophysical Union Annual Meeting, San Francisco, CA. Session Co-Chair and Co-Convener. Session B41B: Biogeochemistry of Rivers and Soils in the Urban Ecosystem and Their Climate Impacts Posters. "Geochemical Characteristics of an Urban River: Influences of an Urban Landscape" Poster Presentation
4. Connor, Nicholas P., Stephanie L. Sarraino, Deborah E. Frantz, Karen Bushaw-Newton, Stephen E. MacAvoy . 2013. American Geophysical Union, Annual Meeting, San Francisco CA. H31H-1282 "Geochemical characteristics of an urban river: Geochemical contamination and urban stream syndrome" Poster Presentation.
5. Sarraino, S.L, D.E. Frantz, K Bushaw-Newton and S.E. MacAvoy. 2011. American Geophysical Union, Annual Meeting. San Francisco CA. " Biogeochemical characteristics of a polluted urban stream (Anacostia River, Washington DC, USA): inorganic minerals, nutrients and allochthonous vs. autochthonous production" Poster Presentation.

DATE: March 10,2016
TO: WRRI Director Tolessa Deksissa
FROM: Professor Stephen MacAvoy
RE: Final Report: Evaluation of "green roof" effectiveness for nitrogen, phosphorus and suspended solid reduction in runoff from precipitation events.
AUTHORS: Sydney Mucha and Stephen E. MacAvoy

Abstract:

One of the challenges urban areas (including Washington DC) face is high storm water flow from resulting from impermeable surfaces. This often results in increased sedimentation, flooding, pollutant flux and combined sewage/storm water discharge to DC rivers. Green roofs are now being considered to reduce the storm flow from buildings, and the Washington DC government is even granting stormwater tax credits to businesses that incorporate water retention practices. An added benefit for having the roofs (in addition to water retention) may be the reduction of suspended solids and nutrients such as nitrogen (N) and phosphorus (P). The roofs support plants and bacteria that may retain excess nutrients and solids that would otherwise end up quickly traveling to waterways. In this report, the effectiveness of green roofs for limiting N, P, dissolved organic carbon (DOC) and suspended solids is evaluated. American University installed traditional green roofs (soil based) and Aqualok roofs (foam based) several years ago. These green roof types will be monitored for nutrient retention (or release) and compared to regular roofs. Collections were made during eight precipitation events. Based on the data gathered, green roofs of any type show higher TSS and phosphorus than rainwater. The planted and unplanted roofs are all better options than asphalt roofs with respect to phosphorous, though neither are better than the asphalt roof with respect to TSS. Planted roofs are a sink for both types of nitrogen, though the unplanted roof released more than the asphalt roof with respect to ammonium, but less with respect to NO_x. The traditional roof did not act as a sink for any of the

nutrients and released more than the asphalt roof with respect to all nutrients. As the planted roof only acted as a sink for half of the nutrients and as a source for the other half, it does not seem that green roofs are the end all solution to urban runoff, though they are better than current asphalt roofs according to these results.

Introduction

The United Nations Habitat Committee estimates that 70% of the world's population will live in urban areas by 2050. This worldwide trend will also be reflected close to home here in Washington DC. Increasingly growing cities are facing issues with the water quality of local streams that have been historically been ignored but are increasingly being seen as treasures that can enhance quality of life and city economies (Washington Post 2012). Urban areas are focusing on the quality of freshwater resources within the metropolitan areas. Included in these resources are streams or rivers within the city limits. Urban areas with increasingly low permeability surfaces also tend to have air pollution problems that are directly linked to polluted runoff following rain events. An additional problem urban areas have seen is the flash flood effects as runoff of impermeable surfaces flows directly to streams causing them to rise and fall very quickly ("pulse" effect). This can deliver a large dose of pollutants that had been accumulating on surfaces as well as strain infrastructure for holding wastewater. Indeed, in Washington DC there is a combined sewage and storm water infrastructure that mixes the two flows when the storm flow system is overwhelmed. This occurs on a regular basis (82 average events per year in 2008).

Washington DC has made a commitment to make the Anacostia swimmable by 2032 (Hawkins 2008). This will require a drastic reduction in nutrients and organics in the river

(reduce biological oxygen demand by 50 to 90%) and suspended sediments (by 86%) just to name two of the many challenges (Hawkins 2008).

One of the ways to reduce heavy runoff in urban areas has been to plan or develop "green roofs". These are either foam or engineered soil based planted surfaces capable of retaining and transpiring water. These roofs keep water from rushing into streets and streams, as well as retain sediment or pollutants that may have accumulated on surfaces.

The fact that green roofs retain water is well documented, however another added benefit maybe excess nutrient removal/sediment from rain and potential runoff. Nitrogen in rainwater is derived from internal combustion engines and is perhaps the most important nitrogen pollution source in cities (Galloway and Cowling 2002). Green roofs can potentially remove N by either using it for plant growth or by supporting bacteria which take up the N. For cities, such as DC, interest in reducing nitrogen pollution to rivers, by the possible removal of nitrogen by green roofs, would be a benefit in addition to the runoff mitigation. Suspended solids are another type of pollution common in urban streams and they are linked to decline in aquatic grass, fish and benthic fauna. In the Anacostia River, approximately 19,000,000 lbs of sediment is deposited every year. DC's goal is to reduce this number by 86% by 2032 (Hawkins 2008).

The objective of the project was to quantify the concentration of pollutants (N, P and suspended solids) in precipitation and runoff from regular roofs vs. the water that flows through green roofs. The volume of rainwater will be estimated from a precipitation gage. Then the total volume of rain falling on the green roof can be estimated as well as the pollution mitigation per liter of water (if it is observed). Then the amount of pollutants taken up by the green roof vs. regular roof can be estimated. Pollutants taken up by plants or bacteria in the green roofs will

effectively removing harmful material from entering local waterways and ultimately the Chesapeake Bay.

Methods.

Water was collected from 2 green roof sites located on American University's grounds (both in the Mary Graydon Center). The first site had water collected (three 500ml containers) from 4 types of surface or collector: Aqualok foam planted, traditional soil roof planted, untreated runoff and precipitation. The second site had water collected from Aqualok foam unplanted. Direct precipitation was collected using 1 cm interior diameter funnels attached to 3-liter amber glass containers, and there were three of these containers located side-by-side. The small 1cm funnels were use to limit evaporation and discourage insects from entering the container. Throughflow was collected in high-density polyethylene (HDPE) pans covered with 1 mm fiberglass screen that were placed directly beneath the Aqualok foam panels (planted and unplanted). Untreated roof runoff was collected in 1L HDPE containers from a downspout draining untreated roof. Water samples were collected by hand into 500 ml acid washed HDPE bottles through 1mm fiberglass mesh (total suspended solids collection protocol excluded large debris from collection (Eaton et al. 1998). All samples were placed on ice/cold packs in coolers for transport. Water samples were filtered onto glass fiber filters (45um GFF) for total suspended solids analysis (TSS) once they reached the lab, while sub-samples were sent to Cornell's Nutrient Analysis Lab for analysis of water nutrients (nitrate, ammonium). Methodology for nutrient and analysis was based on EPA requirements (Eaton et al. 1998). A Colorimetric Bran-Luebbe Automated Ion Analyzer was used for ammonium, and nitrate.

Since exact measurements for rainfall and conditions could not be monitored at each site, sample collection sites were extrapolated using the NOAA website (http://w2.weather.gov/climate/index.php?wfo=lwx). The conditions and rainfall amounts for each site were estimated to be approximately the same as Ronald Regan National Airport. After each rainfall event, details such as rainfall amount (in inches), average wind speed and humidity, high and low temperatures, and weather pattern conditions were gathered from the website and recorded along with the nutrient data.

Results:

Eight rain events were collected from the American University green roofs in the fall of 2014 and summer 2015. Three were from the fall and five from the summer (Tables 1 and 2). This allows for a seasonal comparison of the extensive green roofs. Seasonal averages were compared using averages of each season for the nutrient of interest and a Kruskal Wallis test was used to determine significance. Significance for all Kruskal Wallis tests was set at 0.05. TOC was not analyzed this way as it was only collected for the fall of 2014 due to funding issues. The performance of the roof during its respective season was also examined using Kruskal Wallis tests and seasonal averages. The performance of the extensive roofs were also examined overall by combining the data from the two seasons and using a Kruskal Wallis test and the Dunn procedure to determine significance. TOC performance was just analyzed using data from fall of 2014.

Fall 2014

TSS: There was a significant difference in the treatments with a p value of 0.013. The planted roof was extremely high with respect to solids, releasing over 200 mg/L (Table 1). None

of the treatments released less TSS than rainfall or the downspout runoff (Figure 1). The median value also showed the planted roof released the most and had more variability, followed by the unplanted roof and then the model (Figure 2).

TOC: Significance differences among treatments was also found for total organic carbon (TOC) ($p=0.010$). The median values showed that the planted roof releases the most, followed by the model, unplanted roof and the downspout (Figure 2). The average values also indicated a high amount of TOC released from the planted roof (64 mg/L) and the model (25.3 mg/L) (Table 1). The rainfall, downspout runoff and the unplanted roof means were very similar (Figure 1).

PO_4: The downspout and the model have large variations around their means, while rainfall and the unplanted roof do not (Figure 2). The highest average was found in the model, followed by the downspout runoff, the planted roof, rainfall and then the unplanted roof (Table 1 and Figure 1), however no significance was found in the Kruskal Wallis test (0.088).

Table 1. American University Rainfall, Downspout Runoff, Planted and Unplanted Green Roof Averages for Fall 2014. N=3 in all cases.

	TSS (mg/L)	**TOC (mg/L)**	**TP (mg/L)**	**NH_4 (mg/L)**	**NO_x (mg/L)**
Rainfall	1.00 ± 0.58	1.67 ± 0.05	0.06 ± 0.02	0.21 ± 0.05	0.019 ± 0.06
Runoff	1.89 ± 1.05	5.66 ± 0.14	0.75 ± 0.01	0.08 ± 0.01	1.74 ± 0.01
Planted	234.2 ± 36.2	63.97 ± 1.34	0.34 ± 0.01	0.04 ± 0.0	0.02 ± 0.01
Unplanted	34.3 ± 5.2	9.38 ± 0.59	0.03 ± 0.0	0.13 ± 0.02	0.06 ± 0.0
Model	9.45 ± 2.36	25.30 ± 1.46	1.08 ± 0.02	0.43 ± 0.02	14.03 ± 0.10

NH_4: No significant differences were found among treatments ($p=0.209$). The variation around the mean for the model and the rainfall was rather large, while the median values of the downspout runoff and the planted roof were below that of rainfall (Figure 2). The average value was largest in the model, but the other treatments were similar (Figure 1). The downspout runoff,

the planted and unplanted roofs all had averages lower than that of rainfall, with the planted being the lowest (Table 1).

Table 2. Site Collection Dates and Weather Conditions

Date & Site	Rainfall	Average Wind Speed	Average Humidity	High Temp.	Low Temp.	Conditions
Oct. 7 2014	.15 inches	10.7 mph	58%	75 °F	62 °F	Thunder storms, heavy and light rain
Oct. 15 2014	1.44 inches	9.8 mph	78%	80 °F	61 °F	Thunder storms, heavy rain, fog, haze
Oct. 22 2014	1.09 inches	14.8 mph	72%	58 °F	55 °F	Rain and Fog
June 1 2015	2.49 inches	10.7 mph	67%	92 °F	71 °F	Thunder storms, heavy and light rain
June 4 2015	.37 inches	10 mph	84%	65 °F	59 °F	Rain
June 8 2015	.65 inches	13 mph	70%	88 °F	65 °F	Thunder storms and Rain
June 23 2015	.84 inches	11 mph	68%	96 °F	75 °F	Thunder storms, heavy and light rain
June 27 2015	2.75 inches	11 mph	85%	78 °F	69 °F	Rain

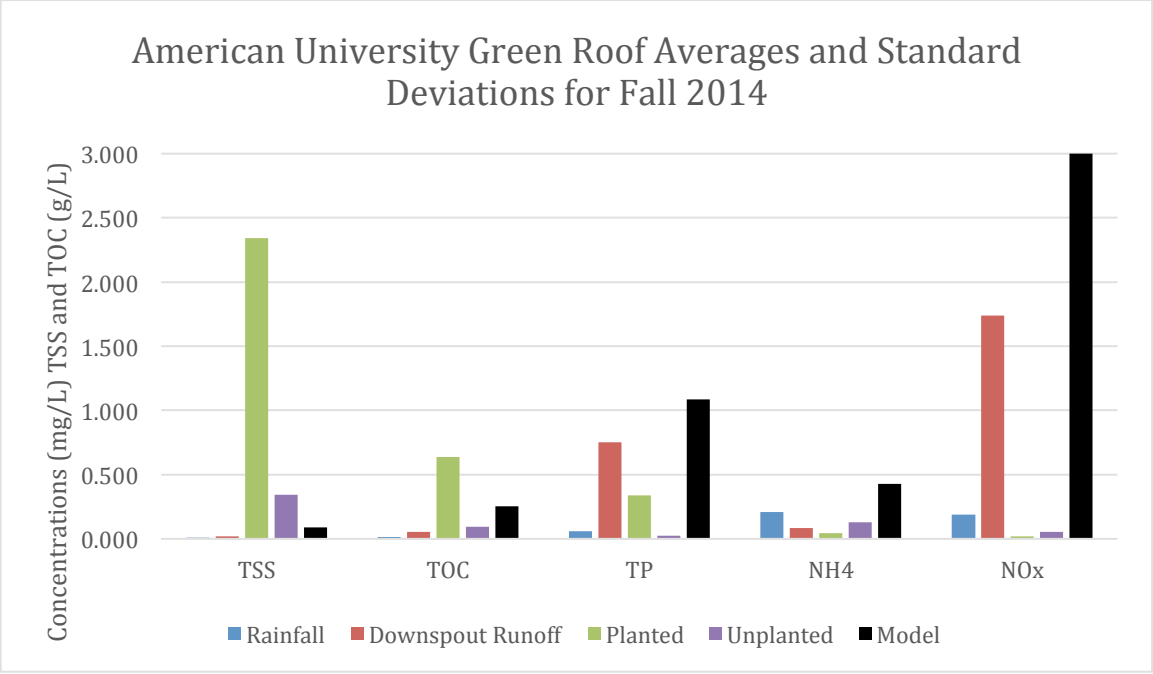

Figure 1: Average total suspended solids (TSS), Total organic carbon (TOC), total phosphate (TP), ammonium (NH$) and nitrate (NO3) collected from Fall 2014. TSS average is highest for the planted roof, then the unplanted roof, then the model, and the rainfall and downspout runoff are similar. The TOC is also highest in the planted roof, followed by the model, unplanted roof, downspout runoff and rainfall. PO_4 is highest in the model, but all are above rainfall input. For ammonium, the model is the highest and all other treatments are lower than rainfall. NO_x is high in the model and the downspout

NO_x: No significance was found using the Kruskal Wallis test (0.729). The model, again, had the highest spread and median value, while the median values of the other treatments were similar (Figure 2). The model also had the highest average followed by downspout runoff, unplanted, rainfall and then planted. (Figure 1). The planted roof retained only 0.001 mg/L more than the rainfall and all other treatments were higher than rainfall (Table 1).

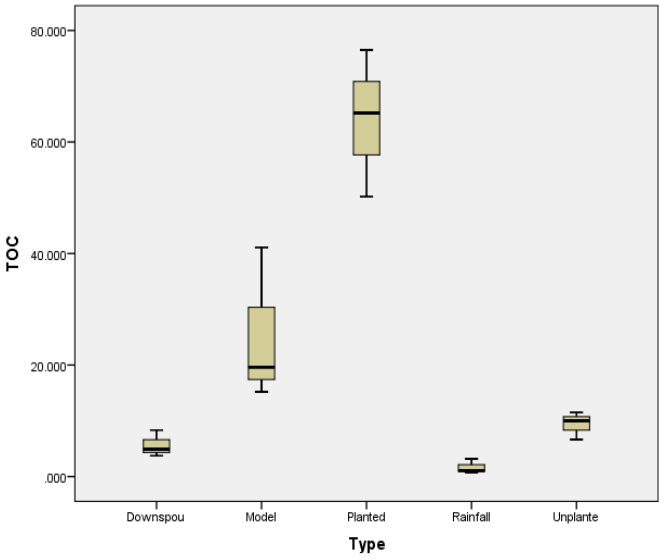

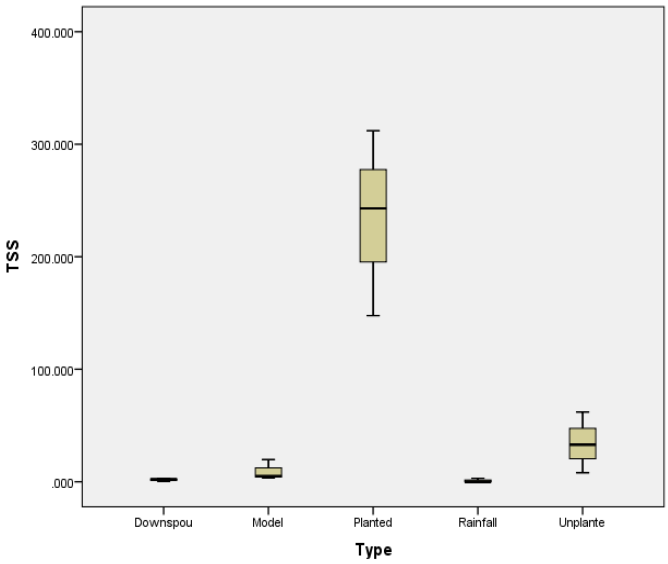

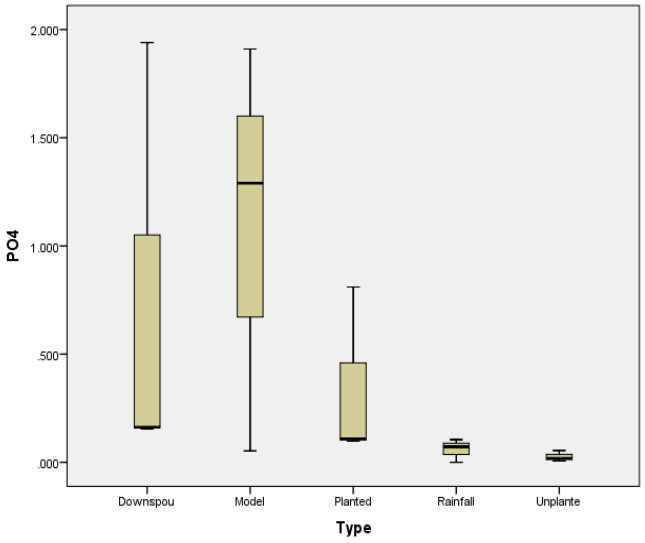

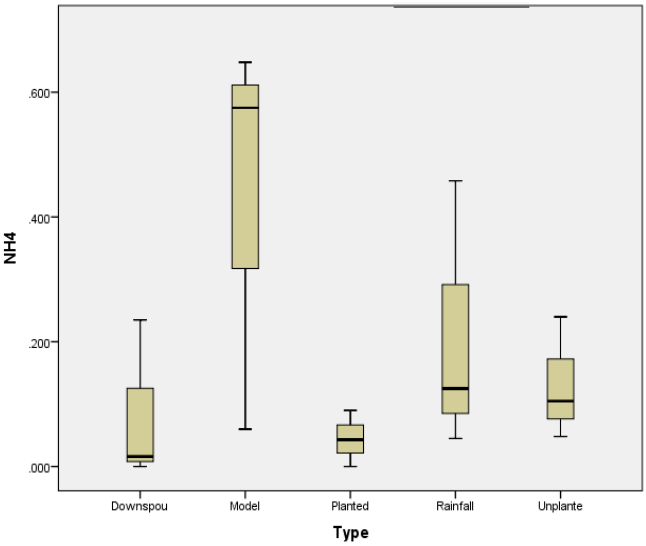

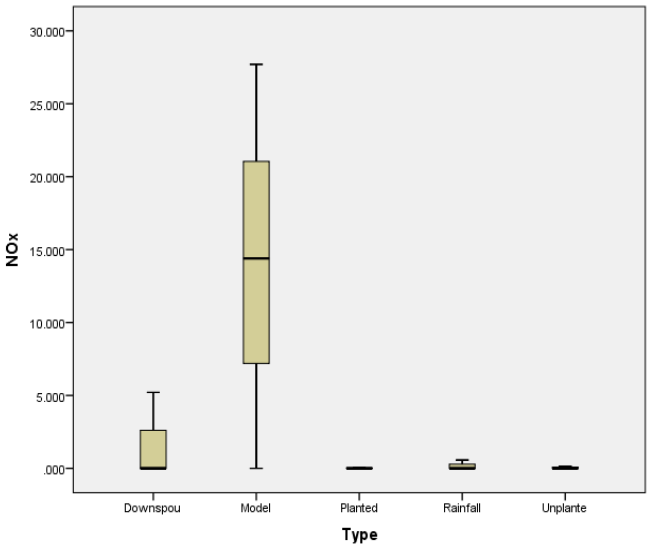

Figure 2: The median values and spread of each of the treatment types for the fall 2014 collection data are illustrated above. The planted roof is highest in TSS and TOC. The model is highest in the rest of the nutrients and has the largest spread. In most cases, the median values of all treatments are not lower than the median rainfall value, thought the unplanted roof is in the case of TP and the planted and unplanted roof in the case of NO_x.

Summer 2015

TSS: There were significant differences among the treatments (p=0.002). The highest amount released was from the planted roof (53.01 mg/L), followed by the unplanted roof, the model and then the downspout runoff (Table 3). None of the treatments outperformed the downspout runoff or rainfall (Figure 3). The spread of the data was largest for the planted roof, while the other treatments were less variable and median scores were closer in value (Figure 4).

Table 3. American University Rainfall, Downspout Runoff, Planted and Unplanted Green Roof Averages and Standard Deviations for Summer 2015

	TSS (mg/L)	TP (mg/L)	NH_4 (mg/L)	NO_x (mg/L)
Rainfall	1.47 ± 0.54 (N=5)	0.03 ± 0.04 (N=5)	0.1 ± 0.08 (N=5)	0.35 ± 0.11 (N=5)
Downspout Runoff	2.07 ± 1.44 (N=5)	0.51 ± 0.01 (N=5)	0.56 ± 0.01 (N=5)	0.86 ± 0.01 (N=5)
Planted	53.01 ± 22.39 (N=5)	0.08 ± 0.02 (N=5)	0.03 ± 0.02 (N=5)	0.04 ± 0.02 (N=5)
Unplanted	7.13 ± 2.72 (N=5)	0.15 ± 0.01 (N=5)	1.09 ± 0.04 (N=5)	0.46 ± 0.15 (N=5)
Model	3.33 ± 1.53 (N=5)	0.89 ± 0.02 (N=5)	0.18 ± 0.02 (N=5)	0.59 ± 0.06 (N=5)

TP: There was significance among the treatments (p=0.008). The spread of the model and downspout runoff was large, while the other three data points were not, with one outlier removed from the unplanted roof data. The median values were highest in the model, followed by the downspout runoff, the unplanted roof, the planted roof and then rainfall (Figure 4). Phosphorous measured in all treatments were under 1 mg/L, with the average value being highest in the model and the lowest in the rainfall (Table 3). The planed and unplanted roofs released less than the downspout runoff, but more than the rainfall (Figure 3).

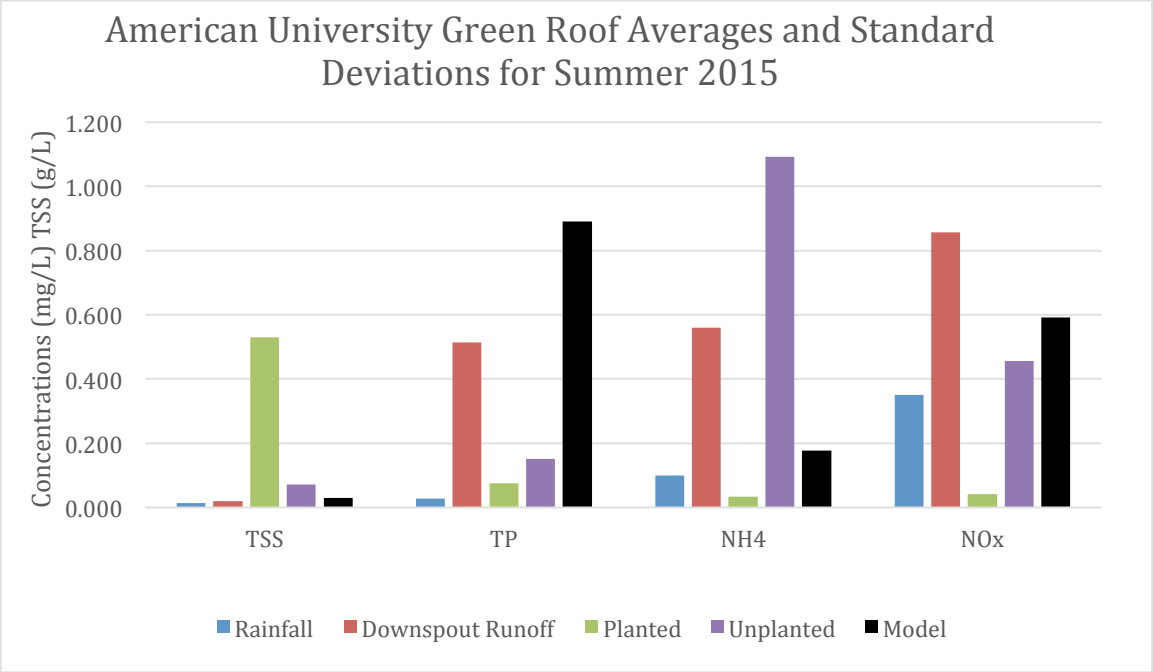

Figure 3: The planted roof had the highest TSS, followed by the unplanted and the model, while none are lower than downspout runoff and rainfall. TP was highest in the model and downspout runoff, though not even the planted and unplanted roof were below the rainfall amount, yet they were below the downspout amount. The planted roof retained ammonium, while the model was lower than both the downspout runoff and the unplanted roof, which was the highest. The planted roof was also the lowest with respect to NO_x. The rainfall was much higher than usual, but still lower than the unplanted, model and downspout runoff. The unplanted and model were both lower than the downspout runoff.

NH_4: There was significance among the treatments ($p=0.049$). The variance around the mean for unplanted and downspout runoff was large, while the other three treatments were not (Table 3). The median value of the unplanted roof was the highest, followed by the model, downspout runoff, the rainfall and then the planted roof (Figure 4). The average value for the unplanted roof

was the highest, but the model and planted roof values were lower than the downspout runoff (Figure 3). The planted roof ammonium value was almost a third of the rainfall value (Table 3).

NO_x: There was significance among the treatments ($p=0.025$). The median value of the downspout runoff was the highest, followed by the model, unplanted roof, rainfall and then the planted roof (Figure 4). The average value also follows this trend (Figure 3). All nitrate concentrations were lower than 1 mg/L, respectively (Table 3).

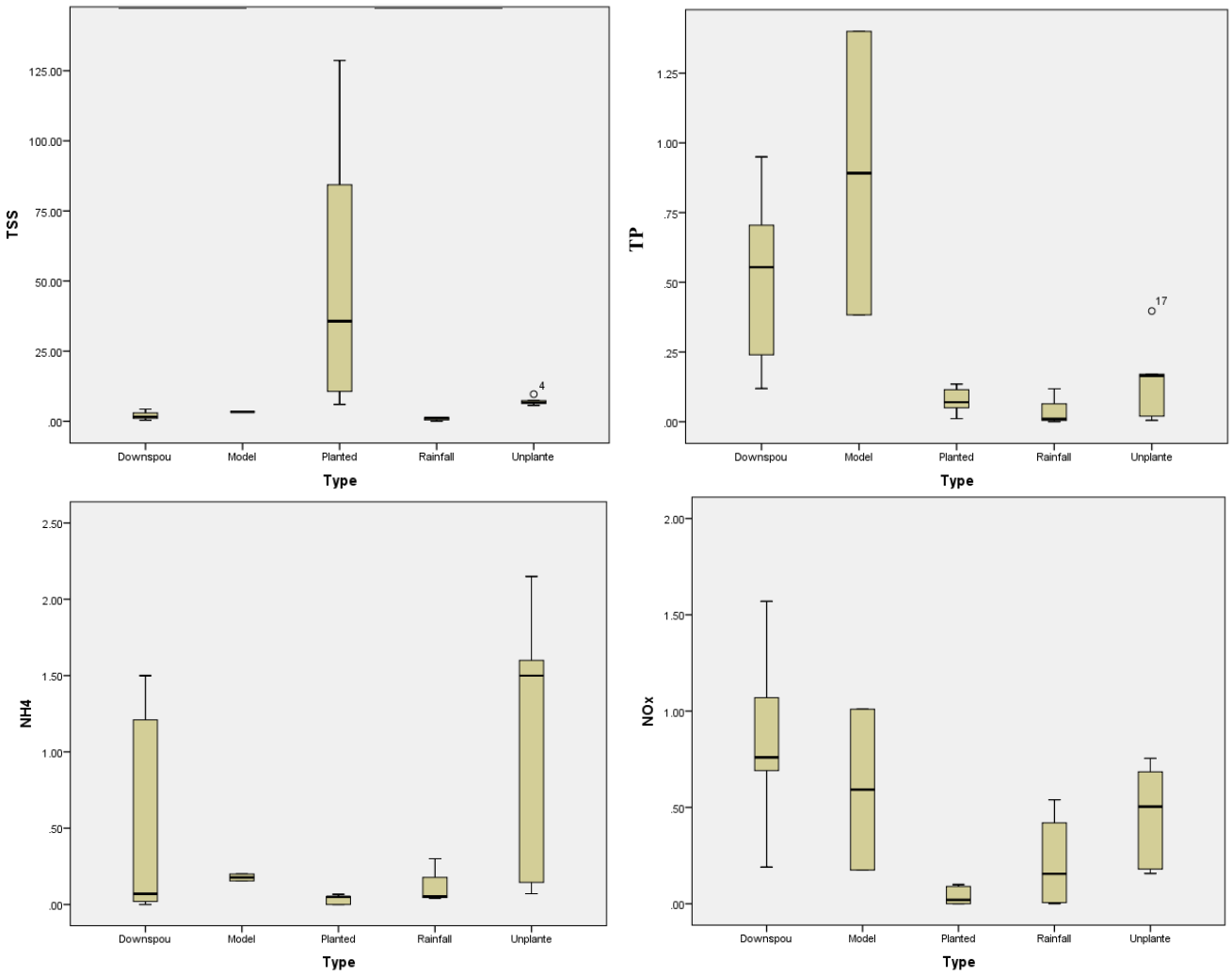

Figure 4: The spread of the planted roof is much greater than any of the other treatments with respect to TSS. The median values are similar for the rest of the treatments with one outlier in the unplanted roof TSS measurement. The spread for the downspout runoff and the model are large with the latter having the largest median value with respect to TP. The unplanted roof has the highest median for NH_4, while the planted and rainfall value are the smallest. The planted roof has the smallest median with respect to NO_x, while the downspout runoff has the highest median.

Seasonal Comparison

Only TSS, TP, NH_4 and NO_x were compared using Kruskal Wallis since TOC was not measured for the summer of 2015. The average concentrations did vary between the seasons although the means were not significantly different.

TSS: The rainfall and downspout runoff were roughly the same. The planted roof decreased TSS throughflow by over 180 mg/L, the unplanted roof decreased over 25 mg/L and

the model decreased by 6 mg/L from fall 2014 to summer of 2015 (Tables 1 and 3). In both seasons, the planted roof released the most and rainfall released the least. The model was the second highest, followed by the unplanted and then the downspout runoff in both seasons.

TP: The model throughflow had the highest concentration the most followed by the downspout runoff (Figure 1 and 3). For the summer of 2015, the next highest TP concentration was from the unplanted roof, followed by the planted roof and then rainfall (Table 3). For the fall of 2014, the planted roof ranked 3rd for TP followed by the rainfall and then the unplanted roof with the lowest TP (Table 1).

NH_4: Ammonium seemed to decrease with time as the values were all higher in the fall of 2014, except for the downspout runoff and the unplanted roof. The planted roof released the least in both years and decreased by 0.01 mg/L between fall 2014 and summer 2015. The rainfall decreased over 0.10 mg/L and the model decreased by almost 0.30 mg/L (Table 1 and 3). In fall 2014, the model released the most, but in summer 2015, the unplanted roof had highest concentrations (Figure 1 and 3).

NO_x: In 2014, the model had the highest concentration in throughflow, but in 2015, the downspout runoff was higher, and the model released 13 mg/L less NO_x (Table 1 and 3). The planted roof remained the treatment that released the least, but increased by 0.03 mg/L in 2015. The unplanted roof also increased by 0.40 mg/L and the downspout runoff decreased by almost 1 mg/L. The concentration in rainfall increased by 0.3 mg/L (Figure 1 and 3).

Overall, the planted, unplanted and model green roofs seem to be improving with age as the amount of nutrients released has decreased from fall of 2014 to summer of 2015. The exceptions include the increase in TP in the unplanted roof, NH_4 in the unplanted roof, NO_x in the planted and unplanted roof. The model was the only one that decreased for each nutrient.

Overall Analysis of AU's Extensive Green Roofs

All collection data from both fall 2014 and summer 2015 were combined to create average values for each of the nutrients of concern, except for TOC. Kruskal Wallis tests were performed to see if significance arose, median values were examined and the averages were also graphed for visualization.

TSS: There was significance among the treatments (p=less than 0.001). The Dunn procedure revealed that the significance was between from the comparison of rainfall/planted, rainfall/model, downspout runoff/planted and downspout runoff/model. The planted roof released the most solids followed by the unplanted, model and then downspout runoff (Figure 14). None were lower than rainfall, which was less than 1 mg/L (Table 4). The median value of the planted roof was the highest, followed by the unplanted roof and the rest of the collection points had similar scores (Figure 5).

Table 4. American University Rainfall, Downspout Runoff, Planted and Unplanted Green Roof Averages combining fall of 2014 and summer 2015

	TSS (mg/L)	TP (mg/L)	NH_4 (mg/L)	NO_x (mg/L)
Rainfall	0.83 (N=8)	0.04 (N=8)	0.14 (N=8)	0.29 (N=8)
Downspout Runoff	2.00 (N=8)	0.60 (N=8)	0.38 (N=8)	1.19 (N=8)
Planted	121.00 (N=8)	0.18 (N=8)	0.04 (N=8)	0.03 (N=8)
Unplanted	17.33 (N=8)	0.11 (N=8)	0.73 (N=8)	0.31 (N=8)
Model	7.00 (N=8)	1.01 (N=8)	0.33 (N=8)	8.66 (N=8)

TP: Phosphorous was also significantly different between treatment types (p=0.001). The significance arose from the comparison of rainfall/downspout runoff, rainfall/model, planted/model, unplanted/model. The model throughflow contained the highest concentration, over 1 mg/L, while rainfall contained the least followed by the unplanted and planted roofs and

then the downspout runoff (Table 4 and Figure 5). The downspout runoff and model had the largest spread and median values. The unplanted roof had the smallest median value followed closely by rainfall and then the planted roof (Figure 6).

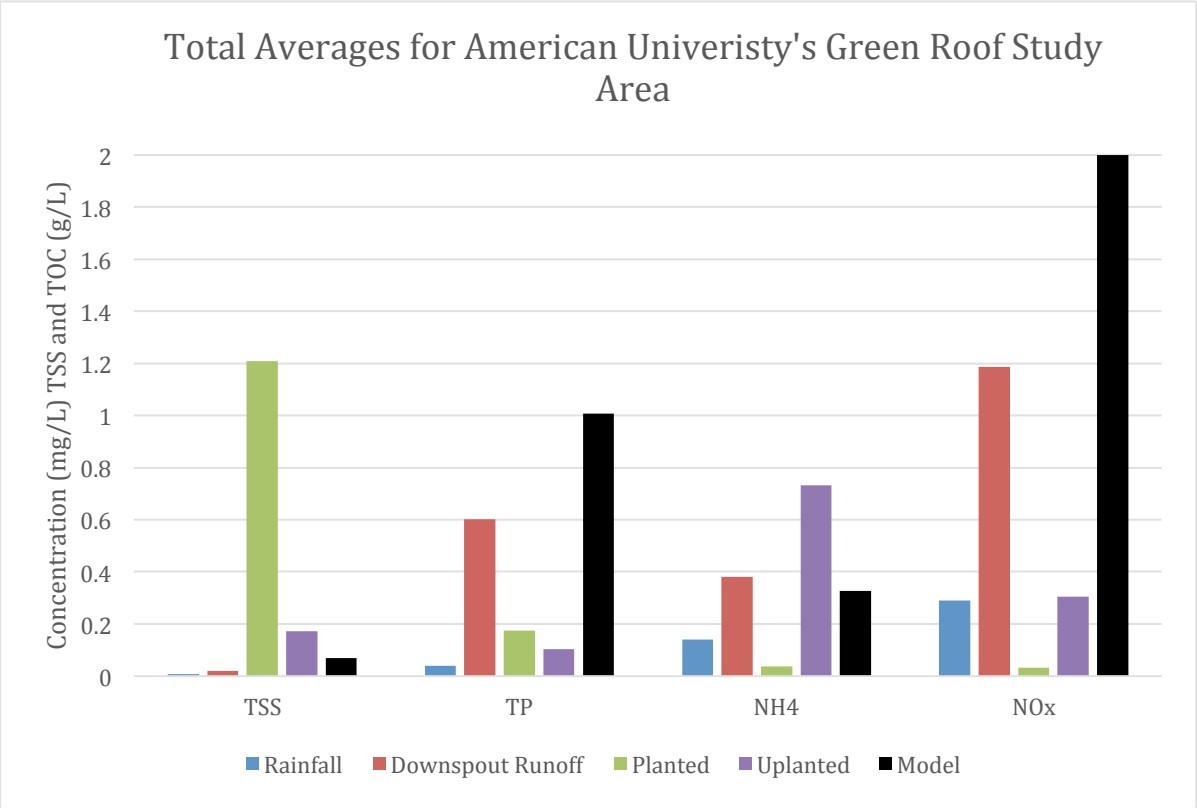

Figure 5: The planted roof released the most solids, but released very little of NH_4 and NO_x, which were all less than the amount present in rainfall. The model released the most TP and NO_x, but released very little of TSS and NH_4- though not lower than rainfall. The unplanted roof released the most NH_4, but was lower in the amount of NO_x and TP released than downspout runoff. The model NO_x value was truncated.

NH_4: There was significance among the treatments ($p=0.023$). This resulted from the following comparisons: rainfall/model, downspout runoff/model, and planted/model. The planted roof retained ammonium from the rainfall (Figure 5). The unplanted roof released the most NH_4, followed closely by the downspout runoff and then the unplanted roof (Table 4). The median value of the model is the highest and has the most variation. The next highest median value was

found in rainfall and the unplanted roof, then the planted roof and lastly the downspout runoff (Figure 6).

NO_x: No significance was indicated (p=0.071). The model released the most nitrite and nitrate, followed by the downspout runoff, the unplanted roof, the rainfall and then the planted

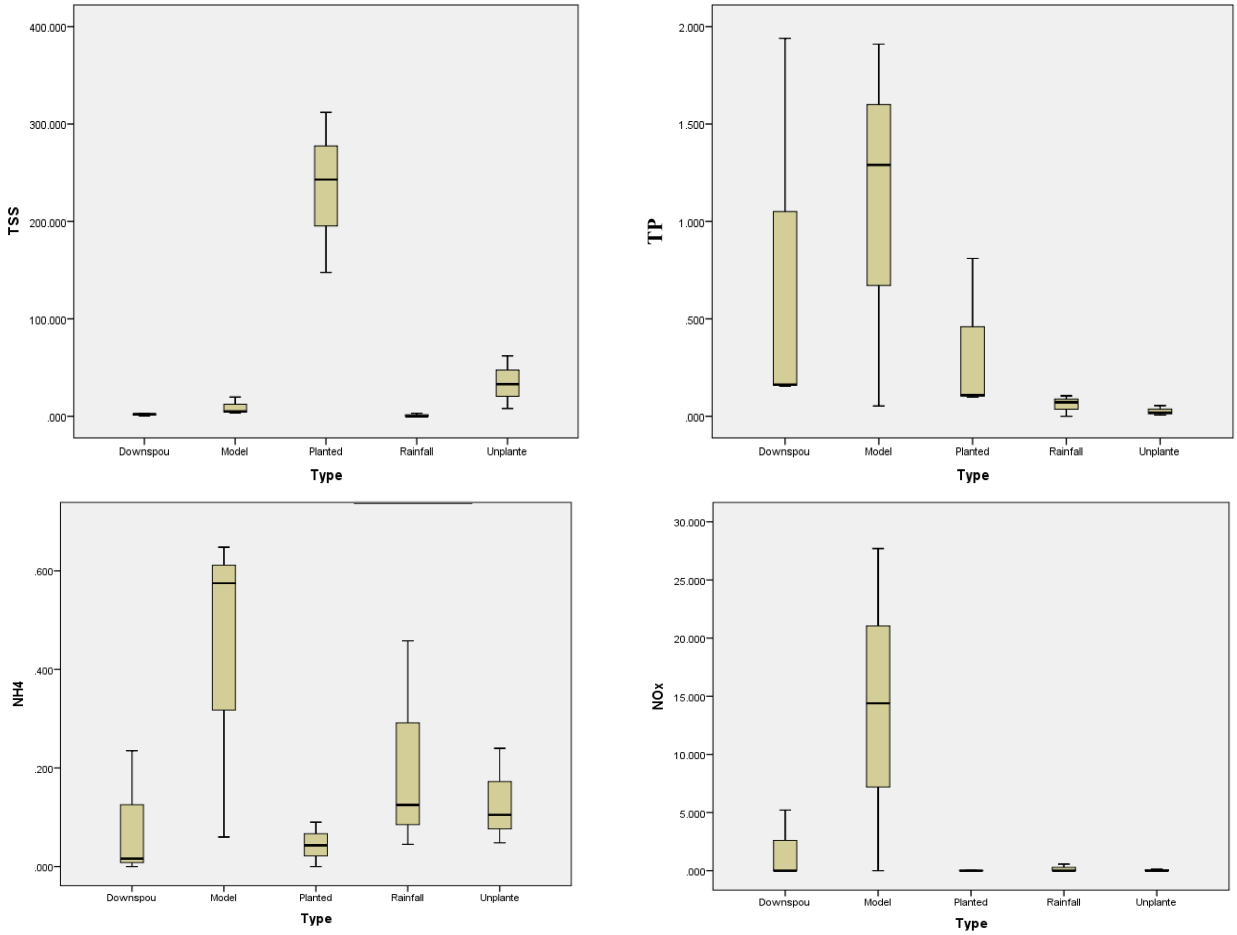

Figure 6: The median value of the planted roof is highest with respect to TSS, followed by the unplanted roof, the model and then the downspout and runoff. The model and the downspout runoff have large variation and the highest medians in terms of phosphorous. The unplanted roof median phosphorous value is less than that of rainfall. The model is again the largest median value in NH_4 and has a large spread. The planted median NH_4 value is the lowest, while the downspout runoff is next followed by the rainfall and unplanted roof. The model has the highest median value for NO_x, while the other treatments are all very similar.

roof (Figure 5). The model measurement contained over 8x's the amount present in any of the other treatments, while the planted roof contained more than 8x's less than the amount present in rainfall (Table 4). The spread and median was also highest in the model, followed by the

downspout runoff. The planted and unplanted roof median values are similar to that of the rainfall (Figure 16).

Discussion:

Fall 2014

TSS: The treatments were significant, with the planted roof releasing the most. This could be due to the fact that the plants were losing leaves during the fall or the amount and intensity of the rainfall. This trend has been indicated in other studies with the growing media and plants cited as the main source of solids (Carpenter and Kaluvakolanu 2011, Harper et al. 2014). The unplanted and model roof also released TSS, which are more likely due to rainfall intensity and amount, though the model could be experiencing its first flush as it was installed during this sampling period. All treatments released more TSS than rainfall, making them a source of pollutants, and they released more than the downspout runoff, not indicating that they are a better option than asphalt roofs.

TOC: The treatments were found to be significant with the planted again releasing the most. This is to be expected as plants contain carbon and the amount released is very dependent on growing media; our results were found to be within range of other green roofs (Harper et al. 2014). The model released 25.3 mg/L, which is also relatively high, but is expected to decrease with time. None of the treatments were lower than rainfall or the downspout runoff indicating that they are a source of TOC and not a more viable option than asphalt roofs.

PO_4: No significance was found with the model releasing just over 1 mg/L and all others less than 0.8 mg/L. This is higher than other studies on planted and unplanted green roofs, which were found to release around 0.2 mg/L (Berndtsson et al. 2006, Teemusk and Mander 2011, Gregoire and Clausen 2011). It is our thought that this will

decrease with time. Our planted green roof released 0.339 mg/L, which is only slightly higher and could be due to any fertilization done by the maintenance department at the University. All the treatments except the unplanted roof were sources for the nutrient, which is consistent to the studies mentioned above, but not with ones conducted by Carpenter and Kaluvakolanu (2011) and Speak et al. (2014). Speak et al. found that their green roofs were not significantly different than rainfall, but released less, though it still exceeded EPA limits of 0.5 mg/L (2014). Only out model roof exceeded that limit. Only the unplanted roof was a sink for phosphorous, but the planted roof released less than the downspout runoff making them better options than asphalt roofs.

NH_4: The model released 2 times that of the rainfall, but all other treatments indicated that green roofs are a sink for ammonium even though no significance was indicated. Teemusk and Mander (2011) found similar results in his study with average throughflow releasing 0.14 mg/L, while ours released 0.044 mg/L for the planted roof and 0.131 for the unplanted roof (Table 3) (2011). Ammonium uptake is dependent on plant type and growing media, and is also often converted to NOx. The plants and algae on the green roofs are the likely sources of this sink phenomena.

NO_x: No significance was found, and only the planted roof did not expel nitrogen (Table 3). The planted roof and rainfall both released 0.019 mg/L, which is lower than the studies done by Teemusk and Mander (2011), Carpenter and Kaluvakolanu (2011), and Gregoire and Clausen (2011), which put releases between 0.21 and 2.33 mg/L. It is unknown why the amount released is so much lower, though plant uptake and rain intensity often influence the amount released. The unplanned roof was also lower than these values and released less than the downspout runoff, therefore both green roofs are a

more viable option than asphalt roofs even though the unplanted roof is a source of pollution. The model released much higher amounts, and is not a viable option.

Summer 2015

TSS: The planted roof was the largest source of TSS 121 mg/L (Table 5). This is again to be expected due to the plant material and growing media, and has been indicated by other studies (Carpenter and Kaluvakolanu 2011, Harper et al. 2014). Carpenter and Kaluvakolanu (2011) reported close to 200 mg/L, while Harper et al. (2014) reported a median value of 10 mg/L. The median range of our planted roof is higher, but the same trend is observed. None of the treatments are sinks for TSS as all release more than rainfall and the downspout runoff, indicating asphalt roofs are the better option.

PO_4: Significant differences were observed, with all treatments staying below 0.9 mg/L. The planted roof value is much lower than reported values and suggesting that retains more phosphorous than other roofs (Berndtsson et al. 2006). This trend is consistent with studies done by Carpenter and Kaluvakolanu (2011) and Speak et al. (2014), though their studies did not indicate significance. Other studies have indicated that green roofs are a source of PO_4 (Teemusk and Mander 2011, Gregoire and Clausen 2011). The increased uptake could be due to the growing season and the intensity of rainfall. The unplanted roof was a source of pollutants, but released less than the downspout runoff, making it also a better option than asphalt roofs (Table 5), but the model released more.

NH_4: The unplanted roof released the most ammonium. The increase in ammonium may be due to the unplanted being shifted many times during this season, which mixed the algae clearly living in the panel tray. The planted roof was a sink for this

nutrient, but the other two treatments were not, though the model roof released less than the downspout runoff, indicating it as a better source than asphalt roofs. The planted roof released less than the amount cited in literature, but the overall trend is consistent (Teemusk and Mander 2011).

NO_x: Only the planted roof was indicated to be a sink for nitrates and nitrites, but all other treatments were still lower than downspout runoff signifying that both the model and unplanted roof are better options than asphalt (in terms of nitrate release). The planted roof released less than the amount found in literature, but the overall trend is consistent (Teemusk and Mander 2011, Carpenter and Kaluvakolanu 2011, and Gregoire and Clausen 2011). The plant type and growing media along with rainfall intensity heavily influence the amount of NO_x released. The movement of the unplanted roof, could have caused the unplanted roof to become a source of the pollutant, and it is still though that the model roof is experiencing a first flush.

Overall Analysis

The overall average comparison of the 2014 and 2015 study sites (planted, unplanted, model, downspout runoff and rainfall) yielded significant results for all nutrients of interest (TSS, TP, NH_4, and NO_x). It is noteworthy that the amount of the nutrients released is in part dependent upon intensity and duration of rainfall, climate, season, growing media, plant type and roof slope.

TSS: The average TSS from the planted roof was by far the highest, though this is expected since all plants and soil media release solids during their lifespan and other studies have also reported this trend with similar average amounts (Harper, et al. 2014, Carpenter and Kaluvakolanu 2011). The unplanted released solids as well, which could

be due to algal growth on the aqualok material. The solids released from the model, rainfall and downspout runoff could be due to the particulate matter landing on the surfaces or in the case of the ladder, tar or asphalt coming loose.

PO_4: The amount of phosphorous released by the green roofs was more than the amount of input rainfall indicating they are a source of pollution (Table 5), which agree with the other studies (Berndtsson et al. 2006). This is could be due to the growing media and any fertilizer that could have been added. The average values reported for the planted and unplanted roof are similar to that of other studies (Gregoire and Clausen 2011, Carpenter and Kaluvakolanu 2011, Mander 2011) and lower than the 0.6 mg/L reported by Speak et al. (2014). The downspout runoff was also higher than the unplanted and planted roof, which indicated these types of surfaces are better, but still a source of phosphorous runoff (Figure 14).

NH_4: Ammonium was retained by the planted roof, which has been observed in other studies (Teemusk and Mander 2011, Berndtsson et al. 2006), but the Aqualok roofs seem have lower throughflow concentrations; 0.038 mg/L as opposed to 0.14 mg/L (Table 5). This nutrient is strongly affected by the age of the roof and the plants, which are able to retain more nitrogen with age. The unplanted roof and model, both released more ammonium than the downspout runoff, making them less effective at nutrient removal.

NO_x: This type of nitrogen follows the same trend as ammonium, as the planted green roofs retain the nutrient. This is consistent with other studies, which even indicate higher output concentrations, 0.21 mg/L as opposed to 0.033 mg/L (Table 5) (Gregoire and Clausen 2011, Carpenter and Kalivakolanu 2011, Teemusk and Mander 2011).

Based on the data gathered, green roofs of any type show higher TSS and phosphorus than rainwater. The planted and unplanted roofs are all better options than asphalt roofs with respect to phosphorous, though neither are better than the asphalt roof with respect to TSS. Planted roofs are a sink for both types of nitrogen, though the unplanted roof released more than the asphalt roof with respect to ammonium, but less with respect to NO_x. The traditional roof did not act as a sink for any of the nutrients and released more than the asphalt roof with respect to all nutrients. As the planted roof only acted as a sink for half of the nutrients and as a source for the other half, it does not seem that green roofs are the end all solution to urban runoff, though they are better than current asphalt roofs according to these results.

Literature Cited

Berndtsson, J.C., Emilsson, T., Bengtsson, L. (2006). *The influence of vegetated roofs on runoff water quality*. Sci. Total Environment 355, 48-63.

Carpenter, D.D., Kaluvakolanu, P. (2011). *Effect of roof surface on storm-water runoff from full-scale roofs in a temperate climate.* Journal of Irrigation and Drainage Engineering 137 (3), 161-169.

Eaton, A.D., Clesceri, L.S., Greenberg, A.E., Franson, M. A. H. 1998. American Public Health Association., American Water Works Association., & Water Environment Federation. *Standard methods for the examination of water and wastewater*. Washington, DC: American Public Health Association.

Galloway JN, Cowling EB. 2002. Reactive nitrogen and the world: 200 years of change. Ambio 31(2):64-71

Gregoire, B.G., Clausen, J.C. (2011). *Effect of a modular extensive green roof on storm water runoff and water quality.* Ecological Engineering 31, 963-969.

Harper, G.E., Limmer, M.A., Showalter, W.E., Burken, J.G. (2014). *Nine-month evaluation of runoff quantity from an experiential green roof in Missouri, USA*. Ecological Engineering 72, 3033-3040.

Hawkins, GS. 2008. Anacostia 2032: Plan for a Fishable and Swimmable Anacostia River. Report to the District Department of the Environment.

Speak, A.F., Rothwell, J.J., Lindley, S.J., Smith, C.L. (2014). *Metal and nutrient dynamics on an aged intensive green roof*. Environmental Pollution 184, 33-43.

Teemusk, A., Mander, Ü. (2011). *The influence of green roofs on runoff water quality: a case study from Estonia*. Water Resource Management 25, 3699-3713.

Washington Post. 2012. Anacostia River Trail system moves toward completion. 10/15 by Mike DeBonis.

A Novel Water Treatment Solution Using Hybrid Mesoporous Materials Embedded with Metallic Oxide Nanoparticle

Basic Information

Title:	A Novel Water Treatment Solution Using Hybrid Mesoporous Materials Embedded with Metallic Oxide Nanoparticle
Project Number:	2015DC171B
Start Date:	3/1/2015
End Date:	2/28/2016
Funding Source:	104B
Congressional District:	District of Columbia
Research Category:	Water Quality
Focus Category:	Treatment, Water Quantity, Wastewater
Descriptors:	None
Principal Investigators:	Xueqing Song, Jiajun Xu

Publications

1. Vu, Trinh, Xueqing, Song, Jiajun Xu. 2016. “Design and Characterization of Nanoparticles Infused Mesoporous Materials for Environmental Applications”, ASME 2016 International Mechanical Engineering Congress & Exposition (IMECE)
2. Vu, Trinh, Xueqing, Song, Jiajun Xu. 2016. “MCM Based Hybrid Mesoporous Materials for Water Treatment” 2016 National Capital Region Water Resources Symposium. Oral Presentation.

Cover Page

A Novel Water Treatment Solution Using Hybrid Mesoporous Materials Embedded with Metallic Oxide Nanoparticle

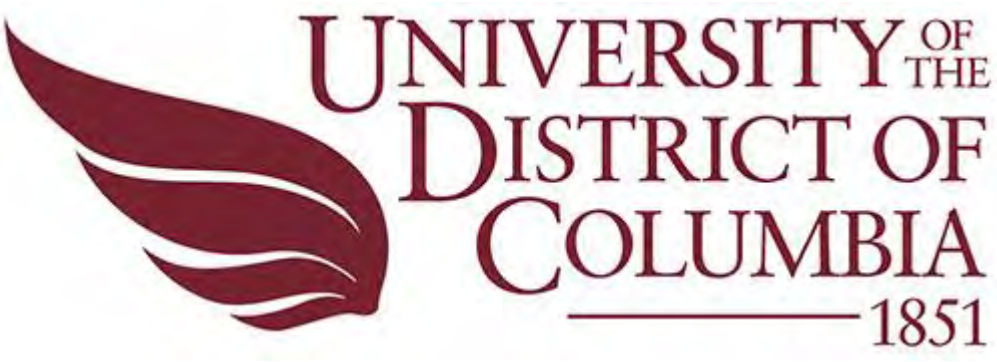

Principal Investigators

Jiajun Xu

Department of Mechanical Engineering, University of the District of Columbia

Xueqing Song

Chemistry and Physics Department, University of the District of Columbia

April 22, 2016

1. Executive Summary

To restore and maintain the physical chemical and biological integrity of water bodies in the United States, there is an urgent need of developing effective and economical feasible solution for the prevention of contamination of water supplies caused by industrial wastes and storm water. In the last decade, many new techniques and methodologies have been proposed to remedy wastewater which include using micro/nanostructured membrane/filtration, nanoparticle catalytic, and chemical reaction etc. However, these methods are still evolving and often times, further cleaning/removal of the nanomaterials/surfactants added inside are needed which usually is time-consuming and expensive. So this research has explored and characterized a hybrid solution by integrating the nanoparticle catalytic into mesoporous material, which can take advantage of the greater surface area of nanostructure and save the trouble of post processing process needed.

The broader goal of this research project is to assist in exploring a new artificial nanocomposite structure that can offer a path way to the development of engineered materials with novel macroscopic properties for a more feasible and efficient pollutants treatment solution. Our approach comprises two components: 1) Preparation of mesoporous material to be used as frame for nanoparticle deposition, and 2) Synthesis and encapsulate the metallic oxide nanoparticle to the mesoporous frame. This research will utilize one family of widely used mesoporous material-M41S. Our proposed research has utilized the most popular member of this family: MCM-48 as the deposition target. The synthesized metallic oxide nanoparticles will be deposited to the porous surface of the MCM48. To ensure the stability and coverage of nanoparticles on the porous surface, the deposition process will be performed inside buffer solution while the temperature, additives and pH value is controlled. The formed hybrid material has be tested and evaluated for its performance. The result has shown a promising solution for water treatment, in particular the heavy metal removal. It is very much useful for the District of Columbia because it can help improve the efficiency and reduce the cost of wastewater treatment to meet the increasing volume of wastewater, especially in metropolitan area.

2. Introduction

Mesoporous materials have pore size from 2 – 50 nm. They are used as adsorbents for environmental contaminants. In 1992, Mobil Oil's scientists discovered a family of mesoporous siliceous materials – M41S. Typical members of M41S family are MCM-41, MCM-48, and MCM-50. MCM-41 has one dimensional hexagonal structure, resembling a honeycomb network. MCM-48 has three dimensional cubic symmetry structure, and the structure of MCM-50 is two dimensional stabilized lamellar. Because of large surface area, highly ordered and uniformly porous structure, MCM material is a good adsorbent and a catalyst for acid catalyzed reactions and petroleum refining process. MCM can be used to break down organic matters such as oxidation of cyclohexene with H_2O_2, photocatalytic reduction of CO_2 and H_2O, peroxidative oxidation of methyl methacrylate and styrene. MCM-41 has been studied since 1992, therefore, this experiment focuses on MCM-48 because MCM-48 has three dimensional channel system which is expected to have more applications than one dimensional hexagonal MCM-41 and two dimensional

lamellar MCM-50[4]. Cubic MCM-48 has a three dimensional network of pores that increases the surface area, leading to more adsorption of molecules. This type of network also minimizes pore clogging and enhances catalytic reactions [10]. A study for Arsenic (As) removal from water using diamino-functionalized MCM-41 and MCM-48 containing different transition metals Fe, Co, Ni, and Cu shows that the adsorption capacity of MCM-48 for As is greater than MCM-41 [11]. Therefore, MCM-48 is studied in this experiment.

TiO_2 nanoparticle (NP) is used widely for its photocatalytic activity in oxidation/reduction reactions. TiO_2 NP can degrade some organic compounds such as benzene, phenolic compounds, and pesticides. It can also disinfect bacteria like E.coli and remove methylene blue and methyl orange dyes [9]. TiO_2 is a good removal material for heavy metals, especially chromium (Cr), arsenic (As), cadmium (Cd), copper (Cu) and lead (Pb). The ability to remove toxic compounds of TiO_2 NP together with the ability to adsorb on large surface area and uniform pores of MCM-48 can be combined to make a great material for water purification.

Together with the developed industrialization is the environmental pollution. A large amount of toxic organic and inorganic compounds from many industries and agriculture is excreted into the soil, air, water, food, and eventually they will be consumed by human. Those compounds take a long time to decompose and they can harm human health if being exposed in a long period. Heavy metals in drinking water are a big concern because they are toxic and can cause death. These metals can get into water through corrosion of the pipes and plumbing system, erosion of natural deposits, or runoff from old paints. Some of the effects heavy metals cause to human are damages in skin, brain, lungs, circulatory system, kidneys, livers, and eventually leading to cancer or death [2]. Studies have shown MCM can adsorb Arsenic (As) and Chromium (Cr) from water. MCM-41-TiO_2 has been studied for its removal of Cr and MCM-48 has been studied to remove As in drinking water [11, 12]. In this experiment, MCM-48-TiO_2 is synthesized to remove As, Cd, Cr, Cu, and Pb from drinking water. These metals in water can be analyzed using Inductively Couple Plasma – Mass Spectrometer (ICP-MS) from PerkinElmer Pure Plus – NexIon 300D model. This instrument is used for detecting elements, hence, it has several applications in environment such as testing trace metals and minerals in soil, water, and tissues.

In this study, MCM-48-TiO_2 NP is synthesized by hydrothermal technique [4]. Three different sizes of TiO_2 NP (15 nm, 50 nm, and 300 nm) are used for the synthesis with MCM-48, and then tested for their adsorptions of heavy metals. DI water is contaminated with trace metals and filtered through MCM-48-TiO_2NP material. After that, the filtrates are analyzed in order to determine the adsorptions.

The first objective of this study is to synthesize MCM-48-TiO_2NP. The second objective is to determine and compare the adsorption for heavy metals in water between three TiO_2 NP sizes 15 nm, 50nm, and 300 nm.

3. Methodologies

Materials and Method:

Materials: TiO_2 NP sizes 15 nm, 50 nm, and 300 nm from US Research Nanomaterials Inc., NH_4OH 28 – 30 % NH_3 basis from Sigma Aldrich, cetyltrimethylammoniumbromide (CTAB) from Sigma Life Science, ETOS from Aldrich Chemistry, Atomic Spectroscopy Standard Mercury (100 mg/L), Instrumental Calibration Standard 2 (100 mg/L), Environmental Mix 2 (1000 mg/L), and Environmental Mix 3 (1000 mg/L) from PerkinElmer Pure Plus.
Method: MCM-48 containing TiO_2 NP is synthesized using hydrothermal technique. Different sizes of TiO_2 NP (15 nm, 50 nm, and 300 nm) are used. The three materials are then tested for their adsorption of heavy metals. DI water is contaminated with trace metals and minerals with the final concentration is 100 ppb of trace metals, 10 ppb of Hg, and 2100 ppb of minerals. The solution of contaminants will be filtered through the three materials. Collected filtrates are analyzed using ICP-MS to determine which NP size has the best adsorption on heavy metals.

Experimental Procedure:

Synthesis of MCM-48-TiO_2 NP:
Synthesis was done in a water bath at 40 – 50oC. 50 mL of DI water was added to a 250 mL beaker in the water bath. About 3 g of 300 nm TiO_2 nanoparticle was added and stirred constantly. 11.077 g CTAB was added and stirred for 30 min. 9.6 mL ETOS and 3 mL NH_4OH were added and stirred for 1 hour [4].
The procedure was repeated for two other sizes of TiO_2 NP: 15 nm and 50 nm. To distinguish between the three solutions, they were labeled as MT15, MT50, and MT300, which are corresponding to MCM-48 with 15 nm, 50 nm, and 300 nm TiO_2 NP, respectively. The solutions were heated in the oven at 90oC for 4 days.
Characterization for dye removal:
Dyed solution was prepared by dissolving 1 drop of blue dye into 100 mL of DI water. 14 mL of the dyed solution were filtered through MT15, MT50, and MT300. Color of filtrates were collected and compared with the initial solution.

Characterization for heavy metals removal:
Contaminated water was prepared by adding 0.5 mL of 100 mg/L Hg Atomic Spectroscopy Standard, 0.5 mL of 100 mg/L Instrumental Calibration Standard 2 (trace metals and minerals), 1 mL of 1000 mg/L Environmental Mix 3 (Al and Fe), and 1 mL of 1000 mg/L Environmental Standard Mix 2 (Ca, K, Mg, and Na) into 497 mL of DI water. For each synthesized material, 90 mL of the solution was filtered slowly through 6 g of the material and collected in six 15 mL tubes. The collected filtrates were then analyzed for trace metals with ICP-MS.

4. Results and Discussion

Include Figures and Tables

Characterization for dyed solution:

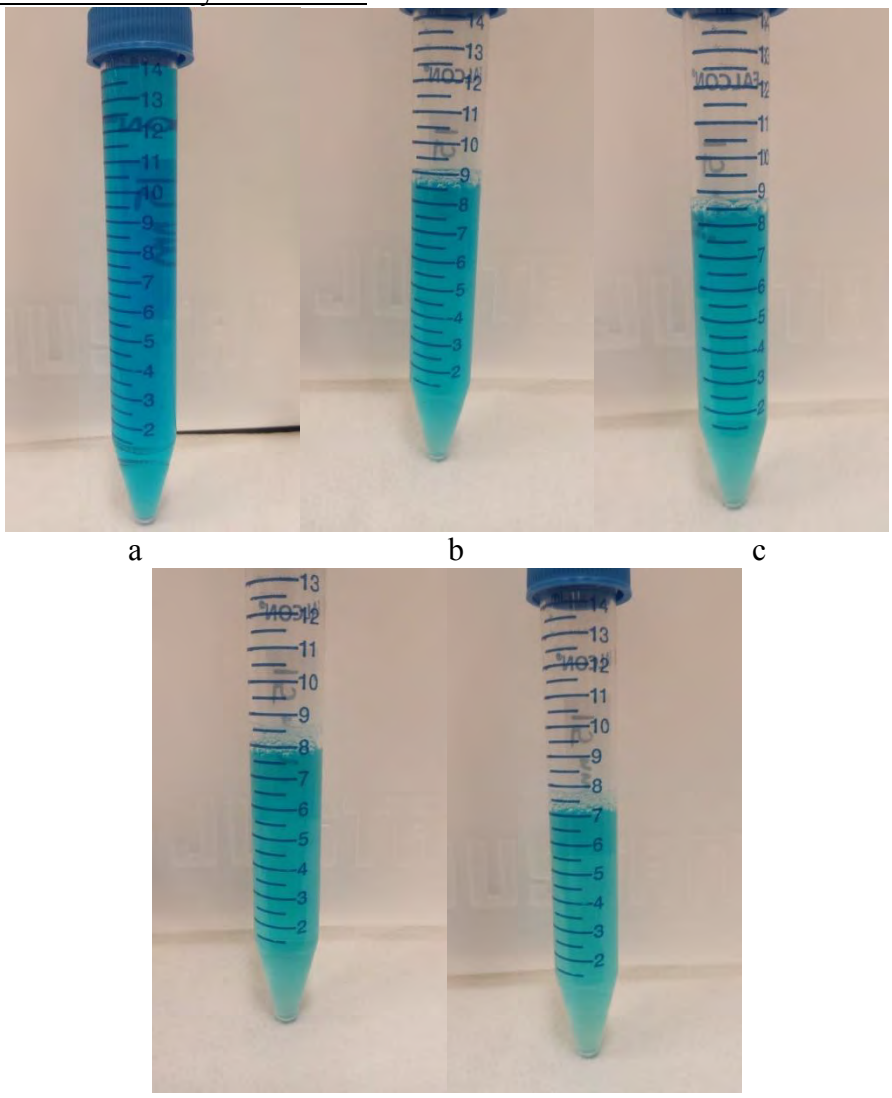

a b c

d e

Figure 1. Filtrates from MT15: a is the initial solution, b, c, d, e are the first, second, third, and fourth filtrates, respectively. The color of the solution after four filtrations is light blue and there is 7 mL left.

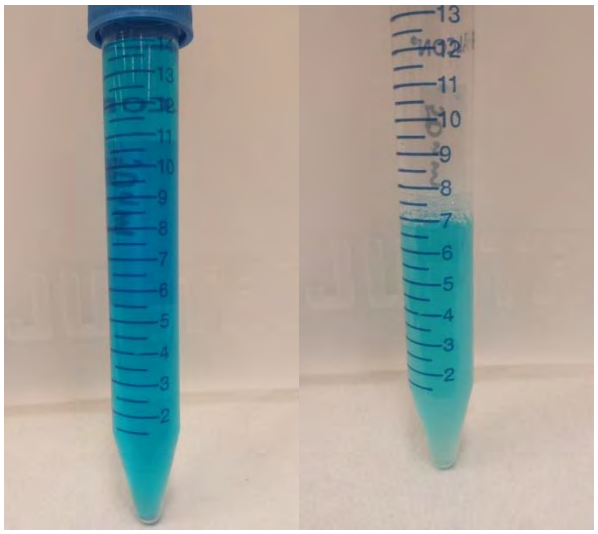

a b

Figure 2. Filtrate from MT50: a is the initial solution and b is the filtrate. After only one filtration, the color becomes much lighter and there is 7 mL left.

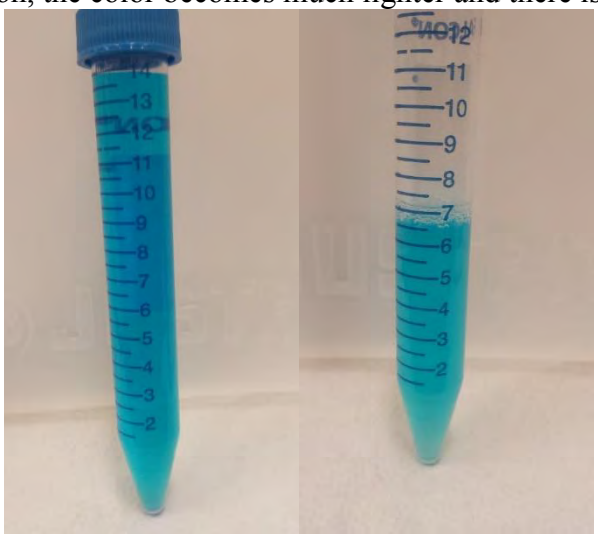

a b

Figure 3. Filtrate from MT300: a is the initial solution and b is the filtrate with a light blue color. There is 6.5 mL left after the filtration.

Characterization for heavy metals:

Table 1. Adsorption data of MCM-48-TiO_2.

Material	No. tubes collected	Amount Adsorbed by MCM-48-TiO_2 (ppb)				
		As	Cd	Cr	Cu	Pb
MT15	1	37.40	19.65	20.90	40.50	35.45
	2	37.65	11.40	16.05	32.55	23.05
	3	32.95	7.55	10.4	14.20	22.35
	4	30.75	5.20	3.15	23.85	22.15

	5	28.55	6.70	2.55	26.50	19.05
	6	36.60	3.25	-10.95	1.15	25.85
MT50	1	24.20	26.90	4.80	19.85	30.30
	2	24.35	9.50	-6.05	-47.85	53.40
	3	23.20	21.75	-6.50	22.85	59.25
	4	16.70	13.60	-5.65	25.95	51.70
	5	13.55	11.55	-10.40	23.95	55.60
	6	24.05	21.65	-23.90	3.00	56.10
MT300	1	44.90	50.85	18.40	50.25	17.50
	2	78.25	71.70	13.65	106.75	88.25
	3	86.20	77.45	-4.65	107.30	92.90
	4	85.40	72.70	-20.35	70.80	88.80
	5	79.65	64.75	-24.65	75.25	87.90
	6	52.10	34.25	-13.85	86.20	50.90

Table 2. Total adsorption of MCM-48-TiO_2 NP with different NP sizes

Material	Total absorption (ppb)				
	Cr	Cu	As	Cd	Pb
MT15	53.05	138.75	203.90	53.75	147.90
MT50	4.80	95.60	126.05	104.95	306.35
MT300	32.05	496.55	426.50	371.70	426.25

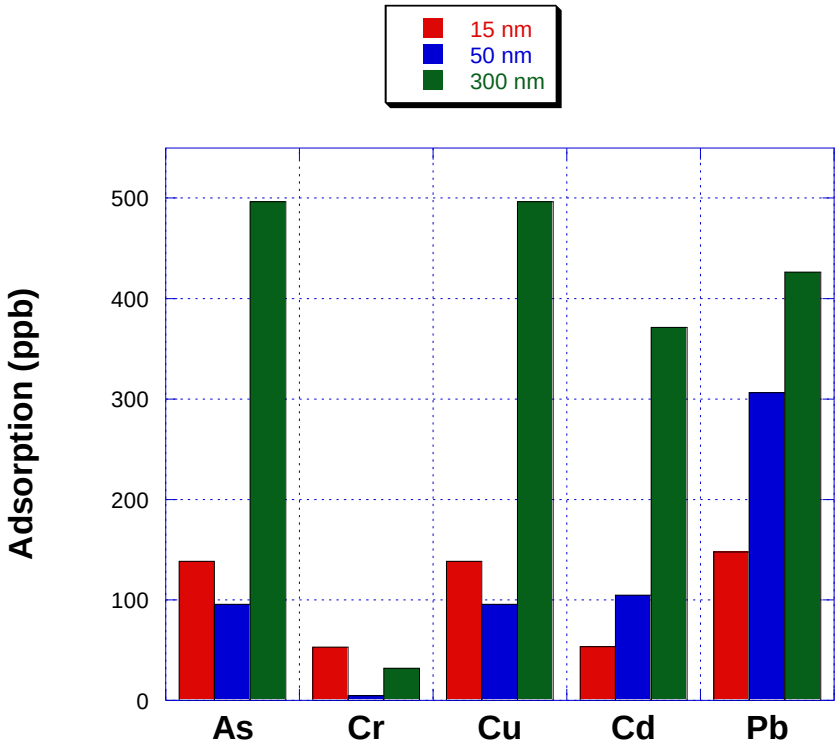

Figure 4. Total adsorption of heavy metals on MCM-48-TiO_2 with three NP sizes 15 nm, 50 nm, and 300 nm.

Discussion:

MCM-48-TiO2NP with different NP sizes were synthesized and used to filter dyed solution and contaminated water. Figure 1 shows that MCM-48 with TiO2 NP size 15 nm could adsorb blue dye from the solution, making the solution's color gets lighter after each filtration. However, the solution only get to light blue after four filtrations through MT15 and the amount of solution left is 7 mL. Figure 2 is the result for MT50, which has the light blue color after just one filtration. There is 7 mL of solution left after the filtration. MT300 could also remove some of the dye from the solution after just one filtration (Figure 3). There is 6.5 mL of solution left after the filtration. Based on the results, MT50 and MT300 adsorb blue dye better than MT15. The amount of solution retained from the filtration is approximately same for all three materials.

From Table 2, the total adsorptions for Cr, Cu, As, Cd, and Pb of MT15 are 53.05 ppb, 138.75 ppb, 203.90 ppb, 53.75 ppb, and 147.90 ppb, respectively. Those values for MT50 are 4.80 ppb Cr, 95.60 ppb Cu, 126.05 ppb As, 104.95 ppb Cd, and 306.35 ppb Pb. MT300 can adsorb 496.55 ppb Cu, 426.50 ppb As, 426.25 ppb Pb, 371.70 ppb Cd, and 32.05 ppb Cr. MT300 has the largest adsorption for Pb, As, Cu, and Cd, but the least adsorption for Cr. On the other hand, MT15 adsorbs the most Cr, but the adsorption for

other metals is less than that of MT50 and MT300. MT15 and MT300 have much lower adsorptions comparing to MT300. MT300 can adsorb Pb, As, Cu, and Cd.

The results show that MCM-48-TiO2 can adsorb heavy metals but cannot determine the maximum amount of heavy metals that it can adsorb for 6 g of material. The maximum adsorption of the material for certain metal can be determined based on the negative values in Table 1, but only Cr has some negative values. Negative adsorption means the material has reached its maximum capacity for the metal. If more water runs through the material, the material cannot adsorb the metal from water, but in fact, some of the adsorbed metal on the material can get back into the water, making the concentration of the metal increase. For example, there is a negative adsorption for Cr (-4.65 ppb) for the third tube when filtering through MT300. That means MT300 has reached its maximum adsorption for Cr after the second tube had been collected (which 30 mL has been run through). Therefore, the water that runs through the material after this point can carry some Cr form the material and gets more contaminated, resulting in a concentration that is higher than the initial concentration 100 ppb, leading to negative adsorption. The maximum concentration of Cr that MT300 could adsorbed was 32.05 ppb Cr based on the adsorption of the first two tubes. Because the other four metals do not have concentration higher than 100 ppb (negative adsorption), the amount adsorbed from Table 2 may not be the maximum adsorption of MCM-48-TiO2 NP for those four metals. It may adsorb more than these values. In general, MT300 has the best adsorption for heavy metals, especially Pb, Cu, Cd, and As. For future experiment, the maximum capacity of the material for these heavy metals will be tested by filtering more contaminated water.

5. Project outcomes, presentations, publications (book chapter journals or conference proceedings)

Technical Presentation:

Vu, Trinh, Xueqing, Song, Jiajun Xu, "MCM Based Hybrid Mesoporous Materials for Water Treatment" 2016 National Capital Region Water Resources Symposium

Conference proceedings:

Vu, Trinh, Xueqing, Song, Jiajun Xu, "Design and Characterization of Nanoparticles Infused Mesoporous Materials for Environmental Applications", ASME 2016 International Mechanical Engineering Congress & Exposition (IMECE)

6. Student supports

It has provided an excellent opportunity for training undergraduate students, researchers and water resources professionals. Two undergraduate students have been involved in the project. Through working on the project the students become familiar with the aspects of wastewater management, nanotechnology, material synthesis and characterization theory and its application to pollutant treatment. The students were also given opportunities to present their work at professional conferences.

7. Extramural funding

The PI has received National Science Foundation funding after receiving this WRRI grant to support his research.

8. Conclusion

Recent advances suggest that many of the issues involving water quality could be resolved or greatly ameliorated using nanoparticles, nanofiltration or other products resulting from the development of nanotechnology. Utilization of specific nanoparticles either embedded in membranes or on other structural media that can effectively, inexpensively and rapidly render unusable water potable is being explored at a variety of institutions. In conclusion, MCM-48-TiO2 NP has been successfully synthesized. The materials have the ability to adsorb heavy metals from drinking water. Among the three NP sizes, 300 nm TiO2 NP gives the best adsorption for Cu, As, Pb, and Cd, but not the best for Cr. Even though 300 nm NP did not adsorb much of Cr, 15 nm NP adsorbed the most Cr (50.05 ppb). Overall, the materials are good adsorbents for Pb, Cd, As, and Cu. The next goal for future research is to determine the maximum capacity of the material (MT300, specifically) and to develop a method of removing organic matters from drinking water. Another goal is to research how to retain as much water as possible during filtration and how to ensure the turbidity of water after it runs through the material.

The impacts of the proposed activity are two-fold: 1. Innovative use of mesoporous nanomaterials with embedded nanoparticles on for treatment of industrial wastewater is another potentially useful application. Many factories generate large amounts of wastewater. Removal of contaminants and recycling of the purified water would provide significant reductions in cost, time, and labor to industry and result in improved environmental stewardship. Aquifer and groundwater remediation are also critical issues, becoming more important as water supplies steadily decrease and demand continues to increase. 2. In addition to obvious advantages for industrialized applications, the benefits for personal usage would also be enormous. Most of the industrial remediation technologies available today, while effective, very often are costly and cumbersome. A mesoporous material with embedded nanomaterials provides an effective way to removal toxic pollutants while maintain versatile and compact. The ultimate goal of developing new nanostructured materials for water filtration is to remove toxic compounds from subsurface and other environments in situ, and doing so rapidly, efficiently and within reasonable costs.
In addition, undergraduate students have been actively involved in the research, technical presentation and publication at regional and national conferences, in which an increase of participation and awareness of pre-university students have been achieved.

9. Acknowledgement

We want to acknownledge the funding support from DCWRRI for this research. We also want to thank Dr. Deksissa and his lab technicans (Yacov Assa and Sebhat Tefera, Lab

Technicians, Water Resources Lab, University of the District of Columbia) for constructive discussion and help with the Inductively Couple Plasma – Mass Spectrometer (ICP-MS) experiment.

9. References

1. Sarojam, Praveen. Analysis of Trace Metals in Drinking Water with the Optima 7000 DV ICP- OES. Shelton, CT: PerkinElmer.

2. U.S.EPA. 2016. Table of Regulated Drinking Water Contaminants.

3. Amin, M. T., Alazba, a a, & Manzoor, U. (2014). A Review of Removal of Pollutants from Water / Wastewater Using Different Types of Nanomaterials, 2014.

4. Bandyopadhyay, M. (2005). Synthesis of mesoporous MCM-48 with nanodispersed metal and metal oxide particles inside the pore system. Synthesis. Retrieved from http://www-brs.ub.ruhr-uni-bochum.de/netahtml/HSS/Diss/BandyopadhyayMahuya/diss.pdf

5. Boote, B., Subramanian, H., & Ranjit, K. T. (2007). Rapid and facile synthesis of siliceous MCM-48 mesoporous materials. Chemical Communications (Cambridge, England), (43), 4543–4545. http://doi.org/10.1039/b706633c

6. Paper, C., Askari, M. J., & Columbia, N. B. (2012). Investigation of water remediation by nanoparticles, (December 2015), 22–27. http://doi.org/10.13140/2.1.3110.2082

7. Lin, K., Pescarmona, P. P., Vandepitte, H., Liang, D., Van Tendeloo, G., & Jacobs, P. A. (2008). Synthesis and catalytic activity of Ti-MCM-41 nanoparticles with highly active titanium sites. Journal of Catalysis, 254(1), 64–70. http://doi.org/10.1016/j.jcat.2007.11.017

8. Tiwari, D. K., Behari, J., & Sen, P. (2008). Application of Nanoparticles in Waste Water Treatment. Carbon Nanotubes, 3(3), 417–433. Retrieved from http://scholar.google.com/scholar?hl=en&btnG=Search&q=intitle:Application+of+Nanoparticles+in+Waste+Water+Treatment#7

9. Lazar, M. A., Varghese, S., & Nair, S. S. (2012). Photocatalytic Water Treatment by Titanium Dioxide: Recent Updates. Catalysts, 2, 572–601. http://doi.org/10.3390/catal2040572

10. Budhi, S., Wu, C.-M., Zhao, D., & Koodali, R. (2015). Investigation of Room Temperature Synthesis of Titanium Dioxide Nanoclusters Dispersed on Cubic MCM-48 Mesoporous Materials. Catalysts, 5(3), 1603–1621. http://doi.org/10.3390/catal5031603

11.Mohan, D., & Pittman, C. U. (2007). Arsenic removal from water/wastewater using adsorbents-A critical review. Journal of Hazardous Materials, 142(1-2), 1–53. http://doi.org/10.1016/j.jhazmat.2007.01.006

12. Parida, K., Mishra, K. G., & Dash, S. K. (2012). Adsorption of toxic metal ion Cr(VI) from aqueous state by TiO2-MCM-41: Equilibrium and kinetic studies. Journal of Hazardous Materials, 241-242(SEPTEMBER), 395–403. http://doi.org/10.1016/j.jhazmat.2012.09.052

Water Pollution Prevention and Removal Using Nanostructured Smart Fluid with Switchable Surfactants

Basic Information

Title:	Water Pollution Prevention and Removal Using Nanostructured Smart Fluid with Switchable Surfactants
Project Number:	2015DC172B
Start Date:	3/1/2015
End Date:	2/28/2016
Funding Source:	104B
Congressional District:	District of Columbia
Research Category:	Water Quality
Focus Category:	Treatment, Wastewater, Hydrology
Descriptors:	None
Principal Investigators:	Jiajun Xu, Xueqing Song

Publications

1. Poudel,Naresh, Xueqing Song, Jiajun Xu. 2016. “Nanostructured Smart Fluid with UV Switchable Surfactants for Water Pollution Prevention and Removal”, ASME 2016 International Mechanical Engineering Congress & Exposition (IMECE)
2. Poudel, Naresh, Xueqing Song, Jiajun Xu. 2016. “Nanostructured Smart Fluid with UV Switchable Surfactants for Water Pollution Prevention and Removal” 2016 National Capital Region Water Resources Symposium. Oral Presentation.

Cover Page

Water Pollution Prevention and Removal Using Nanostructured Smart Fluid with Switchable Surfactants

Principal Investigators

Jiajun Xu

Department of Mechanical Engineering, University of the District of Columbia

Xueqing Song

Chemistry and Physics Department, University of the District of Columbia

April 22, 2016

1. Executive Summary

To restore and maintain the physical chemical and biological integrity of water bodies in the United States, there is an urgent need of developing effective and economical feasible solution for the prevention and treatment of contamination of water supplies caused by industrial wastes and storm water. In the last decade, many new techniques and methodologies have been proposed to remedy contaminated water which includes using micro/nanostructured membrane/filtration, nanoparticle catalytic, and chemical reaction etc. However, these methods are still evolving and often times, further cleaning/removal of the nanomaterials/surfactants added inside are needed which usually is time-consuming and expensive. This proposal research has explored and characterized a new nanostructured smart fluid system with switchable surfactants, which can "smartly" remove the pollutants along with itself under certain external stimulus.

More importantly, those methods are more focused on restoration rather than prevention of wastes in water. The broader goal of this research project is to assist in exploring a new water pollution prevention and restoration solution which can change the way industry operate the cleaning, manufacturing, oil recovery and other processes by providing a more feasible and efficient approach. Especially the surfactant, which is widely used in most industrial applications to enhance stability or reduce heat and mass transport limitations, rarely is an integral component of the final product. In these cases, surfactant removal and the breaking of the emulsion usually entails addition of heat, mechanical agitation, or chemical interfacial modification with the addition of an emulsion neutralizing agent. These treatments are not only costly; they often lead to product contamination and produce large volumes of surfactant-contaminated aqueous wastes. Via developing a "smart" switchable surfactant which can replace existing surfactant used in various industrial processes and perform "self-clean" process under external stimulus after finish its job, it is not only economically appealing, but also environmentally sustainable.

In this study, one "smart" switchable surfactant responsive to UV light has been developed by one of the PIs, and it will serve as a template system for water pollutant removal. The proposed research is very much useful for the District of Columbia because it can help improve the efficiency and capacity of wastewater treatment to meet the increasing volume of wastewater, especially in metropolitan area.

2. Introduction

Water pollution is a serious problem for human health and the environment and is one of main threats and challenges humanity faces today[12, 13]. Pollution loading from point and non-point sources continues to have significant impacts on our receiving waters, i.e., rivers, streams and lakes; in spite of massive public investments in drainage infrastructure (i.e., sewer systems and treatment plants) and the implementation of several federal and state regulations. Across our nation, thousands of waters are listed as impaired waters by a wide variety of pollutants. Based on the most recent state 303(d) lists, as of mid-2009, the national list encompassed over 43,000 impaired waters with over 73,000 impairments[2]. The pollutants including sediments, nutrients, metals and pathogens are

the most common pollutants included on state lists and the top ten listed impairments account over 75% of the total listings in the nation.

Especially, contamination of drinking water supplies from industrial waste is a result of various types of industrial processes and disposal practices. Industries that use large amounts of water for processing have the potential to pollute waterways through the discharge of their waste into streams and rivers, or by run-off and seepage of stored wastes into nearby water sources[1, 2]. Other disposal practices which cause water contamination include deep well injection and improper disposal of wastes in surface impoundments. More than 200,000 sources of waste water are regulated by the National Pollutant Discharge Elimination System (NPDES) permit program: 1. Agriculture (Run-off from crops contains pesticides, fertilizer, and sediment); 2. Fruit and Vegetable Processing (Waste water contains high concentrations of dissolved organic matter and may be highly alkaline from the use of lye); 3. Petroleum Refining (Oil is mixed with water in the refining process to remove salts and other impurities); 4. Pulp and Paper (The use of bisulfite and sulfurous acid or sulfur dioxide in the pulping process yields a waste sulfite liquor containing various wood by-products). In addition, the waste disposal practices which presently pose a threat to drinking water supplies include deep well injection of wastes and wastes that are dumped and retained in surface impoundments or evaporation ponds. A vast variety of industrial waste adds unto the difficulty and complexity of wastewater treatment.

In 2008, there were 14,780 municipal wastewater treatment plants operating in the United States. These plants ranged in size from a few hundred gallons per day (GPD) to more than 1440 million gallons per day (MGD). Early efforts in water pollution control began in the late 1800s with construction of facilities to prevent human waste from reaching drinking water supplies. Since the passage of the 1972 Amendments to the Federal Water Pollution Control Act (known as the Clean Water Act [CWA]), municipal wastewater treatment facilities have been designed and built or upgraded to abate an ever-increasing volume and diversity of pollutants. The CWA requires that municipal wastewater treatment plant discharges meet a minimum of secondary treatment. However, in 2008, nearly 37 percent of the municipal facilities produced and discharged effluent at higher levels of treatment than the minimum federal standards for secondary treatment[1].

To meet the challenge of keeping progress in wastewater pollution abatement ahead of population growth, changes in industrial processes and wastewater treatment technological developments are urgently needed. Many industrial applications reply on stabilization of emulsion during certain stages in cleaning, manufacturing, oil recovery and other processes. Surfactants are widely used during these processes to form emulsion during certain stage which, however, is useless after or before that process and becomes a liability that hinders separation of components. Eventually, untreated surfactants will mix with other industrial discharges such as metals, oil and grease, and other pollutants, and they can interfere with the operation of local sanitary sewers and waste water treatment plants, leading to the discharge of untreated or inadequately treated pollutants into local waterways [14-16]. On the other side, the Clean Water Act has standards for the permitted release of a limited amount of contaminants into waterways. This is an

incentive for industry to pre-treat their water by neutralizing the chemically active components, recycling, dilution or extraction and collection for proper disposal.
Developing an efficient and effective water pollution prevention and restoration solution which can dramatically reduce and remove the wastes generated in industrial process is critical to help business, federal facilities, local governments and tribes meet environmental regulatory requirements. The EPA‟ National Enforcement Initiatives, identified the needs for development of new regulations, systems and tools in waste water management. This study has answered this call.

While many waste water pretreatment and remediation technologies are available today, most of them very often are costly and/or time consuming, particularly pump-and-treat methods. Recent advances suggest that many of the issues involving water quality could be resolved or greatly ameliorated using nanostructure materials resulting from the development of nanotechnology [3-11, 17]. Nanostructured materials have two key properties that make them particularly attractive as waste water treatment: 1. on a mass basis, they have much larger surface areas than bulk particles; 2. they can also be functionalized with various chemical groups to increase their affinity towards target compounds. The waste water treatment using nanostructured materials provide an alternative approach.

This project proposed an innovative approach of waste water pollutant removal by using nanostructured smart fluids with switchable surfactants. It combines the state-of-art intelligent materials that dynamically alter their structures and properties on demand or in response to environmental changes, and can be switched between an „on‟ and „off‟ state, during which a switchable surfactant can undergo fully reversible interconversion between active and inactive form to „grab‟ and „deposit‟ unwanted chemical pollutants along with itself using external stimulus. This unique approach can bring breakthrough to waste water pollutants removal techniques and possibility of greatly reduce the cost while increase the capacity of wastewater treatment at little or no extra cost. More importantly, this project will not only conquer the problems in wastewater treatment, but will also advance the industrial processing techniques by replacing existing surfactants used in various industrial processes with this smart “self-cleanable” switchable surfactant which can greatly reduce the environmental impact.

This research has successfully synthesized and tested the “smart” switchable surfactant responsive to UV light, and it will serve as a template system for water pollutant removal. Common chemicals used for pesticide and phosphorus removal will be integrated into the switchable surfactant to remove these targeted pollutants from aqueous solution.

3. Methodologies

Materials and Method:

Materials: cetyltrimethylammonium bromide (CTAB), trans-ortho-methoxycinnamic acid (OMCA) were used to form the smart fluid. Solutions containing OMCA were prepared with a slight excess of base (NaOH), and CTAB was then added to these solutions to reach the final composition. Samples were stirred continuously under mild heat until they

became homogeneous. The solutions were then left to equilibrate overnight at room temperature before any experiments were conducted. CTAB/OMCA samples were irradiated with UV light. The samples were used for the following tests using appropriate techniques such as UV-vis spectroscopy, rheology, and SANS.

Characterization for heavy metals removal:

Rheological Studies: steady and dynamic rheological experiments were performed on an Brookfield rheometer. Samples were run at 25 °C on a cone-andplate geometry. Dynamic frequency spectra were obtained in the linear viscoelastic regime of each sample as determined by dynamic stress-sweep experiments.

Small Angle Neutron Scattering (SANS). SANS measurements were made on the NG-7 (30 m) beamline at NIST in Gaithersburg, MD. Neutrons with a wavelength of 6 Å were selected. A wide range of wave vectors from 0.004 to 0.4 Å-1 were used. Samples were studied in 2 mm quartz cells at 25 °C. The scattering spectra were corrected and placed on an absolute scale using calibration standards provided by NIST. The data are shown for the radially averaged intensity I versus the wave vector q) (4ð/ì) sin(õ/2), where ì is the wavelength of incident neutrons and õ is the scattering angle.

4. Results and Discussion

The structural diagram and rheological behavior of the UV sensitive smart fluid is shown below in the Figure 1.

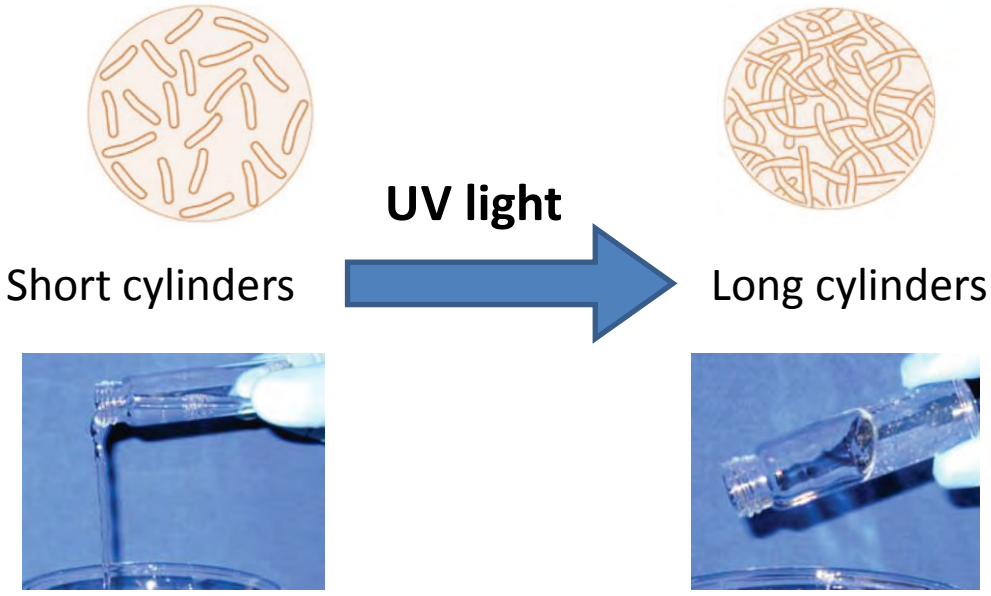

Figure 1. Structure digram of CTAB/OMCA smart fluid before and after UV irradiation

As shown here in Figure 1, the viscosity of the fluid changed dramatically after UV irradiation which changes from fluidic status to very viscoelastic form. The microstructure inside is proven to change from short cylinders to long cylinders after UV irradiation which has also been confirmed by the SANS study showed later.

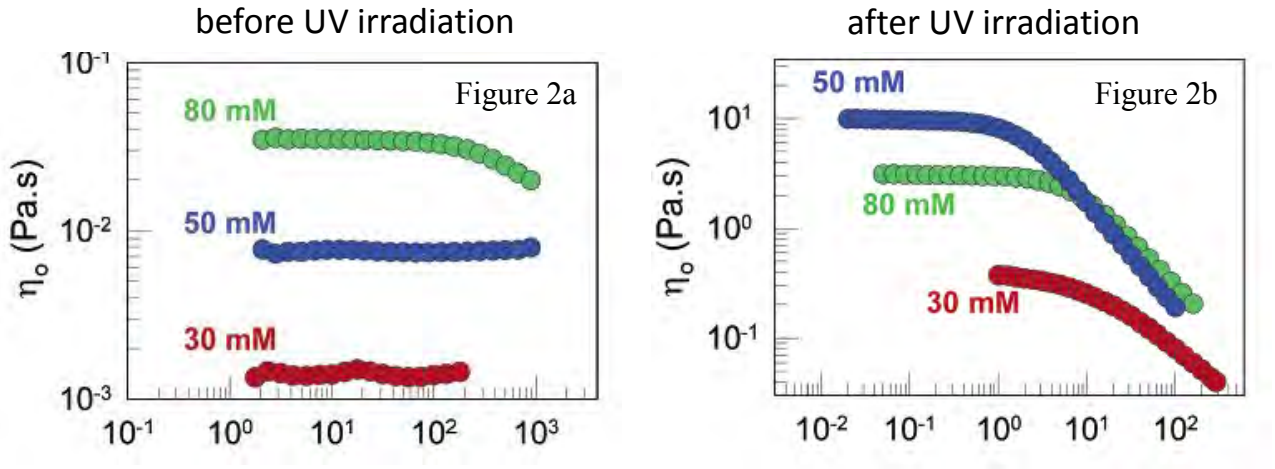

Figure 2. Rheological property of PR fluid before irradiation, and after UV irradiation.

In addition, the rheological data on selected CTAB/OMCA samples has also been shown here to quantify the light-induced rheological changes. Note that, following irradiation, CTAB/OMCA samples remain unaltered when stored under ambient conditions (exposure to visible light has no effect because OMCA has a negligible absorbance in the visible range of the spectrum). Thus, irradiated bsamples could be tested subsequently on the rheometer. Figure 2 shows steady-shear rheological data (viscosity vs shear rate) for three samples, each containing 60 mM CTAB, with OMCA concentrations of 30, 50, and 80 mM, respectively. Before irradiation (Figure 2a), the irradiated samples show negligible shear rate-dependence of their viscosities; i.e., their behavior is mostly Newtonian (only the 80 mM OMCA sample shows slight shear-thinning). Moreover, the viscosities are much lower compared to Figure 2a, with each sample showing a drop in viscosity by several orders of magnitude due to UV irradiation. Figure 2b shows the rheology of the same three samples after UV irradiation for 30 min. all three samples show shear-thinning behavior, with a plateau in the viscosity at low shear rates, followed by a decrease in viscosity at higher shear rates. The zero-shear viscosity is highest for the 50 mM OMCA sample, with a value of about 10 Pa.s (i.e., about 10,000 times the viscosity of water). With further increases in OMCA content, there is a drop in viscosity , and the 80 mM OMCA sample has a viscosity value of about 2 Pa.s. The measurements thus confirm the visual observations reported in Figure 1.

To better understand the microsrcture change inside the fluid before and after UV irradiation, samples were tested using SANS, in which the D_2O was used to achieve the required contrast between the micellar structures and solvent. SANS spectra (I vs q) are

shown in Figure 3 for the sample with CTAB/OMCA concentrations of 50/50 mM, respectively.

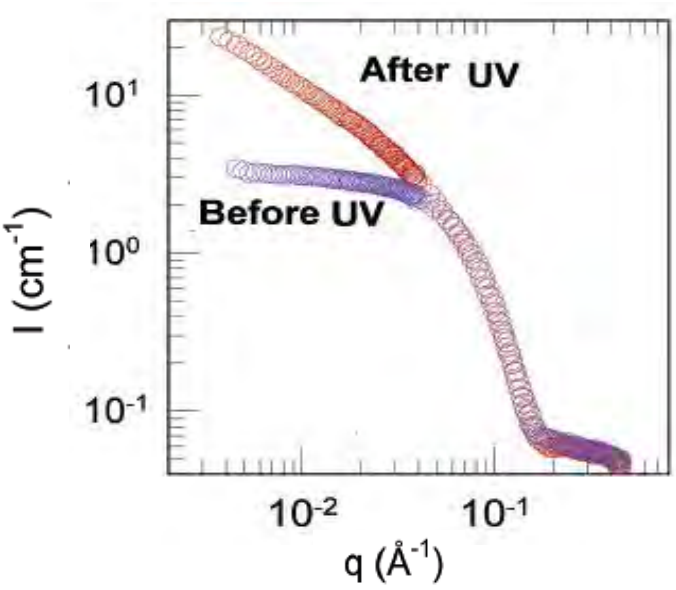

Figure 3. SANS curve of PR fluid before irradiation, and after UV irradiation.

As it can be seen from Figure 3, the irradiation causes a significant drop in the scattered intensity at low q. The drop in intensity is a direct, qualitative indication of a decrease in micelle size, which is consistent with our expectation. To obtain a more quantitative measure of micellar sizes, the SANS data was fitted using the standard modelingprotocol provided by NIST NCNR. For this sample (Figure 3), a large decrease in intensity is seen upon UV irradiation, presumably because the micelle sizes fall within the window probed by SANS. Before irradiation shows a plateau in SANS intensity at low q, which suggests the presence of smaller and more globular structures. The micelles in this case is ellipsoids of revolution. A good fit is obtained for prolate ellipsoids with radii of 22 and 40 Å, respectively, for their major and minor axes. After irradiation, the intensity asymptotes at low q to a slope of about -1, which is indicative of long, cylindrical structures. From the fit, the micellar radius is obtained to be about 22 Å, while their length is about 3000 Å. Thus, as expected, there is a dramatic increase in the largest dimension of the micelles (a factor of about 100) due to UV irradiation.

The SANS data thus confirm that the light-induced viscosity reduction in CTAB/OMCA mixtures is due to an increase in micelle size. The micellar size also suggests that there is a photoisomerization of sample under UV irradiation.

5. Project outcomes, presentations, publications (book chapter journals or conference proceedings)

Technical Presentation:

Naresh Poudel, Xueqing, Song, Jiajun Xu, "Nanostructured Smart Fluid with UV Switchable Surfactants for Water Pollution Prevention and Removal" 2016 National Capital Region Water Resources Symposium

Conference proceedings:

Naresh Poudel, Xueqing, Song, Jiajun Xu, "Nanostructured Smart Fluid with UV Switchable Surfactants for Water Pollution Prevention and Removal", ASME 2016 International Mechanical Engineering Congress & Exposition (IMECE)

6. Student supports

It has provided an excellent opportunity for training undergraduate students, researchers and water resources professionals. Two undergraduate students have been involved in the project. Through working on the project the students become familiar with the aspects of wastewater management, nanotechnology, material synthesis and characterization theory and its application to pollutant treatment. The students were also given opportunities to present their work at professional conferences.

7. Extramural funding

The PI has received National Science Foundation funding after receiving this WRRI grant to support his research.

8. Conclusion

It has shown here that a UV sensitive smart fluid has been successfully synthesized and characterized. The result has shown that this type of CTAB/OMCA based smart fluid can change their rheological property dramatically after UV irradiation and it can be dissolved in water for water pollutant removal.

This project provided an innovative approach of waste water pollutant removal by using nanostructured smart fluids with switchable surfactants. It combines the state-of-art intelligent materials that dynamically alter their structures and properties on demand or in response to environmental changes, and can be switched between an „on" and „off" state, during which a switchable surfactant can undergo fully reversible interconversion between active and inactive form to „grab" and „deposit" unwanted chemical pollutants along with itself using external stimulus. This unique approach will bring breakthrough to waste water pollutants removal techniques and possibility of greatly reduce the cost while increase the capacity of wastewater treatment at little or no extra cost. More importantly, this project will not only conquer the problems in wastewater treatment, but will also advance the industrial processing techniques by replacing existing surfactants used in

various industrial processes with this smart “self-cleanable” switchable surfactant which can greatly reduce the environmental impact.

The next step is to study the efficiency of pollutant removal using this smart fluid as a template. In general, there are two approaches for that: 1. CTAB itself is a common surfactant used in many chemical process so it can be removed directly using this smart fluid and UV irradiation; 2. the CTAB surfactant and OMCA combination can servce as a carrier which can be used with specific functioning group to remove certain pollutant.

In addition, undergraduate students have been actively involved in the research, technical presentation and publication at regional and national conferences, in which an increase of participation and awareness of pre-university students have been achieved.

9. Acknowledgement

We want to acknownledge the funding support from DCWRRI for this research. We also want to thank Dr. Hamouda from NIST NCNR for constructive discussion and help with the SANS experiment.

10. References

[1] 2013, "Emerging Technologies for Wastewater Treatment and In-Plant Wet Weather Management ", EPA.

[2] 2011, "Introduction to the National Pretreatment Program," EPA

[3] Cross, K. M., Lu, Y. F., Zheng, T. H., Zhan, J. J., McPherson, G., and John, V., 2009, "Water Decontamination Using Iron and Iron Oxide Nanoparticles," Nanotechnology Applications for Clean Water, pp. 347-364.

[4] Wiesner, M., Li, Q. L., Burgess, J., Kaegi, R., and Dixon, D., 2013, "Progress towards the responsible application of nanotechnology for water treatment," Water Research, 47(12), pp. 3865-3865.

[5] Kar, S., Subramanian, M., Ghosh, A. K., Bindal, R. C., Prabhakar, S., Nuwad, J., Pillai, C. G. S., Chattopadhyay, S., and Tewari, P. K., 2011, "Potential of nanoparticles for water purification: a case-study on anti-biofouling behaviour of metal based polymeric nanocomposite membrane," Desalination and Water Treatment, 27(1-3), pp. 224-230.

[6] Brame, J., Li, Q. L., and Alvarez, P. J. J., 2011, "Nanotechnology-enabled water treatment and reuse: emerging opportunities and challenges for developing countries," Trends in Food Science & Technology, 22(11), pp. 618-624.

[7] Kumar, S., Ahlawat, W., Bhanjana, G., Heydarifard, S., Nazhad, M. M., and Dilbaghi, N., 2014, "Nanotechnology-Based Water Treatment Strategies," Journal of Nanoscience and Nanotechnology, 14(2), pp. 1838-1858.

[8] Laera, G., Lens, P. N. L., Virkutyte, J., Jegatheesan, V., Kim, S. H., and AlAbed, S., 2013, Nanotechnology for water and wastewater treatment: potentials and limitations.

[9] Lens, P. N. L., Virkutyte, J., Jegatheesan, V., Kim, S. H., and AlAbed, S., 2013, Nanotechnology for Water and Wastewater Treatment.

[10] Savage, N., and Diallo, M. S., 2005, "Nanomaterials and water purification: Opportunities and challenges," Journal of Nanoparticle Research, 7(4-5), pp. 331-342.

[11] Qu, X. L., Alvarez, P. J. J., and Li, Q. L., 2013, "Applications of nanotechnology in water and wastewater treatment," Water Research, 47(12), pp. 3931-3946.

[12] Perkins, F., 1993, "HUMAN-DEVELOPMENT REPORTS 1990-92, UNITED-NATIONS DEVELOPMENT PROGRAM - UNDP," Economic Record, 69(204), pp. 83-84.

[13] Skip, B., 2009, "WATER POLLUTION IMPACT ON IMMUNE STATUS OF HUMAN ORGANISM AND TYPICAL EPIDEMIC PROCESSES: MATHEMATIC MODEL, OBTAINING RESULTS, THEIR ANALYSIS AND PROPOSALS TO MANAGE RISK FACTORS," Risk Management of Water Supply and Sanitation Systems, pp. 199-204.

[14] 2006, ""Switchable" surfactants to beat oil spills," Tce(783), pp. 15-15.

[15] Liu, Y. X., Jessop, P. G., Cunningham, M., Eckert, C. A., and Liotta, C. L., 2006, "Switchable surfactants," Science, 313(5789), pp. 958-960.

[16] Chu, Z. L., Dreiss, C. A., and Feng, Y. J., 2013, "Smart wormlike micelles," Chemical Society Reviews, 42(17), pp. 7174-7203.

[17] Bang, I. C., and Jeong, J. H., 2011, "NANOTECHNOLOGY FOR ADVANCED NUCLEAR THERMAL-HYDRAULICS AND SAFETY: BOILING AND CONDENSATION," Nuclear Engineering and Technology, 43(3), pp. 217-242.

Evaluating Impacts of Urban Water Ways on the Transportation Networks for the District of Columbia

Basic Information

Title:	Evaluating Impacts of Urban Water Ways on the Transportation Networks for the District of Columbia
Project Number:	2015DC173B
Start Date:	3/1/2015
End Date:	2/28/2016
Funding Source:	104B
Congressional District:	District of Columbia
Research Category:	Engineering
Focus Category:	Hydrology, Water Quantity, Management and Planning
Descriptors:	None
Principal Investigators:	Yao Yu, Pradeep K. Behera

Publication

1. Laura Rojas, Pradeep K Behera, Yao Yu. 2016. Impacts of Urban Water Bodies on the Transportation Networks for the District of Columbia. 2016 National Capital Region American Water Resources Association 4th Annual Water Resources Symposium: Rethinking the Value of Water: Innovations in Research, Technology, Policy, and Management, Washington, DC, Oral Presentation.

Impacts of Urban Water bodies on the Transportation Networks for the District of Columbia

Progress Report

Dr. Pradeep K. Behera, PE, Principal Investigator
Laura Rojas, Civil Engineering Major
Department of Civil Engineering
University of the District of Columbia

April 22, 2016

1. Executive Summary

Transportation infrastructure is intrinsically connected with water bodies in many ways that include bridges, culverts, and road systems adjacent to any type of water bodies. Transportation infrastructure has been typically developed under the assumption that climate and weather patterns remain constant through its service life of road system. However, under climate change scenario, there is a need to analyze the interaction between urban water ways and transportation infrastructure from not only public safety view point but also operation and maintenance of transportation systems. The potential climate change can have significant impacts on our water resources and related sectors such as water availability, flooding, urban infrastructures, water quality, ecosystems, coastal areas navigation, hydropower, economy and other energy (USGS, 2009). In order to understand the impact of water bodies on the transportation infrastructure, this research has collected, integrated and utilized available information about extreme wet-weather events, urban water way in the district, elevations of flood plain and local transportation infrastructure. The study considers the extreme events include 100 year storms and a 10 ft river surge during hurricanes or extreme events. During the extreme events, what percentage of roads are affected is assessed through digital maps which provides the vulnerability assessment of transportation network during the extreme events.

2. Introduction

Long-term weather and climate play significant roles in the planning, design, construction, operation, maintenance of the transportation system. For example, from trivial events like a light rain or light fog that can slow down traffic flow, to extreme events, such as

floods and hurricanes, which can significantly disrupt, and even shut down large parts of transportation network for extended time periods. The core transportation infrastructure of Washington DC include streets and highways, bridges, culverts, traffic lighting systems and traffic signage etc. District of Columbia Department of Transportation (DDOT) owns and maintains over 4,000 lane miles of roadways and streets, 240 bridges and tunnels, 68,000 streetlights and over 1400 signalized intersections. The planning, design, maintenance, operation, and development of this huge infrastructure requires DDOT to develop systematic methods to ensure that its infrastructure can tolerate the extreme events and minimize effects of local disturbance, malfunction and system failures. Moreover, public safety has been a key issue during extreme weather related to issues in most of the metropolitan areas, including Washington DC. Almost half a million people come to nation's capital on the working days from the surrounding counties from Maryland and Virginia for work, business, education and visits.

Since the publication of Intergovernmental Panel on Climate Change (IPCC) Report in 2007, many federal, state and local agencies have been developing guidelines for planning, design, operation of transportation systems that include the potential impacts of climate change on the system in a short-term and long-term basis. The primary urban waterways of the DC include Potomac River, Anacostia River and Rock Creek and their tributaries. There are a number of hydraulic structures in the form of culverts to bridges are located within the waterways which facilitate the transportation. Typically, transportation infrastructure has been designed based on event scenarios occurring with short return-period or developed under the assumption that climate and weather patterns remain constant through its service life. With growing climate change impacts and changing land use composition, a better understanding of

these changes and impacts is needed such as: climate projections and uncertainties in these projections; vulnerabilities of transportation infrastructure; and strategies needed to adapt the infrastructure to address these changes. This information can help local agencies to come up with an adaptation plan to prepare and adapt its assets for changes in climate.

3. Research Methodology

This research is focused on analyzing the relationship between the Transportation Network with the adjacent water bodies (i.e., rivers, lakes) in order to identify how the transportation infrastructures are going to be mainly affected during the extreme events. The extreme events include 100 year storms and river surge during hurricanes or extreme events. The research will utilize the available data for the Washington DC, specifically focused on the Federal Triangle area. The research methodology includes as follows:

- Collect GIS transportation data from OCTO for the Washington DC.
- Analyze the total miles of roads located in Washington DC.
- Collect GIS flooding data from FEMA, OCTO and US Army Corps of Engineers public domain web sites (the extreme events considered in this study include 100-yr storm event and 10 ft. elevation of surge data).
- Add flooding data to the transportation layout in order to create one complete digital map of transportation network and water bodies.
- Evaluate the total miles of roads affected by the elevation of the water.
- Determine the total miles of roads affected by the water in the Federal Triangle area.
- Tabulate the results to get the percentage of roads under the water under various conditions to show the vulnerability during the extreme events.

4. Results and Discussion

The capital of the United States, Washington DC, was designed by the engineer-architect; Pierre-Charles L'Enfant. His design is represented in the following map from 1835 (figure 1). As you can see, the National Mall and adjacent areas were originally underwater and were filled as L'Enfant's plan was realized. That is why this are of DC is one of the most vulnerable for flooding.

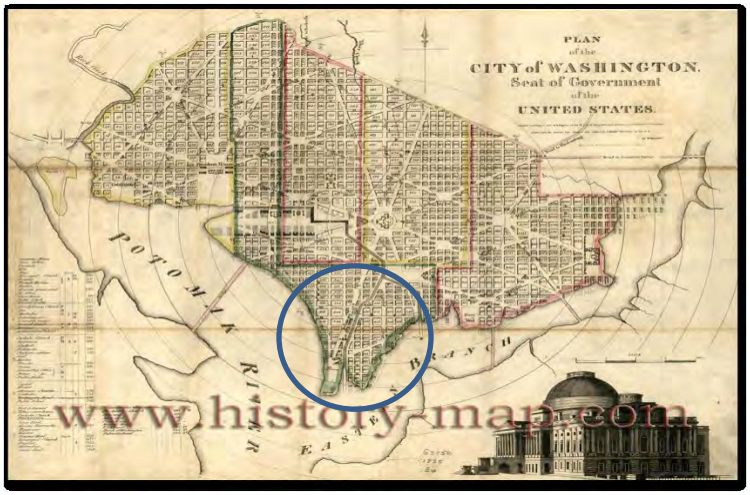

Figure 1: Map of Washington DC in 1835

Washington DC Transportation System

Based on the ASCE Report Card (2013), *"Washington DC is rank as one of America's most congested cities"*. In the Metropolitan DC area, approximately 9.7 million motorists cover 3,814 miles causing drivers an estimated 204 million hours of delay, and this is one of the value is one of the highest in United States. On the other hand, 47% of DC.'s roads are in good condition, and 25% of which are in poor or worse condition. Following Table 1 presents classification of transportation networks of Washington DC: Interstates, Local, Public Access, Minor Arterial and Collectors [1].

Type of Road	Miles	Lane Miles
Interstate	11.82	77.51
Public Access	122.43	510.83
Minor Arterials	163.32	429.51
Collectors	156.64	305.32
Local	1047.23	2094.45

Table 1: Types and lengths of Transportation Infrastructures

While the number of miles driven in D.C. is expected to increase by a modest 14% by 2040, the total hours of delay caused by congestion are expected to increase by 43%. If this projection comes true, it will translate into significant costs for drivers and the broader society, in longer travel times, increased fuel consumption, increased greenhouse gas emissions, and worsening air quality. It is attributed that these estimations have been collected taking into the consideration mainly an increase on the population and the number of drivers in Washington DC.

Flooding and Storm water in Washington DC

Since the publication of the Intergovernmental Panel on Climate Change documents (IPCC, 2007), there has been a growing interests among scientists, engineers, governments and public to understand climate change issues and its associated impacts. Climate change and water resources management are closely related because climate change affects the hydrologic cycle directly. The potential climate change can have significant impacts on our water resources and related sectors such as water availability, flooding, urban infrastructures, water quality, ecosystems, coastal areas navigation, hydropower, economy and other energy (USGS, 2009). As a results water resources managers who play an active role in planning, designing, operating and maintaining these water resources related systems will also be impacted by climate change (Brekke, et. al, 2009). With the Climate Change, sea level rise is one of the consequences. It is

estimated that there is a certain chance of flooding above 6 feet by 2040 and 10 feet by the end of Century. [3]. Washington DC is located at the confluence of the Potomac and Anacostia Rivers, which is relatively low land area highly susceptible to periodic flooding. Over the period , urban development has increased impervious areas significantly, reduced vegetation coverage, and further exacerbated flooding and storm water runoff through the entire watershed. [2]

The drainage system of Downtown DC which was planned and designed Century ago has been at the limited sewer capacity which makes the area susceptible to interior flooding. The vulnerability of the Federal Triangle during the flooding is very high and as per the NCPC report "While flooding in downtown DC is relatively infrequent, the concentration of key federal agencies and the huge federal, local, and private costs associated with recovering from even periodic floods warrants a close examination of cost-effective solutions. Moreover, future growth will further strain the system's already limited capacity." [2]

Federal Triangle Area

The Federal Triangle is a triangular area formed by 15th Street NW, Constitution Avenue NW, Pennsylvania Avenue NW, and E Street NW. Seven of the buildings in Federal Triangle were built by the U.S. federal government in the early and mid-1930s as part of a coordinated construction plan that has been called "one of the greatest building projects ever undertaken"[4]

The Federal Triangle study area is in the lowest point of a large drainage basin in DC, which is responsible for Constitution Avenue is prone to flooding, even during small rain events.

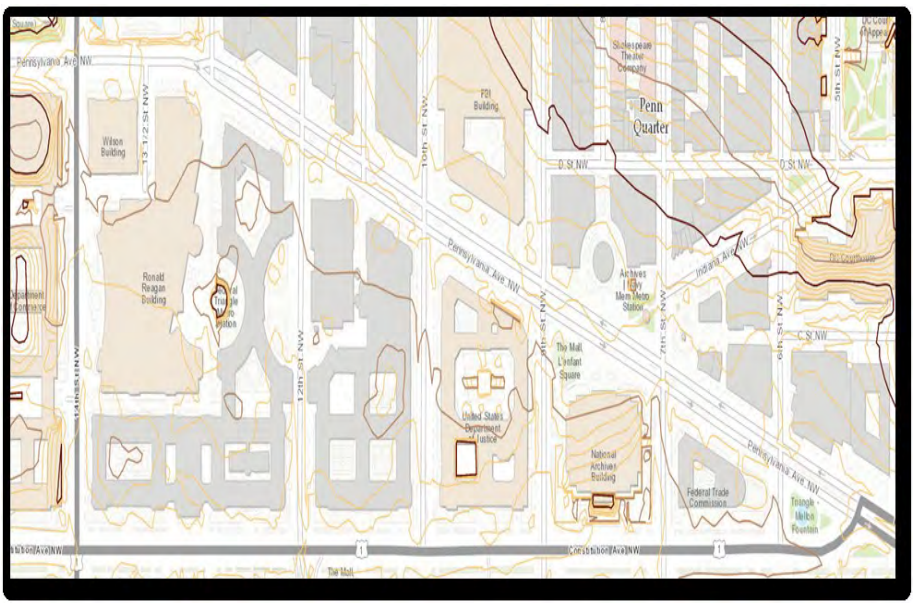

Figure 2. Federal Triangle Topographic Map

One of the main problems in this area is because the sewer lines in the study area is not designed to handle storm water volumes exceeding a 15-year storm event. Mainly, The Federal Triangle study area is in the lowest point of a large drainage basin in DC, which is why Constitution Avenue is prone to flooding, even during small rain events. Also, the existing sewer system is not designed to absorb and discharge storm water, when there is a big storm the combined sewer system was discharging the storm water. [2]

Interaction of 100 Year flood on the Transportation Network

Figure 1 presents the 100 year flood inundation areas. This flood inundation area was layered over the transportation network layer using the GIS analysis. The estimation of length of transportation network was obtained with and without the flood inundation. Table 1 presents the results.

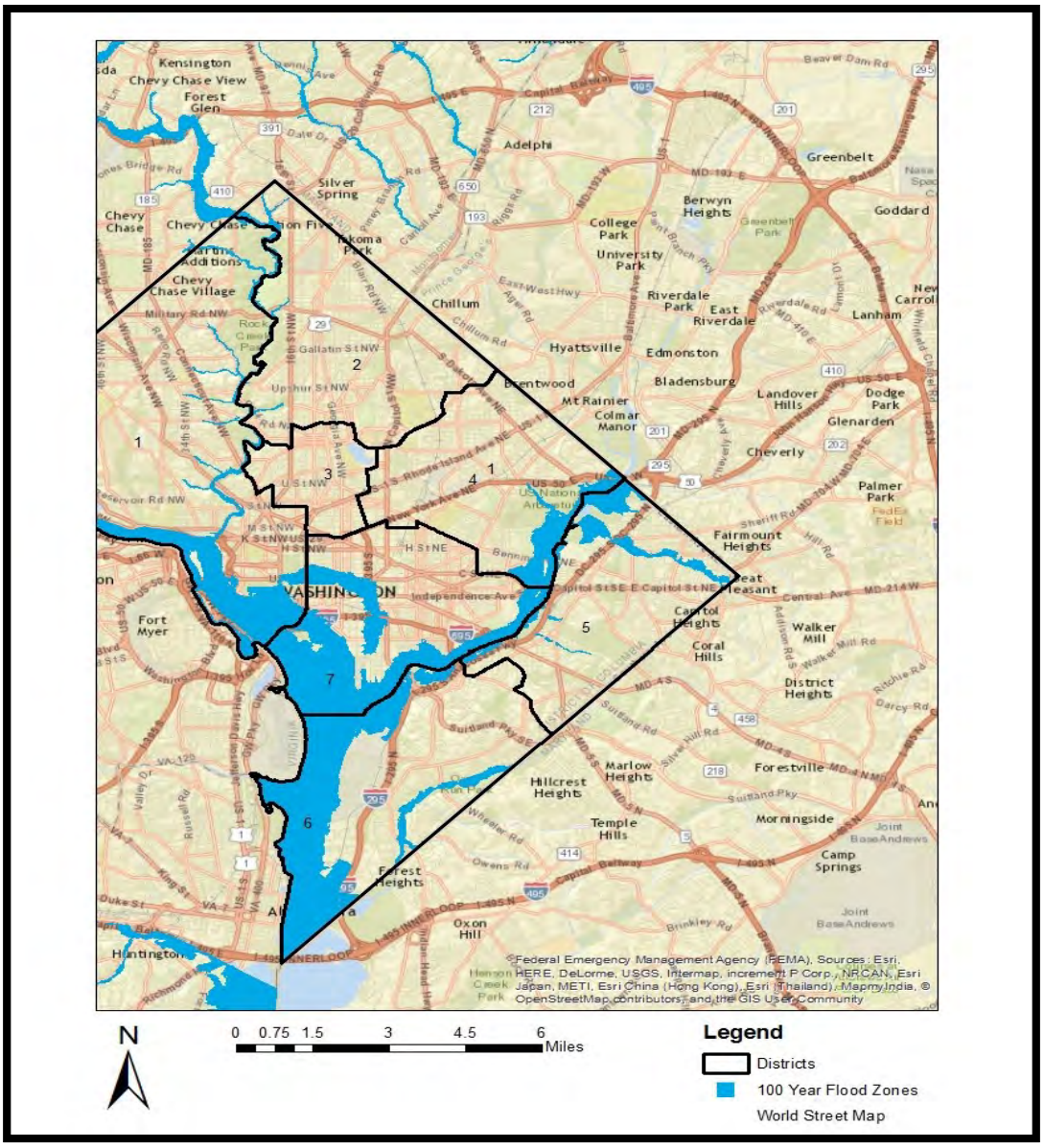

Figure 3: Inundation of areas during a 100 year Storm Event

Table 2. Total Roads affected 100 yr. Storm

Zone	Street Name Close to the water bodies	Total miles	Estimation of Inundation Length in Miles	Percentage of Length affected
1	Canal Road NW	5.09	0.00	0.0
	US Route 29	3.19	1.42	44.5
	Rock Creek and Potomac Pky	6.16	6.16	100.0
	I 66 W	2.08	0.70	33.7

Zone	Street Name Close to the water bodies	Total miles	Estimation of Inundation Length in Miles	Percentage of Length affected
	George Washington Memorial Pky	2.46	0.65	26.6
	Constitution Avenue	2.62	0.12	4.6
	Ohio DR SW	2.30	2.30	100.0
	Independece Ave	0.46	0.46	100.0
	17th Street	2.50	0.00	0.0
	M Street	2.43	0.53	21.8
	Masashutess Av	3.24	0.34	10.6
	Wisconcin Ave	6.69	0.00	0.0
	US -50	2.85		0.0
	Connecticut Ave	7.41	0.21	2.9
	Military Road	3.66		0.0
	Oregon Ave	2.57	0.36	14.0
	Chain B	0.39	0.19	48.0
	Broad Branch Road	4.29	2.45	57.1
2	----			
3	----			
4	Benning Road	**3.75**	**0.69**	18.4
5	Nanni Helenn Bourroughs	**2.71**	**2.46**	90.9
6	Anacostia Rdw	**7.41**	**1.31**	17.6
7	1695-S	4.67	1.43	30.6
	US - 1	2.68	2.68	100.0
	Pennsylvania Ave	1.01	1.01	100.0
	Independence Ave	4.45	0.41	9.3
	12th Street	1.32	1.32	100.0

Federal Triangle Area Analysis

To understand the impact of extreme events on the transportation systems within the Federal Triangle area, a GIS analysis was conducted. Figure 4 presents the 100 year flood inundation areas within the Federal Triangle Area. Table 4 presents the total lengths of road and inundation length of each road. Figure 5 and Table 5 presents the road lengths and inundation lengths during a 15 year storm. Figure 6 presents the graphical representation of inundation of individual roads which depicts the vulnerability of transportations network during the extreme events.

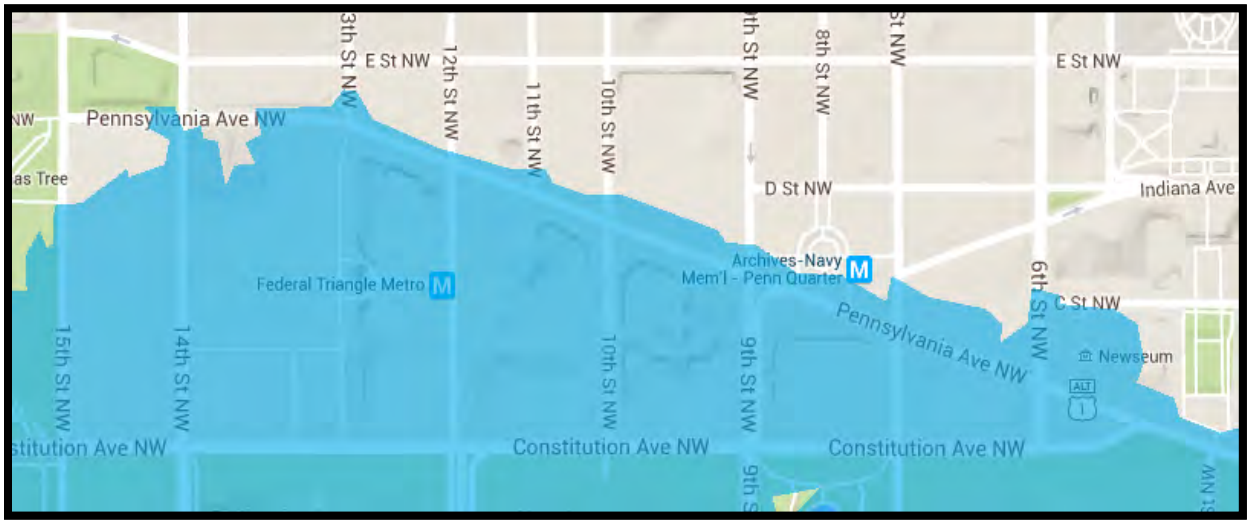

Figure 4: GIS Analysis Federal Triangle Area for a 100 Yr. Storm

Table 4. Total Roads affected 100 yr. Storm

Street Name Close to the water bodies	Total miles	Estimation of Inundation Length in Miles	Percentage of Length affected
6th	0.04	0.04	100
7th	0.08	0.08	100
9th	0.11	0.11	100
10th	0.16	0.16	100
12th	0.19	0.19	100
13th	0.07	0.07	100
14th	0.23	0.23	100
15th	0.23	0.17	74
Constitution Av	0.82	0.82	100
Pennsylvania Av	0.78	0.12	15

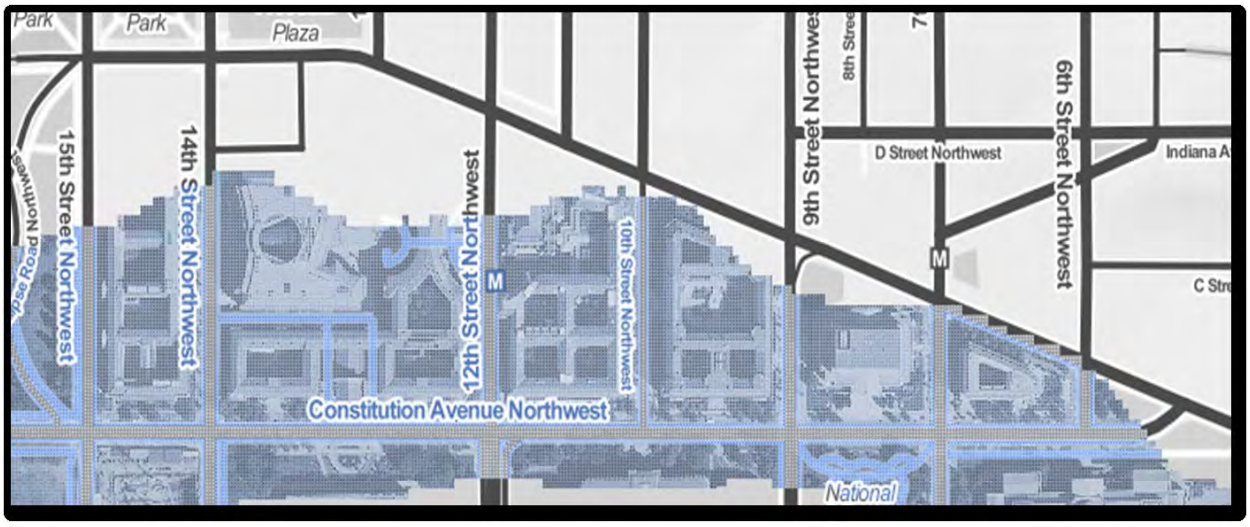

Figure 5. GIS Analysis Federal Triangle 15 yr. Storm

Table 5. Total Roads affected 15 yr. Storm

Street Name Close to the water bodies	Total miles	Estimation of Inundation Length in Miles	Percentage of Length affected
6th	0.04	0.04	100
7th	0.08	0.08	100
9th	0.11	0.08	73
10th	0.16	0.14	88
12th	0.19	0.13	68
13th	0.07	0	0
14th	0.23	0.15	65
15th	0.23	0.12	52
Constitution Av	0.82	0.78	95
Pennsylvania Av	0.78	0.11	14

- Total miles of roads cover for a 100yr storms event

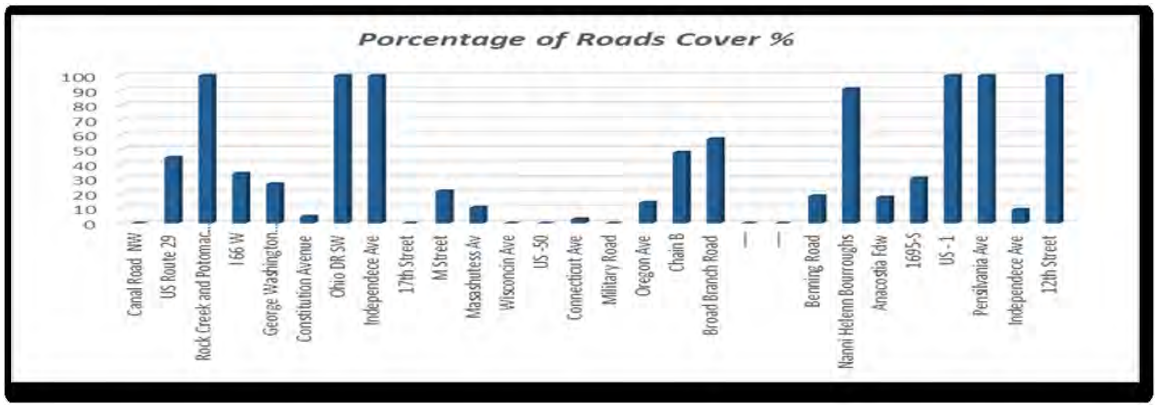

- Total miles of roads cover for a 100yr storms event Federal Tringle

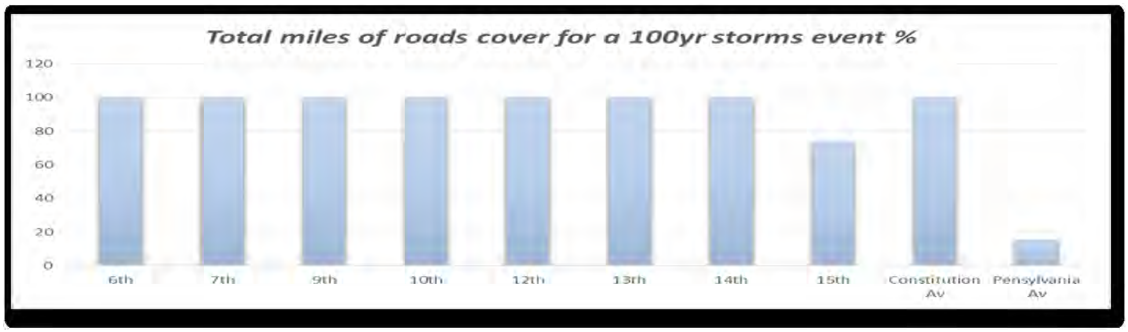

- Total miles of roads cover for a 15 yr. storms event Federal Tringle

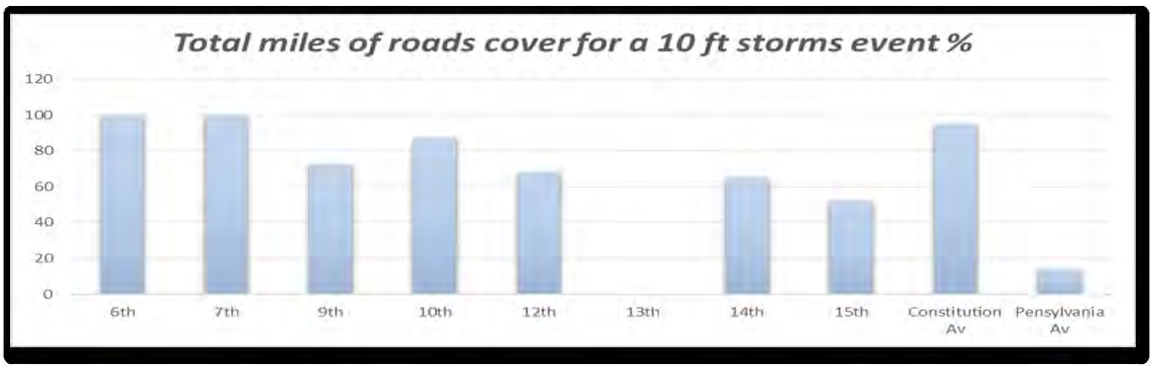

Figure 6: Graphical representation of inundation by each of the roads

5. Project outcomes, presentations, publications (book chapter journals or conference proceedings)

The research results were presented in the following symposium

Impacts of Urban Water Bodies on the Transportation Networks for the District of Columbia. 2016 National Capital Region Water Resources Symposium: Rethinking the Value of Water: Innovations in Research, Technology, Policy, and Management, Laura Rojas, Undergraduate Student, Pradeep K Behera, Professor, Yao Yu, Assistant Professor, Department of Civil Engineering, University of the District of Columbia, Washington D.C.

6. Student supports

Two civil engineering students were trained in the project. One student was directly involved in the research. Through the research, the student was able to learn the GIS and apply to a problem.

7. Conclusions

This research collected data on transportation network and water surface elevation during extreme wet weather events for Washington DC and analyzed. According with the results it is found that Washington DC transportation network and adjacent water bodies are strongly related and road network will be affected by the high depth of water during extreme events, especially in the Downtown area. Federal Triangle is one of the most important areas in Washington DC which will be one of the most affected by both river and interior drainage flood events. A 100 yr. storm event will directly inundate 31% of the roads within the Washington DC and 15 yr. storm will inundate 19% of the roads located within the Washington DC. In the federal triangle area, 100 year storm will inundate most of the roads and a 15 year storm will inundate half of the roads. There is a need to analyze the interaction between transportation network and adjacent water body elevation for various return period storms.

Acknowledgement

The authors of the report acknowledges the funding support by DC WRRI and modeling and simulation lab facilities of School of Engineering and Applied Science of the University of the District of Columbia, Washington DC.

Reference

[1] http://www.infrastructurereportcard.org/district_of_columbia/dc-overview/

[2] https://www.ncpc.gov/DocumentDepot/Publications/FloodReport2008.pdf

[3] http://ss2.climatecentral.org/#16/38.8946/-77.0282?show=satellite&projections=0-RCP85-SLR&level=10&unit=feet&pois=hide

[4] https://en.wikipedia.org/wiki/Federal_Triangle

[5] http://opendata.dc.gov/

[6] http://nld.usace.army.mil/egis/f?p=471:32:7321415511608::NO:::

[7] http://www.infrastructurereportcard.org/district_of_columbia/dc-overview/

[8] htttp://www.history –map.com

[9] USGS Report (2009), "Climate Change and Water resources Management: A Federal Perspective, Circular 1331, U.S. Department of Interior and U.S. Geological Survey.

[10] Brekke, L.D., Julie E. Kiang, J. R. Olsen, R. S. Pulwarty, D. A. Raff, D. P. Turnipseed, R. S. Webb and K. D. White., "Climate Change and Water Resources Management: A Federal Perspective", 2009, Circular 1331, U.S. Department of Interior and U.S. Geological Survey

Potomac River Stage Forecasting Using a Hybrid Particle Swarm Optimization and Evolutionary Algorithm (PSO-EA) Algorithm with LS-SVM

Basic Information

Title:	Potomac River Stage Forecasting Using a Hybrid Particle Swarm Optimization and Evolutionary Algorithm (PSO-EA) Algorithm with LS-SVM
Project Number:	2015DC174B
Start Date:	3/1/2015
End Date:	2/28/2016
Funding Source:	104B
Congressional District:	District of Columbia
Research Category:	Engineering
Focus Category:	Education, Hydrology, Models
Descriptors:	None
Principal Investigators:	Nian Zhang, Pradeep K. Behera

Publications

1. Zhang, Nian, Tilaye Alemayehu, and Pradeep Behera. 2015. “Nonlinear Autoregressive (NAR) Forecasting Model for Potomac River Stage Using Least Squares Support Vector Machines (LS-SVM)”, International Journal of Innovative Technology and Exploring Engineering (IJITEE), vol. 4, no. 9, pp. 1-9.
2. Zhang, Nian, Roussel Kamaha, and Pradeep Behera .2015. “Prediction of Surface Water Supply Sources for the District of Columbia Using Least Squares Support Vector Machines (LS-SVM) Method”, Advances in Computer Science: an International Journal (ACSIJ), vol. 4, issue 1, no.13, pp. 47-51.
3. Rochac, J. F. Ramirez, Nian Zhang, and Pradeep Behera. 2016. “Design of Adaptive Feature Extraction Algorithm Based on Fuzzy Classifier in Hyperspectral Imagery Classification for Big Data Analysis,” The 12th World Congress on Intelligent Control and Automation (WCICA 2016), Guilin, China.
4. Zhang, Nian. 2016. “Cost-Sensitive Spectral Clustering for Photo-Thermal Infrared Imaging Data,” 2016 Sixth International Conference on Information Science and Technology (ICIST), Dalian, China.
5. Rochac, Juan F. Ramirez Rochac and Nian Zhang, 2016. “Reference Clusters Based Feature Extraction Approach for Mixed Spectral Signatures with Dimensionality Disparity,” 10th Annual IEEE International Systems Conference (IEEE SysCon 2016), Orlando, Florida.

Potomac River Stage Forecasting Using a Hybrid Particle Swarm Optimization and Evolutionary Algorithm (PSO-EA) Algorithm with LS-SVM

Final Report

Nian Zhang, Ph.D.
Department of Electrical and Computer Engineering

Pradeep K. Behera, Ph.D., P.E., D. WRE
Department of Civil Engineering

Submitted to DC Water Resources Research Institute,
University of the District of Columbia

April 2016

1. Executive Summary

This research project investigates the ability of a least-squares support vector machine (LS-SVM) model to improve the accuracy of streamflow forecasting. Cross-validation and grid-search methods are used to automatically determine the LS-SVM parameters in the forecasting process. To assess the effectiveness of this model, streamflow records from Geological Survey (USGS) gaging station 1652500 on Four Mile Run of the Potomac River, were used as case studies. The performance of the LS-SVM model is compared with the recurrent neural networks model trained by Levenberg-Marquardt backpropagation algorithm. The results of the comparison indicate that the LS-SVM model is a useful tool and a promising new method for streamflow forecasting.

2. Introduction

In regard to stormwater runoff, how urbanized a watershed is or how developed a watershed is can be characterized by the degree of imperviousness found in the watershed [1]. A more urbanized watershed will have a greater percentage of area covered by impervious structures, i.e., roadways, rooftops, sidewalks, parking lots, etc. The effects of these impervious areas create higher peak flows and lower base flows in the watershed tributaries. These effects are most evident in the higher frequency rain/flood events, and they diminish as the range of magnitudes increases, i.e. the initial abstractions (infiltration, interception, and surface storage) become less significant when measured against rainfall for a large event, e.g. a 100-year rainfall event.

Potomac River was determined to be one of the most polluted water bodies in the nation mainly due to the CSOs and stormwater discharges and wastewater treatment plant discharges. This highly urbanized Potomac River watershed suffers from serious water quantity problems including flooding and stream bank erosion. Of approximately 10,000 stream miles assessed in the watershed, more than 3,800 miles were deemed “threatened” or “impaired”. The middle Potomac sub-watershed, including Washington, DC, contains both the greatest percent impervious area and the greatest population density, which is home to 3.72 million or about 70% of the watershed’s population. In the next 20 years, the population of the Potomac watershed is expected to grow 10% each decade, adding 1 million inhabitants to reach a population of 6.25 million.

In this regard, it is imperative to provide a reliable streamflow forecasting tool at various locations on the middle Potomac sub-watershed. Engineers, water resources professionals, and regulatory authorities need this streamflow information for planning, analysis, design, and operation & maintenance of water resources systems (e.g., water supply systems, dams, and hydraulic structures). Currently USGS provides the streamflow data at various locations in the form of gage height and discharge volume at specific locations, and we used this input to design a reliable prediction model.

Recently a variety of computational intelligence has been proposed to address the water quantity prediction problem. In [2][3][4], a predictive model based on recurrent neural networks with the Levenberg-Marquardt backpropagation training algorithm to forecast the stormwater runoff. In [5], a recurrent neural network based predictive model was trained by a combination of particle

swarm optimization and evolutionary algorithm to forecast the stormwater runoff discharge. Recent developments of least squares support vector machine (LS-SVM) has attracted an increasing attention in the fields of time series prediction [6]-[17]. However the investigation of the LS-SVM method on water quantity prediction has been very limited. Therefore, this paper will present a promising nonlinear autoregressive (NAR) model optimized by the LS-SVM using the previous discharge time series.

3. Method

3.1 NAR Model with Time-Delay

In the nonlinear autoregressive model (NAR) time series predictive model, the output is feedback to the input and the future values of time series y(t) could be predicted from past values of that time series, as shown in Fig. 1. Extending backward from time t, we have time series (y(t), y(t-1), y(t-2), · · ·).

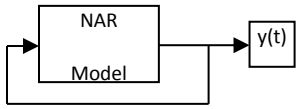

Fig. 1. The NAR based prediction model. The future values of y(t) can be predicted from past values of y(t).

This form of prediction can be written as follows:

$$y(t+s) = f(y(t-1),\ldots,y(t-d))$$

where s is called the horizon of prediction. If s = 1, then this prediction is called one time step ahead prediction; otherwise, it is called multi-step ahead prediction. d is the time delay, giving the number of past predictions fed into the model.

3.2 Least Squares Support Vector Machine Regression with Symmetry Constraints

Least Squares Support Vector Machines (LS-SVM) is a powerful nonlinear kernel methods, which use positive-definite kernel functions to build a linear model in the high-dimensional feature space where the inputs have been transformed by means of a nonlinear mapping $\emptyset$ [18]. This is converted to the dual space by means of the Mercer's theorem and the use of a positive definite kernel, without computing explicitly the mapping $\emptyset$. The LS-SVM formulation solves a linear system in dual space under a least-squares cost function [19], where the sparseness property can be obtained by sequentially pruning the support value spectrum [20] or via a fixed-size subset selection approach. The LS-SVM training procedure involves the selection of a kernel parameter and the regularization parameter of the cost function, which can be done e.g. by cross-validation, Bayesian techniques [21] or others. Given the sample of N points $\{x_i, y_i\}_{i=1}^{N}$, with input vectors $x_i \in \mathbb{R}^p$ and output values $y_i \in \mathbb{R}$, the goal is to estimate a model of the form:

$$y_i = w^T \emptyset(x_i) + b + \varepsilon_i (\text{i=1,2,…,l}) \qquad (1)$$

where $\emptyset(\cdot)$: $\mathbb{R}^p \longrightarrow \mathbb{R}^{n_h}$ is the mapping to a high dimensional (and possibly infinite dimensional) feature space, and the residuals e are assumed to be independent and identically distributed with zero mean and constant and finite variance.

Least squares support vector machine (LS-SVM) formulates a regularized cost function and changes its inequation restriction to equation restriction. As a result, the solution process becomes a solution of a group of equations which greatly accelerates the solution speed [19]. The following optimization problem with a regularized cost function is formulated:

$$min_{w,b,\varepsilon_i} \frac{1}{2} w^T w + \frac{C}{2} \sum_{i=1}^{l} \varepsilon_i^2 \qquad (2)$$

The solution of LS-SVM regressor will be obtained after we construct the Lagrangian function. The extreme point of Q is a saddle point, and differentiating Q can provide the formulas as follows, using Lagrangian multiplier method to solve the formulas. The conditions for optimality are

$$\frac{\partial Q}{\partial w} = w - \sum_{i=1}^{l} \alpha_i \emptyset(x_i) = 0 \qquad (3)$$

$$\frac{\partial Q}{\partial b} = -\sum_{i=1}^{l} \alpha_i = 0 \qquad (4)$$

$$\frac{\partial Q}{\partial \alpha} = w^T - \emptyset(\mathrm{x_i}) + \mathrm{b} + \varepsilon_i - y_i = 0 \qquad (5)$$

$$\frac{\partial Q}{\partial \varepsilon_i} = C\varepsilon_i - \alpha_i = 0 \qquad (6)$$

where $\alpha \in \mathbb{R}$ are the Lagrange multipliers. From formulas above, we can obtain:

$$\frac{1}{2} \sum_{i=1}^{l} \alpha_i \emptyset(x_i) \sum_{j=1}^{l} \alpha_j \emptyset(x_j) + \frac{1}{2C} \sum_{i=1}^{l} \alpha_i^2 + b \sum_{i=1}^{l} \alpha_i = \sum_{i=1}^{l} \alpha_i y_i \qquad (7)$$

The formula above can be expressed in matrix form:

$$\begin{bmatrix} 0 & e^T \\ e & \Omega + C^{-1} I \end{bmatrix} (\mathrm{l}+1)(\mathrm{l}+1) \begin{bmatrix} \mathrm{b} \\ \alpha \end{bmatrix} = \begin{bmatrix} 0 \\ \mathrm{Y} \end{bmatrix} \qquad (8)$$

In this equation,

$$e = [1, \ldots, 1]_x^T$$

$$\Omega_{ij} = K(x_i, x_j) = \emptyset(x_i)^T \emptyset(x_j) \qquad (9)$$

Formula (7) is a linear equation set corresponding to the optimization problem and can provide us with α and b. Thus, the prediction output decision function is:

$$\bar{y}(x) = \sum_{i=1}^{l} \alpha_i K(x_i x) + b \qquad (10)$$

where $K(x_i, x)$ is the core function.

3.3 Practical Implementation

The training process of LS-SVM involves the selection of kernel parameter: the squared bandwidth, σ2 (sig2) and the regularization constant, γ (gam). The regularization constant, γ (gam) determines the trade-off between the training error minimization and smoothness A good choice of these parameters is crucial for the performance of the estimator. The tuning parameters were found by using a combination of coupled simulated annealing (CSA) and a standard simplex method. The CSA finds good starting values and these values were passed to the simplex method in order to fine tune the result. We use 10-fold cross-validation for selecting these parameters.

Another important choice is the selection of regressors, i.e., which lags of inputs and outputs are going to be included in the regression vector. This selection is done by using a large number of initial components and then performing a greedy search to prune non-informative lags on a cross-validation basis. Therefore an initial model containing all regressors is estimated and optimal choices for the parameters are made. On each stage of the greedy backwards elimination process, a regressor is removed if the cross-validation mean absolute error or mean squared error improves. For the purpose of model estimation, all series are normalized to zero mean and unit variance. Once the parameters are calculated, the final set of regressors is then used for the predictions. By using only a subset of the total data available, we can compare the predictions against real values to see how accurate the prediction is.

4. Results

4.1 Study Area

The study area will focus on the Four Mile Run at Alexandria, VA, as shown in Fig. 2. The US Geological Survey (USGS) gaging station 1652500 on Four Mile Run located at the Shirlington Road Bridge has collected stream flow data since 1951 [1]. The Four Mile Run is 9.2 miles long, and is a direct tributary of the Potomac River.

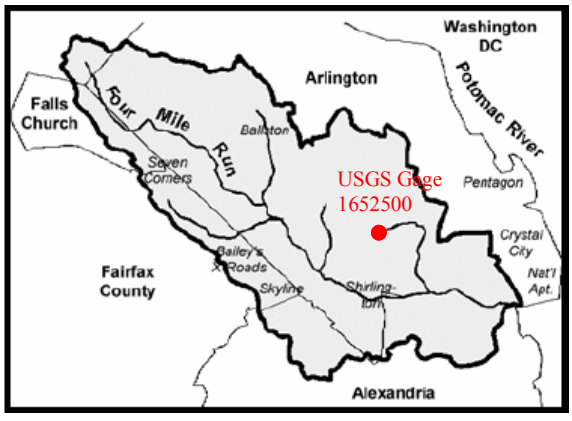

Fig. 2. Four Mile Run at Alexandria, VA is a nine-mile long stream located in a highly urbanized area in Northern Virginia. It is a direct tributary of the Potomac River, which ultimately carries the water flowing from Four Mile Run to the Chesapeake Bay.

The entire watershed can be classified as highly urbanized, which ultimately flows through some of Northern Virginia's most densely populated areas to the Chesapeake Bay. In addition, because of the highly urbanized nature of the Four Mile Run watershed, the neighborhoods and businesses adjacent to this portion of the run were subjected to repeated flooding, beginning in the 1940s. Therefore, the flood-control solutions are the major concern. Runoff prediction would provide a promising solution for flood-control.

4.2 Time Series Data from USGS

The real-time USGS data for the Four Mile Run station include the discharge data, which is useful for investigating its impact to the long-run discharge forecast. The discharge is the volume of water flowing past a certain point in a water-flow. For example, the amount of cubic feet passing through a drain per second is a measure of discharge. The discharge data was retrieved for 120 days between August 28, 2010 and December 4, 2010. Because the real-time data typically are recorded at 15-minute intervals, the runoff discharge (cubic feet per second) data plots 34721 data during the 120 days, as shown in Fig. 8. The discharge will be presented to the system as an input. It is a 34721x1 vector, representing dynamic data, i.e. 34721 time steps. It is challenging that these discharge values vary significantly over time. As shown in Fig. 3, the baseline is at around 4 on the Y-axis, with peaks reaching 8, with very little repetition to the pattern, making it more difficult to predict future values.

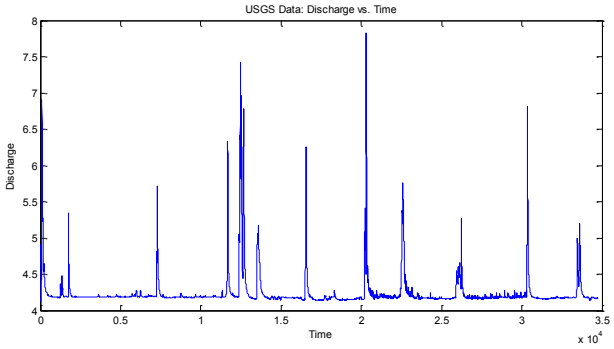

Fig. 3 Plot of entire discharge data set vs. time.

4.3 Training Data and Time Delays

The first 500 time series data from the original sample of about 34,721 were used for our analysis. To determine an appropriate time delay or lag, we increase the number of delays lags until the network performed well. After a number of experiments, 80 is determined to be the smallest lag number that ensures a good performance. That means the model will use the past 80 input data to predict a future data.

Before parameter tuning and network training, we should use the function *windowize* to convert the time-series into a Hankel matrix useful for training a nonlinear function approximation [22]. For example, assume there is a matrix X which is defined below.

$$X = \begin{bmatrix} a_1 & a_2 & a_3 \\ b_1 & b_2 & b_3 \\ c_1 & c_2 & c_3 \\ d_1 & d_2 & d_3 \\ e_1 & e_2 & e_3 \\ f_1 & f_2 & f_3 \\ g_1 & g_2 & g_3 \end{bmatrix}$$

1st window

Now we want to convert matrix *X* to a new matrix *Xu* by running the Matlab command:

Xu = windowize(X, [1 2 3])

This command will select 3 rows of data (i.e. circled by the blue dashed line) from matrix *X* to make a window, and pout this window in a row of matrix *Xu*. For example, row 1 to 3 from matrix *X* will be selected to make the 1st window, and put in the 1st row of matrix Xu. Similarly, row 2 to 4 from matrix X will be selected to make the 2nd window, and put in the 2nd row of matrix Xu. Thus, the matrix Xu will look as follows.

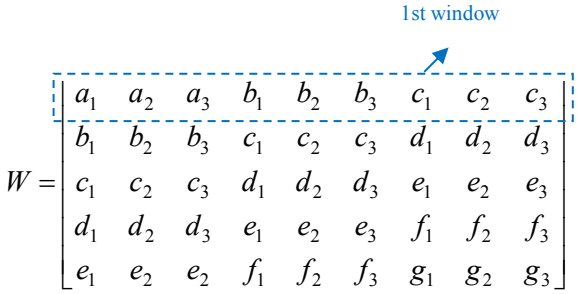

$$W = \begin{bmatrix} a_1 & a_2 & a_3 & b_1 & b_2 & b_3 & c_1 & c_2 & c_3 \\ b_1 & b_2 & b_3 & c_1 & c_2 & c_3 & d_1 & d_2 & d_3 \\ c_1 & c_2 & c_3 & d_1 & d_2 & d_3 & e_1 & e_2 & e_3 \\ d_1 & d_2 & d_3 & e_1 & e_2 & e_3 & f_1 & f_2 & f_3 \\ e_1 & e_2 & e_2 & f_1 & f_2 & f_3 & g_1 & g_2 & g_3 \end{bmatrix}$$

In our case, Xu = windowize(X, 1:lag+1) will convert the discharge data set into a new input vector including the past measurements and the future output by *windowize*.

The size of the discharge data set contains 500 data points, which consists of 500 rows. With the 80 lags, it will generate 420 rows and 81 columns. The last column of the resulting matrix *Xu* contains the future values of the time-series, and the previous 80 columns contain the past inputs. The first 340 data points (i.e. 70%) will be used as training data, and the remaining 160 data (i.e. 30%) will be used as test data. Xtra = Xu(1:end-lag,1:lag) will generate 80 past inputs, i.e. x(t-1), x(t-2), … x(t-80), while Ytra = Xu(1:end-lag,end) contains their actual future value, x(t). Ytra will be used as the target for those past inputs.

4.4 Tuning the Parameters

In order to build an LS-SVM model, we need to tune the regularization constant, *gam* and the kernel parameter, *sig2*. γ (gam) determines the trade-off between the training error minimization and smoothness. In the common case of the Gaussian RBF kernel, the kernel parameter, *sig2* is the squared bandwidth. We use the following statement to tune these parameters:

```
[gam,sig2] = tunelssvm({Xtra,Ytra,'f',[],[],'RBF_kernel'},...
'simplex','crossvalidatelssvm',{10,'mae'})
```

Where *f* stands for function estimation. The Kernel type is chosen to be the default RBF kernel. The optimization function is specified as simplex. The simplex is a multidimensional unconstrained non-linear optimization method. Simplex finds a local minimum of a function starting from an initial point X. The local minimum is located via the Nelder-Mead simplex algorithm [23]. The model adopts *crossvalidatelssvm* as the cost function. It estimates the generalization performance of the model. It is based upon feedforward simulation on the validation set using the feedforwardly trained model.

In addition, 10 means 10-fold. We use 10-fold cross-validation because the input size is greater than 300 points. Otherwise, leave-one-out cross-validation will be used when the input size is less or equal than 300 points. The 10-fold cross-validation method will break data (the size of the data is assumed to be *n*) into 10 sets of size n/10, then train on 9 datasets and test on 1, and then repeat 10 times and take a mean accuracy. *mae* is the mean absolute error and is used in combination with the 10-fold cross-validation method. It is the absolute value of the difference between the forecasted value and the actual value. It tells us how big of an error we can expect from the forecast on average.

The tuning of the parameters is conducted in two steps. First, a state-of-the-art global optimization technique, Coupled Simulated Annealing (CSA) [24], determines suitable parameters according to some criterion. Second, these parameters are then given to a second optimization procedure *simplex* to perform a fine-tuning step. The parameter tuning results are shown in Fig. 4. Coupled Simulated Annealing chosen the initial *gam* to be 1364.706, and *sig2* to be 13.989. They serve as the starting values for the *simplex* optimization routine. After 11 iterations, the *gam* and *sig2* are optimized to be 83.2188 and 15.298, respectively.

4.5 Network Training and Prediction

Once the *gam* and *sig2* parameters were tuned, we should train the network. It will train the support values and the bias term of an LS-SVM for function approximation. The Matlab command is

```
[alpha,b] = trainlssvm({Xtra,Ytra,'f',gam,sig2,'RBF_kernel'})
```

Xtra and Ytra are the training data we defined before. *f* stands for function estimation. The Kernel type is chosen to be the default RBF kernel. Because the network has 80 lags, it helps generate 80 past inputs. For each iteration, the past 80 Xtra data points will be used to predict the 81th data point. Ytra is the desired target. The 340 samples in the Xtra and Ytra will be used to train the network.

After the network has been well trained, we can test the prediction performance by testing on the new data, which have never been seen by the network. We will use the remaining 160 data points as the testing data. The Matlab command is

```
prediction = predict({Xtra,Ytra,'f',gam,sig2, 'RBF_kernel'},Xs,500)
```

Xtra and Ytra are the training data we used before. ‘f’ stands for function estimation. The Kernel type is chosen to be the default RBF kernel. Xs is the starting point for iterative prediction. Since we want to check both the training performance and prediction performance, we set Xs=X(1:end-lag,1). The model will start predicting from the 1st data point, and will predict the next 500 points from the start point.

The predicted discharge value and the actual discharge value were shown in Fig. 5. The prediction is shown in the red dashdot while the real USGS discharge data points are shown in blue line. The first 340 samples are training data, and the remaining 160 samples are testing data. As shown in Fig. 5, the prediction on the training data matches the actual values perfectly. This makes sense because these training samples have been seen by the network during training. The

prediction on these data should have already been trained to be very close to the actual value. In addition, when we test the new data from time step 341 to 500, we find the predicted values match very well with the actual values. This demonstrated that the LS-SVM model has excellent prediction ability.

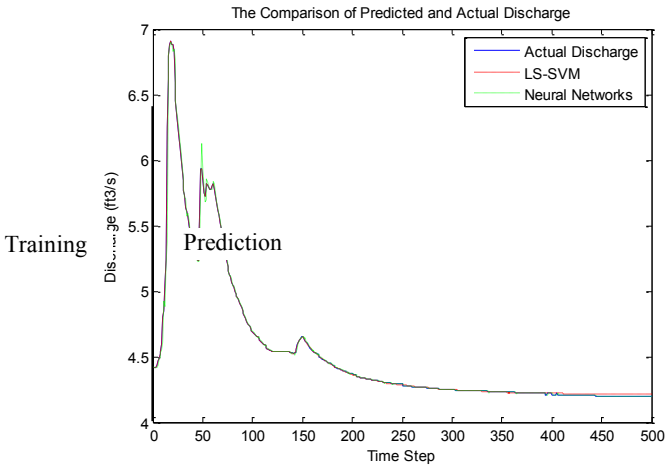

Fig. 4 The LS-SVM prediction is shown in red dashdot, the USGS discharge is shown in blue line, and the recurrent neural networks model trained by Levenberg-Marquardt backpropagation algorithm is shown in green dash colon. The first 340 samples are training data, and the remaining 160 samples are test data.

In order to further evaluate the performance of the proposed LS-SVM method, we compare the results with the recurrent neural networks model trained by Levenberg-Marquardt backpropagation algorithm [4]. The simulation result is shown in Fig. 5. The USGS discharge is shown in blue line, the LS-SVM prediction is shown in red dashdot, and the recurrent neural networks model trained by Levenberg-Marquardt backpropagation algorithm is shown in green dash colon. The first 340 samples are training data, and the remaining 160 samples are test data.

5. Accomplishments

The PIs and the student published 8 referred papers and 7 posters from this project. Please see the list from the appendix. The DCWRRI grant were acknowledged.

6. Conclusions

In this research project, the least squares support vector machine (LS-SVM) based algorithm is developed to forecast the future streamflow based on the previous streamflow. The first 340 data points are used as training data, and the remaining 160 data are testing data. First we convert the time-series into a Hankel matrix useful for training a nonlinear function approximation. Next we build an LS-SVM model by tuning the regularization constant, *gam* and the kernel parameter, *sig2*. A Gaussian Radial Basis Function (RBF) kernel framework was built on the data set to optimize the tuning parameters. The 10-fold cross-validation method is used to estimate the generalization performance of the model. Then we train the LS-SVM network. It trains the support values and the bias term of an LS-SVM for function approximation. We developed an

effective training scheme. After the network has been well trained, we test the prediction performance by predicting new values on the testing samples, as well as the training samples.

The performance of the LS-SVM model is compared with the recurrent neural networks model trained by Levenberg-Marquardt backpropagation algorithm. The excellent experimental results of the comparison indicate that the LS-SVM model is a useful tool and a promising new method for streamflow forecasting. The excellent experimental results demonstrated that the proposed LS-SVM based predictive model has superior prediction performance on not only the training samples, but also the testing samples. In addition, the proposed parameter tuning method and the training scheme worked effectively, which ensure an accurate prediction of streamflow.

6. References

[1] Northern Virginia Regional Commission (NVRC), "Flood Frequency Analysis for Four Mile Run at USGS Gaging Station 1652500," 2004. https://www.novaregion.org/DocumentCenter/Home/View/301.

[2] N. Zhang, "Urban Stormwater Runoff Prediction Using Recurrent Neural Networks," The Eighth International Symposium on Neural Networks (ISNN), Guilin, China, 2011.

[3] N. Zhang, "Prediction of Urban Stormwater Runoff in Chesapeake Bay Using Neural Networks," The Eighth International Symposium on Neural Networks (ISNN), Guilin, China, 2011.

[4] N. Zhang and S.H. Lai, "Runoff Quantity Analysis of Urban Catchments Based on Neural Networks Method," The IASTED International Symposia on Imaging and Signal Processing in Healthcare and Technology (ISPHT), Washington, DC, May 16-18, 2011.

[5] N. Zhang and S.H. Lai, "Water Quantity Prediction Based on Particle Swarm Optimization and Evolutionary Algorithm Using Recurrent Neural Networks," 2011 International Joint Conference on Neural Networks (IJCNN), San Jose, CA, July 31-August 5, 2011.

[6] G. Ji, J.C. Wang, Y. Ge, and H.J. Liu, "Urban Water Demand Forecasting by LS-SVM with Tuning Based on Elitist Teaching-Learning-Based Optimization", The 26th Chinese Control and Decision Conference (2014 CCDC), pp. 3997-4002, 2014.

[7] Z. Liu, X. Wang, L. Cui, X. Lian, J. Xu, "Research on Water Bloom Prediction Based on Least Squares Support Vector Machine," 2009 WRI World Congress on Computer Science and Information Engineering, vol.5, pp. 764 - 768, 2009.

[8] Y. Xiang and L. Jiang, "Water Quality Prediction Using LS-SVM and Particle Swarm Optimization," Second International Workshop on Knowledge Discovery and Data Mining, 2009. pp. 900- 904, 2009.

[9] W. Liu, K. Chen, and L. Liu, "Prediction model of water consumption using least square support vector machines optimized by hybrid intelligent algorithm," 2011 Second International Conference on Mechanic Automation and Control Engineering (MACE), pp. 3298- 3300, 2011.

[10] L. Liang and F. Xie, "Applied research on wastewater treatment based on least squares support vector machine," 2011 International Conference on Remote Sensing, Environment and Transportation Engineering (RSETE), pp. 4825- 4827, 2011.

[11] X. Zhang, S. Wang, and Y. Zhao, "Application of support vector machine and least squares vector machine to freight volume forecast," 2011 International Conference on Remote Sensing, Environment and Transportation Engineering (RSETE), pp. 104- 107, 2011.

[12] R.J. Liao, J.P. Bian, L.J. Yang, S. Grzybowski, Y.Y. Wang, and J. Li, "Forecasting dissolved gases content in power transformer oil based on weakening buffer operator and least square support vector machine–Markov," Generation, Transmission & Distribution, IET, vol. 6, no. 2, pp. 142- 151, 2012.
[13] L. Hou, Q. Yang, J. An, "An Improved LSSVM Regression Algorithm," International Conference on Computational Intelligence and Natural Computing, vol. 2, pp. 138- 140, 2009.
[14] X. Zhang, Y. Zhao, and S. Wang, "Reliability prediction of engine systems using least square support vector machine," 2011 International Conference on Electronics, Communications and Control (ICECC), pp. 3856- 3859, 2011.
[15] N. Zhang, C. Williams, E. Ososanya, and W. Mahmoud, "Streamflow Prediction Based on Least Squares Support Vector Machines," ASEE-2013 Mid-Atlantic Fall Conference, Washington, D.C., October 11-13, 2013.
[16] T. A. Stolarski, "System for wear prediction in lubricated sliding contacts," Lubrication Science, 1996, 8 (4): 315 -351.
[17] Suykens J A K,Vandewalle J, "Least squares support vector machine classifiers," Neural Processing Letter, 1999, 9(3):293-300.
[18] J.A.K. Suykens, T. Van Gestel, J. De Brabanter, B. De Moor, and J. Vandewalle, "Least Squares Support Vector Machines. World Scientific," Singapore, 2002.
[19] J.A.K. Suykens and J. Vandewalle, "Least squares support vector machine classifiers," Neural Processing Letters, 9:293–300, 1999.
[20] J.A.K. Suykens, J. De Brabanter, L. Lukas, and J. Vandewalle, "Weighted least squares support vector machines: robustness and sparse approximation," Neurocomputing, vol. 48, no. 1-4, pp. 85–105, 2002.
[21] D.J.C. MacKay, "Comparison of approximate methods for handling hyperparameters," Neural Computation, vol. 11, pp. 1035–1068, 1999.
[22] De Brabanter K., Karsmakers P., Ojeda F., Alzate C., De Brabanter J., Pelckmans K., De Moor B., Vandewalle J., Suykens J.A.K., "LS-SVMlab Toolbox User's Guide version 1.8," Internal Report 10-146, ESAT-SISTA, K.U.Leuven (Leuven, Belgium), 2010.
[23] J. A. Nelder and R. Mead, "A Simplex Method for Function Minimization," Computer Journal, 7, 308-313, 1965.
[24] S. Xavier-de-Souza, J.A.K. Suykens, J. Vandewalle, and D. Bolle, "Coupled Simulated Annealing," IEEE Transactions on Systems, Man and Cybernetics - Part B, vol. 40, no. 2, pp. 320–335, 2010.

Appendix

1. Student Support

Category	Number of Students Supported
Undergraduate	1
Master	0
Ph.D.	0
Post Doc.	0
Total	1

2.. List of publications (APA format)

Peer reviewed journal article (DCWRRI grant was acknowledged)

- **Nian Zhang** and Devdas Shetty, An Effective LS-SVM Based Approach for Surface Roughness Prediction in Machined Surfaces, *Neurocomputing*. (In press)
- **Nian Zhang**, Tilaye Alemayehu, and **Pradeep Behera**, "Nonlinear Autoregressive (NAR) Forecasting Model for Potomac River Stage Using Least Squares Support Vector Machines (LS-SVM)", *International Journal of Innovative Technology and Exploring Engineering (IJITEE)*, vol. 4, no. 9, pp. 1-9, 2015. (DCWRRI student co-author)
- **Nian Zhang**, Roussel Kamaha, and **Pradeep Behera**, "Prediction of Surface Water Supply Sources for the District of Columbia Using Least Squares Support Vector Machines (LS-SVM) Method", *Advances in Computer Science: an International Journal (ACSIJ)*, vol. 4, issue 1, no.13, pp. 47-51, 2015. (DCWRRI student co-author)

Conference proceeding (DCWRRI grant was acknowledged)

- Juan F. Ramirez Rochac, **Nian Zhang**, and **Pradeep Behera**, "Design of Adaptive Feature Extraction Algorithm Based on Fuzzy Classifier in Hyperspectral Imagery Classification for Big Data Analysis," *The 12th World Congress on Intelligent Control and Automation (WCICA 2016)*, Guilin, China, 2016.
- **Nian Zhang**, "Cost-Sensitive Spectral Clustering for Photo-Thermal Infrared Imaging Data," *2016 Sixth International Conference on Information Science and Technology (ICIST)*, Dalian, China, 2016.
- Juan F. Ramirez Rochac and **Nian Zhang**, "Reference Clusters Based Feature Extraction Approach for Mixed Spectral Signatures with Dimensionality Disparity," *10th Annual IEEE International Systems Conference (IEEE SysCon 2016)*, Orlando, Florida, 2016.
- Juan F. Ramirez Rochac and **Nian Zhang**, "Feature Extraction in Hyperspectral Imaging Using Adaptive Feature Selection Approach," *The Eighth International Conference on Advanced Computational Intelligence (ICACI2016)*, Chiang Mai, Thailand, pp. 36-40, 2016.
- Francisco Lourenco, **Nian Zhang** and Sasan Haghani, "Prediction of Surface Water Supply Sources for the District of Columbia Using Neural Networks Methods," *ASEE Zone III Meeting 2015*, Springfield, MO, September 23-25, 2015.

Poster presentation (attach poster): Title, Author, and title of the symposium or conference (DCWRRI grant was acknowledged)

- Tilaye Alemayehu, Omar Abbas, **Nian Zhang**, and **Pradeep K. Behera**, "A Nearest-Neighbor Method (NNM) for Annual Streamflow Prediction," *National Capital Region Water Resources Symposium*, Washington D. C., April 8, 2016.
- Tilaye Alemayehu and **Nian Zhang**, "Optimization-Based Extreme Learning Machine with Multi-kernel Learning Approach for Classification," *The 73rd Joint Annual Meeting BKX and NIS*, Hampton, Virginia, April 6 – 9, 2016, 2016.
- Tilaye Alemayehu, **Nian Zhang**, and Sasan Haghani, "Application of Weighted Extreme Learning Machine for Imbalanced Data classification," *2016 Emerging Researchers National (ERN) Conference in STEM*, Washington, D.C., February 25-27, 2016.
- Tilaye Alemayehu, **Nian Zhang**, and Sasan Haghani, "Weighted Extreme Learning Machine for Imbalance Learning," *2015 Annual Biomedical Research Conference for Minority Students (ABRCMS)*, Seattle, WA, November 11-14, 2015.
- Tilaye Alemayehu, **Nian Zhang**, and **Pradeep K. Behera**, "Water Quality Classification of Potomac River Using Principal Component Analysis Method," *National Capital Region Water Resources Symposium*, Washington D.C., April 10, 2015.
- Roussel Kamaha and **Nian Zhang**, "Amelioration of an ECG Signal Using Noise Neutralizer Adaptive Filtering Algorithms," *The 72nd Joint Annual Meeting BKX and NIS*, Jackson, Mississippi, March 11-14, 2015.
- Roussel Kamaha and **Nian Zhang**, "Performance Study of Adaptive Filtering Algorithms for Noise Cancellation of ECG Signal," *2015 Emerging Researchers National (ERN) Conference in STEM* , Washington, D.C., February 19-21, 2015.

Identifying Sources of Chlordane Contamination in Anacostia River Food Fish

Basic Information

Title:	Identifying Sources of Chlordane Contamination in Anacostia River Food Fish
Project Number:	2015DC175B
Start Date:	3/1/2015
End Date:	2/28/2016
Funding Source:	104B
Congressional District:	DC
Research Category:	Water Quality
Focus Category:	Toxic Substances, Ecology, Surface Water
Descriptors:	None
Principal Investigators:	Harriette Phelps, Sebhat Tefera

Publication

1. Phelps H.L. 2015. Active biomonitoring with Corbicula for USEPA priority pollutant and metal sources in the Anacostia River (DC, Maryland, USA), Integrated Environmental Assessment and Management, 999 (999): 1-11.

SOURCES OF CHLORDANE IN ANACOSTIA RIVER FISH

Progress Report

Dr. Harriette L. Phelps
Department of Environmental Science

April 22 2016

EXECUTIVE SUMMARY

High chlordane in fish tissue is a major reason for banning the consumption of fish caught in DC's Anacostia River. Chlordane is a top EPA Priority Pollutant because it is one of the Persistent Bioaccumulated and Toxic (PBT) compounds that can bioaccumulate to toxic concentrations in fish, birds and man that are dangerous for health and survival. Several legacy chlordane sources were located in the MD tributaries (Phelps 2015). The present project looked for the path transferring chlordane from MD tributary sources to DC food fish Fish of three trophic levels were obtained from the MD tributaries and the tidal Anacostia River. Fish tissue was analyzed for chlordane, which is bioaccumulated, and heptachlor epoxide which is not bioaccumulated but specifically indicates legacy chlordane. The fish species included small minnows trapped at two sites in MD and edible perch caught nearby in the tidal Anacostia (Bladensburg) which has recreational fishing. Tidal Anacostia River DC fish included smallmummichug and gizzard shad obtained by seining and white catfish by electrofishing at three sites from Anacostia Park DC to near Bladensburg MD. Chlordane in Bladensburg perch was significantly greater than tributary minnows, confirming bioconcentration. Tidal Anacostia fish chlordane was highest (2-3X) in the non-edible gizzard shad which is a small migratory member of the herring family that feeds on small organisms living in the upper sediment . Gizzard shad cannot be hooked and are not consumed due to small size and bad taste but they are a favorite food of many DC edible food fish but not catfish (lowest chlordane). This study identified chlordane-contaminated surface sediment from MD the likely source of chlordane DC's food fish via the contaminated/sediment/ gizzard shad/food fish chain. Heptachlor epoxide confirmed a legacy chlordane source. The contaminated/sediment/ gizzard shad/food path is probably responsible for other contaminants like PSBs found with sources in MD.

INTRODUCTION

Earlier WRRI studies had surveyed for EPA Priority Pollutants and metals at 45 sites in the Anacostia River watershed (MD and DC) by using active biomonitoring (ABM) with the local freshwater Asiatic clam *Corbicula fluminea.* From 1999 to 2011 *Corbicula* were translocated from the tidal Potomac River reference site to 45 tidal and nontidal sites in the Anacostia River watershed. Clams were analyzed by TestAmerica (Burlington VT) for 66 EPA Priority Pollutants including PCBs, PAHs and Pesticides and technical chlordane. Translocation using clams found contaminants were accumulated from the water column. Pollutants in the tidal Anacostia River were highest upstream (Bladensburg Marina). Five Anacostia tributaries (94% of flow) held 17 sites with high levels of bioavailable contaminants. PAHs were highest near industrial parks and Metro stations. PCBs originated at one industrial park. Total pesticides (80% technical chlordane) exceeded fish consumption advisory starting at upstream urban sites in four MD tributaries with high heptachlor epoxide indicating legacy chlordane dumpsites. Upper Sligo Creek had a site with technical chlordane 3X the EPA advisory in clams, 5X advisory in minnows and sediment contamination. Below a large Sligo Creek sediment trap pond the bioavailable chlordane fell to reference, suggesting a precipitation loss of chlordane-contaminated suspended sediment.

METHODOLOGIES

The first study (Onyinye and Phelps) compared chlordane and heptachlor concentrations of minnows trapped in Still Creek MD and three edible yellow perch caught nearby at tidal Bladensburg MD by a local fisherman. Analyses reported no significant difference among species in heptachlor epoxide concentration and significant bioaccumulation of chlordane in Bladensburg perch which was confirmed by statistical analysis.

To study chlordane accumulation in tidal Anacostia trophic levels, fish species were obtained during a 7/16/15 boat trip conducted by DC Fisheries from upper Anacostia Park DC to just below Bladensburg Marina MD. Seining was used to collect small mummichug and gizzard shad at three locations. Three white catfish were obtained midway by electrofishing. The freshly caught fish were held in a cooler and received a triple water rinse. Small fish (mummichug and gizzard shad) were combined by species and weight and measured for average weight and length. Whole fish (perch and catfish) were handled individually. Clean catfish tissue samples were obtained by dissection. Duplicate frozen fish samples for analysis of heptachlor and technical chlordane were sent (chain of command) to UDC Analytical Research Laboratory and Test America of Burlington VT. Only the Test America results are available.

RESULTS, DISCUSSION AND CONCLUSIONS

ANACOSTIA FISH DATA (ppt)

	Chlordane	Heptachlor epoxide
Minnows (trapped, combined)		
Sligo Creek MD (Phelps 2012)	1500	37
NW Branch, MD	150	8
NE Branch, MD	350	36
Individual Yellow Perch	270	17
Bladensburg Marina, MD	650	33
	650	40
Mummichug (seined, combined)	85	6.7
Tidal Anacostia, DC		
Gizzard Shad (seined, combined)	210	13
Tidal Anacostia, DC		
White Catfish (electrofished, combined tissue)	49	3.7
Tidal Anacostia, DC		

The 2015 Onyinye and Phelps study found low levels of chlordane in both MD tributary minnows with heptachlor epoxide indicating upstream legacy chlordane sources. The chlordane concentration in perch food fish caught at tidal Bladensburg was nearby was up to 2X greater

which confirmed bioconcentration. The concentration of heptachlor epoxide was not significantly higher as expected.

The 2015-2016 Rose and Phelps study of chlordane and heptachlor epoxide concentrations in Anacostia River fish (Test America analysis) found considerable difference chlordane concentrations and little in heptachlor epoxide. Chlordane was highest in American Gizzard Shad (210 ppt) followed by mummichug (85 ppt) and catfish (49 ppt). Gizzard Shad migrate upstream with other herring species in spring It is not fished due to small size and bad taste. The gizzard shad feeds on organisms living in surface sediment and are a favorite food of the Anacostia River food fish favored by DC residents, putting them at risk of chlordane poisoning. The mummichug feeds on small organisms in the water and white catfish do not eat gizzard shad. The presence of heptachlor epoxide indicated legacy chlordane sources located in the MD watershed (Phelps 2005). The completed study shows a significant contaminated sediment/gizzard shad/fish relationship among MD sources of legacy chlordane and DC Anacostia River food fish.

Considerable DC financing is now available to locate and remediate the DC sources of fish contaminants. The RI/RS (Remedial Investigation/Remediation Study) prepared by Tetra Tech is still open for comment. I have not seen a copy but recently attended the (only) openTetra Tech presentation. It recommended an extensive study of the DC sources of fish contaminants to be followed by remediation including extensive sediment dredging in the DC Anacostia River. There was no mention of reports on contaminant sources in MD, continual deposition of contaminated suspended sediment (Phelps 2015) and dredging Anacostia River sediment followed by a two-year 2X to 3X increase in bioavailable toxics (Phelps 2001). The present study suggests a relationship among MD sources of legacy chlordane and high DC food fish chlordane via chlordane-contaminated DC surface sediment/gizzard shad/ food fish. That may be used by additional toxics. In my opinion the present DC RI/RS is going the wrong way. Much better alternatives are available and on record.

REFERENCES

Phelps HL. 2000. DC's Contaminated Anacostia Estuary Sediments: A Biomonitoring Approach. 10p. www.udc.edu/wrri/

Phelps, HL. 2001. PCB Congenors and Chlordane in Anacostia Estuary Sediments and Asiatic Clams (*Corbicula fluminea*): Possible Effects of Dredging. www.udc.edu/wrri/

Phelps HL. 2002. Sources of Bioavailable Toxic Pollutants in the Anacostia. 17 p. www.udc.edu/wrri/

Phelps HL. 2003. *Corbicula* Biomonitoring in the Anacostia Watershed. www.udc.edu/wrri/

Phelps HL. 2004. Sources of Bioavailable Toxic Pollutants in the Anacostia Watershed (Part III). www.udc.edu/wrri/

Phelps,HL. 2005. Identification of PCB, PAH and chlordane source areas in the Anacostia River watershed. www.udc.edu/wrri/

Phelps,HL. 2008. Active Biomonitoring for PCB, PAH and Chlordane sources in the Anacostia Watershed. www.udc.edu/wrri/

Phelps HL. 2010. Clam Active Biomonitoring and POM Passive Monitoring for Anacostia Watershed Contaminant Point Sources. 11p. www.udc.edu/wrri/

Phelps HL. 2011. Active (*Corbicula fluminea*) and Passive (Polyoxymethylene) Chlordane Monitoring in Upper Sligo Creek of the Anacostia River (MD). 8pp.17 p. www.udc.edu/wrri/

Phelps H.L. 2015. Active Biomonitoring with *Corbicula* for USEPA Priority Pollutant and Metal Sources in the Anacostia River (DC, Maryland, USA). 2015. Integrated Environmental Assessment and Management vol 9999 number 9999 pp1-11.

STUDENTS AND PRESENTATIONS

"Chlordane and Heptachlor Epoxide in Anacostia River Fish." 2015. Onyinye Okidoh and Harriette Phelps. Paper and poster presented at Elizabeth Roosevelt High School, MD

"Chlordane and Heptachlor Epoxide in Anacostia Fish." 2016. Sania Rose and Harriette Phelps. University of the District of Columbia, Washington, DC Poster presented at USMC. 2015

ACKNOWLEGEMENTS
Grateful acknowledgment to the UDC Water Resources Center (WRRI) for arranging essential long-term USGS funding,
DC Fisheries
William Hare and Dr. Tolessa Dikcessa, directors of DC's Water Resources Research Program (WRRI).
Ms. Onyinye Okidoh of the Eleanor Roosevelt High School (MD) science program, and Ms. Sania Rose, UDC major in Environment Science.

CHLORDANE AND HEPTACHLOR EPOXIDE IN ANACOSTIA FISH (DC, MD)

SANIA ROSE and DR. HARRIETTE PHELPS: *University of the District of Columbia, (DC).*
and ONYINYE OKIDOH: *Eleanor Roosevelt High School (MD).*

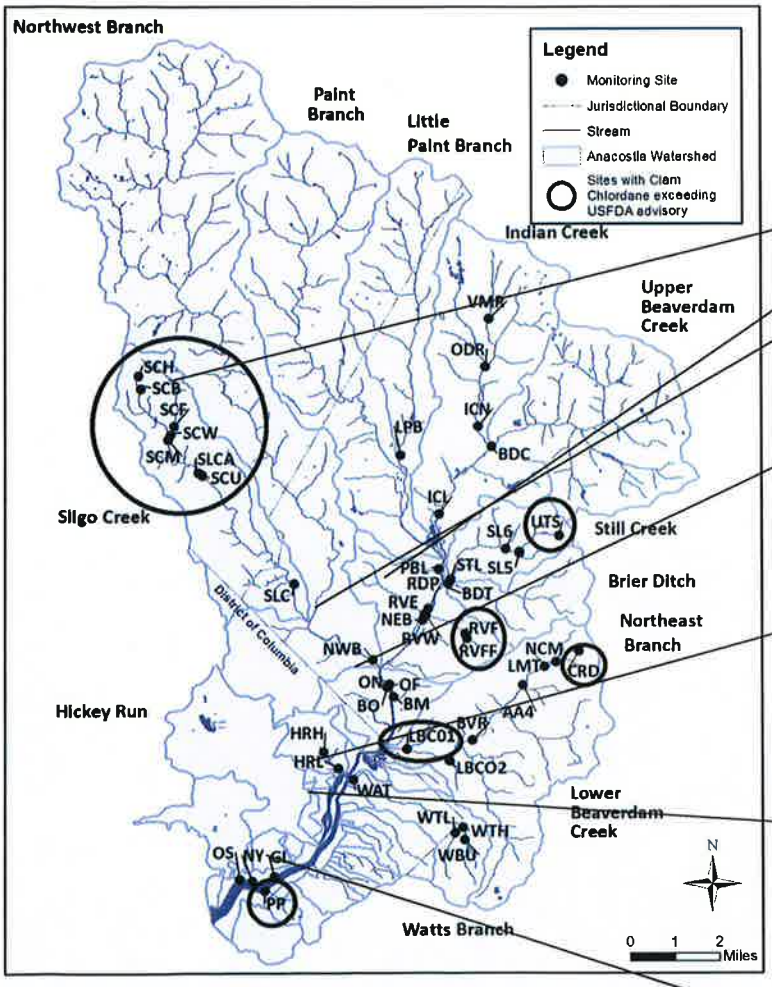

	Chlordane ug/g	Heptachlor Epoxide ug/g
MINNOWS (trapped, MD)		
Sligo Creek	1500	42
NW Branch	150	8
NE Branch	350	36

	270	17
	650	33
YELLOW PERCH (fished, Bladensburg MD	650	40

MUMMICHUG (seined, DC)	85	6.7

GIZZARD SHAD (seined, DC)	210	13

WHITE CATFISH (Fished, DC)	49	3.7

The Anacostia River (DC,MD) has fishing advisories for PCBs, and chlordane that can accumulate in fish, birds and man over USDA limits (300 ppt). Legacy sources of chlordane (having heptachlor epoxide) were located upstream in four MD tributaries by active biomonitoring with the *Corbicula* clam (Phelps 2015). NE and NW Branch minnows had chlordane found significently bioaccumulated in yellow perch fished downstream at Bladensburg Marina. DC Anacostia has the inedible migratory gizzard shad that feeds on organisms in (contaminated) surface sediment, has high chlordane and a favorite food of DC game fish but not catfish.

Chlordane is carried on suspended sediment. Reducing chlordane bioaccumulation in DC fish could follow the capping of DC sediment by natural uncontaminated MD sediment following the strategic placement of sediment trap ponds below the MD sources.

Information Transfer Program Introduction

None.

USGS Summer Intern Program

None.

Student Support					
Category	**Section 104 Base Grant**	**Section 104 NCGP Award**	**NIWR-USGS Internship**	**Supplemental Awards**	**Total**
Undergraduate	16	0	0	3	19
Masters	7	0	0	3	10
Ph.D.	0	0	0	0	0
Post-Doc.	0	0	0	0	0
Total	23	0	0	6	29

Notable Awards and Achievements

The UDC's Water Resources Lab is now NELAP accredited with NELAC standard in potable and non-potable water analysis for trace metals, hardness and minerals. This is a big deal for the university as well as for the city. Nationally certified lab with NELAC standard is crucial for unbiased compliance test to the DC area.